Further Re-Os Arsenopyrite Geochronology from Selected Meguma Au Deposits, Meguma Terrane, Nova Scotia: Possible Evidence for a Protracted Gold-forming System

by

Lin Chen

A thesis submitted in partial fulfillment of the requirements for the degree of

Master of Science

Department of Earth and Atmospheric Sciences
University of Alberta

Abstract

The Meguma terrane, Nova Scotia, is dominated by two rock types; regionally deformed and metamorphosed Cambro-Ordovician metasedimentary rocks and ca. 380-370 Ma meta- to peraluminous granites. The metasedimentary rocks host numerous orogenic-type, vein-hosted gold deposits which occur throughout the metasandstone-dominated Goldenville Group rather than the overlying metasiltstone- and metamudstone-dominated Halifax Group. These mineralized veins are dominated by quartz-carbonate-sulfide assemblages and occupy structures consistent with emplacement during late-stage fold tightening of the regional, northeast-trending, upright folds that formed during the Acadian orogenic event at ca. 410-400 Ma. From previous work, vein formation, hence gold emplacement, spanned 30-40 Ma, as constrained from field observations and radiometric dating. The former indicates veins post-date cleavage formation given that cleaved wall-rock fragments occur in some veins, and that rarely; veins post-date hornfels related to 380 Ma granites. Existing absolute age dating indicates two events at 408 Ma (Re-Os Arsenopyrite; $^{40}Ar/^{39}Ar$ whole rock) and 380-362 Ma (Re-Os Arsenopyrite; $^{40}Ar/^{39}Ar$ Muscovite, Biotite, whole rock). Here we report new Re-Os geochronological data generated from arsenopyrite in gold-bearing veins for two deposits sampled, all of which lie in the same stratigraphic-structural position in the lower part of the Goldenville Group. The Re-Os analysis of arsenopyrite from three veins from the Beaver Dam deposit, which is dominated by bedding-concordant type veins, yielded the ages of ca. 461 Ma, 464 Ma and complex ages of 456 Ma and 446 Ma. In contrast, Re-Os analysis of one vein-hosted arsenopyrite sample from the Touquoy deposit of the Moose River gold district, where mineralization occurs in a vein-poor sequence of carbonate-rich metasiltstone rocks, yielded two isochron ages of ca. 380 Ma and 438 Ma; the

other one sample from the same deposit but from a different vein provided Re-Os model ages from ca. 400 Ma to 440 Ma. Obvious zoning patterns are observed from thin sections, SEM images and EDS element mapping of the arsenopyrite, which indicates multiple generations of mineral growth. From the host rock Re-Os analyses, the extremely low Re and Os concentrations are recorded, indicating that the host rocks are unlikely to significantly affect the sulfide Re-Os ages. The new data suggests that in the Meguma terrane there exists more than two periods of gold mineralization, which started before the Acadian deformation and metamorphism of the host rocks, implying the gold deposit type in the Meguma terrane is not only orogenic related. Similar 440-460 Ma Ordovician and Silurian ages are reported in the adjacent Avalon terrane and Yarmouth area of the Meguma terrane respectively, representing tectonic related magmatic events. Therefore the 460 Ma and 440 Ma vein ages in this study may provide new evidence for the pre-Acadian history of the Meguma terrane. The Meguma terrane might be close to the Avalon terrane during Middle Ordovician age and there may be a wide-spread magmatic event in the Meguma terrane around 440 Ma.

Preface

This thesis is an original work by Lin Chen. No sections of this thesis have been previously published except in abstract form:

Chen, L., Creaser, R.A., Kontak, D.J., 2014, Further Re-Os arsenopyrite geochronology from selected Meguma Au deposits, Meguma Terrane, Nova Scotia: Possible evidence for a protracted gold-forming system: Geological Association of Canada–Mineralogical Association of Canada, Annual meeting abstract with programs, Vol. 37, p.166-167

Chen, L., Creaser, R.A., Kontak, D.J., 2014, Further Re-Os arsenopyrite geochronology from selected Meguma Au deposits, Meguma Terrane, Nova Scotia: Possible evidence for a protracted gold-forming system: Geological Society of America, Annual meeting abstract with programs, Vol. 46, No. 6, p.165

Acknowledgement

This thesis was completed under the supervision of Dr. Robert A. Creaser. I would like to express my sincerest appreciation and thanks to Dr. Robert A. Creaser for his expertise and suggestions. Without his support and guidance throughout the work, this thesis would not be achievable. Additional thanks are expressed for Dr. Daniel Kontak, who provided valuable insights of this study, allowing me to have a comprehensive understanding of the working area. I also would like to thank to Dr. John Waldron and Dr. Brendan Murphy for the tectonic discussion and Dr. Larry Heaman for the zircon U-Pb work support.

Acadian Mining is thanked for providing the access to the drill cores of the Beaver Dam and the Moose River gold deposits in Nova Scotia. I am so thankful for the Radiogenic Isotope Facility, the Canadian Centre for Isotopic Microanalysis and the Scanning Electron Microscope Lab at the University of Alberta for offering the opportunities for all the sample analyses.

I would like to thank to Martin von Dollen, Mark Simms, Krystle Moore, Barbara Ziger, Andy DuFrane, Robert Dokken, Richard Stern and Nathan Gerein for the help with thin section making, sample preparation, Re-Os chemistry, TIMS analysis, U-Pb LA-ICPMS analysis and SEM analysis respectively. In particular, I would like to say many thanks to my colleagues and friends, Danny Hnatyshin, Naomi Miles, Rui Wang, Jingao Liu, Lijuan Liu and Wenjing Wan for the ideas, helps and discussions on my thesis work.

This research was funded by a Natural Sciences and Engineering Research Council (NSERC) Discovery Grant to Dr. Robert A. Creaser.

Table of Contents

List of Tables

List of Figures

List of Symbols/Abbreviations

~ - Approximately

Ar - Argon

Abs - Absolute

As - Arsenic

Aspy - Arsenopyrite

BSE - Backscattered Scanning Electron

BD - Beaver Dam

Bt - Biotite

Blk - Blank

CL - Cathodoluminescence

Cal - Calcite

Cpy - Chalcopyrite

Cps - Counts Per Second

EDX - Energy-Dispersive X-Ray Spectroscopy

Fsp - Feldspar

Fig - Figure

Au - Gold

$Ba(OH)_2$ - Barium Hydroxide

$Ba(NO_3)_2$ - Barium Nitrate

cm - Centimetre

CrO_3 - Chromium Trioxide

ca. - Circa

cf. - Compare

d - diameter

ºC - Degree Celsius

g - Gram

Hz -Hertz

HBr - Hydrobromic Acid

HCl - Hydrochloric Acid

Hbl - Hornblende

HR - Host Rock

ICP-MS - Inductively Coupled Plasma Mass Spectrometer

Fe - Iron

J/cm^2 - Joule Per Centimeter Square

km - Kilometer

LA - Laser Ablation

Pb - Lead

MSWD - Mean square weighted deviation

m - Meter

Ma - Mega-annum

MC - Multi-Collector

MI - Methylene Iodide

μm - Micrometre

μL - Microlitre

mbar - Millibar

mg - Milligram

mL - Millilitre

MR - Moose River

Ms - Muscovite

N - Normality

N/A - Not Available

Ni - Nickel

HNO_3 - Nitric Acid

No. - Number

Or - Orthoclase

Os - Osmium

Os_i - $^{187}Os/^{188}Os$ Initial

O - Oxygen

ppm - Parts Per Million

ppb - Parts Per Billion

ppt - Parts Per Trillion

pg - Picogram

Pl -Plagioclase

Pt - Platinum

Py - Pyrite

Pyr - Pyrrhotite

Qtz - Quartz

Re - Rhenium

λ - Rhenium Decay Constant

S - Sulphur

SEM - Scanning Electron Microscope

NaOH - Sodium Hydroxide

σ - Standard Deviation

H_2SO_4 - Sulphuric Acid

t - Ton

TIMS - Thermal Ionization Mass Spectrometer

U - Uranium

wt - Weight

wt % - Weight Percent

W - Wolfram

Y - Yes

1.0 Introduction:

Numerous vein-hosted gold deposits and showings occur throughout the Meguma terrane, Nova Scotia, Canada. The Meguma terrane consists of a ca. 10 km thick succession of the Cambro-Ordovician metasandstone-dominated Goldenville Group and the overlying metasiltstone-dominated Halifax Group (Kontak et al., 2011). The sequence was deformed into northeast-trending, upright folds during the Acadian orogenic event at ca. 410-400 Ma (Keppie and Dallmeyer, 1987; Muecke et al., 1988; Kontak et al., 1998; Hicks et al., 1999), then intruded by peraluminous granitoids between 380-370 Ma (Reynolds et al., 1981; Keppie et al., 1993, 1999; Clarke and Halliday, 1980). The gold deposits, hosted by the metasandstone-dominated Goldenville Group, can be divided into three types: strata-bound vein associated, bedding-discordant vein related, and disseminated (Horne and Culshaw, 2001; Ryan and Smith, 1998). The mineralized veins are dominated by quartz-carbonate-sulfide assemblages and arsenopyrite is the predominant sulfide phase.

The formation of the gold deposits is controversial, and several ore deposit models have been proposed. Models can be grouped according to the auriferous vein emplacement time with respect to regional deformation. An early proposal was forwarded that auriferous veins formed pre-folding and the source of gold was within the Goldenville-Halifax Group (Hunt, 1968; McBride, 1978; Haynes and Smith, 1983; Henderson and Henderson, 1990). But the new findings of structure features and geochemical data have rejected these theories (Mawer, 1987; Morelli et al., 2005; Kontak and Horne, 2010). Others, however, prefer a synchronous (Mawer, 1987) to prolonged Acadian regional tectonic origin (Kontak et al., 1990a; Kontak et al., 1998). The syn-folding model is forwarded based on the vein structure features described by Mawer

(1987) and the isotope evidence showing a metamorphic origin (Kontak et al., 2010, 2011). The post-folding proposal is supported by $^{40}Ar/^{39}Ar$ vein-fill mica ages of 380 Ma to 362 Ma, suggesting that the metamorphic fluid, as the source of veins, was moved by post-folding magmatic heat (Kontak et al., 1990b, 1993, 1995, 1997). More recently, two Re-Os arsenopyrite ages of ca. 380 Ma and 408 Ma indicated that at least two gold mineralization events happened in the Meguma terrane, spanning 30-40 Ma, coinciding with the syn-Acadian regional deformation and late-Acadian granitoid emplacement respectively (Morelli et al., 2005).

Determining the absolute age of the gold mineralization is crucial in understanding the formation environment of the gold deposit. However, accurate and reliable formation ages for vein-hosted gold deposits are, in most cases, absent due to limitations of applying commonly used geochronometers such as U-Pb, Rb-Sr, Sm-Nd and $^{40}Ar/^{39}Ar$ systems (Selby et al., 2002; Creaser et al., 2002). Previous geochronology work in the Meguma terrane has focused on determining $^{40}Ar/^{39}Ar$ plateau ages of whole rock and vein-fill minerals: mica (most commonly used), amphibole, and K-feldspar (Muecke et al., 1988; Kontak et al., 1990, 1998; Hicks et al., 1999). However, due to the low closure temperature of Ar diffusion in mica, the dating results might only represent the thermal resetting or the prolonged cooling ages. Uranium and lead dating of vein-hosted zircon, monazite and titanite has been applied to date vein-hosted gold ores, but the unknown relationship between the minerals and the vein hosted gold might challenge the interpretation of the U-Pb ages (Lin and Corfu, 2002). Moreover, the rare appearance and complex origins of hydrothermal zircons and monazites hinder the widespread use of U-Pb age in vein systems. Rubidium-strontium dating of hydrothermal minerals is typically not applicable to vein-host gold systems due to the variability of fluid Sr isotopic composition, recrystallization of the Rb-rich vein minerals and the potential of partial resetting during younger hydrothermal

events. Collectively, various limitations hamper the routine use of these approaches and as such, the ^{187}Re-^{187}Os system is becoming more extensively used (Selby et al., 2002, 2003; Morelli et al., 2005, 2007).

Rhenium and osmium are inherently chalcophile in nature and therefore are often sufficiently enriched in sulfide minerals to allow for Re-Os geochronology. Sulfide Re-Os geochronology has been successfully used to determine the mineralization ages of molybdenite, pyrite, and arsenopyrite (Arne et al., 2001; Selby et al., 2001b, 2002; Morelli et al., 2005, 2007; Ootes et al., 2011; Hnatyshin et al., 2015). A considerable number of sediment-hosted orogenic gold deposits contain auriferous veins that are dominated by quartz, carbonates and Fe-As-S phases (e.g. arsenopyrite, pyrite and pyrrhotite). Arsenopyrite, which is often cogenetic with gold mineralization, offers a unique opportunity to determine precise gold mineralization ages by applying Re-Os geochronology (Kontak and Horne, 2010; Christie and Corner, 2000; Fleet et al., 1997; Ayora et al., 1992; Arne et al., 2001; Morelli et al., 2005, 2007). The Re and Os content of the asenopyrite are typically at ppb (parts per billion) and ppt (parts per trillion) level, respectively. At these concentrations, in-situ analysis is impossible based on the current technology. Therefore arsenopyrite crystal fractions are dissolved for the Re-Os chemistry and analyzed using the negative thermal ionization mass spectrometer (e.g., Morelli et al., 2005).

Two previous Re-Os ages of 380 Ma and 407 Ma from the Meguma terrane were determined from vein bearing arsenopyrite, from bedding-concordant veins and bedding-discordant veins, respectively (Morelli et al., 2005). For the third type of gold deposit—the disseminated gold deposit (Touquoy zone of the Moose River deposit), Morelli et al. (2005) failed to define a precise gold formation age by dating disseminated arsenopyrite. However, the availability of new drill holes at that deposit now makes it feasible to collect arsenopyrite

samples from quartz veins, which are used in this study to constrain the gold mineralization age of the Moose River deposit. In addition, more gold deposit Re-Os arsenopyrite ages are required to understand and verify the multi-stage gold mineralization model.

This study aims to precisely determine the formation age of two meta-sediment hosted gold deposits (vein-associated and disseminated type) in the Meguma terrane, namely the Beaver Dam deposit and the Moose River deposit, by using Re-Os arsenopyrite geochronology. These ages will be compared to the Ar-Ar ages of the whole rock and vein fill minerals from the same deposits (Kontak et al., 1990b, 1993) and the previous Re-Os arsenopyrite ages derived from three gold deposits in the Meguma terrane (Morelli et al., 2005). From the existing models, the granite intrusion at 380 Ma is considered to drive the mobilization of vein fluids. In order to comprehend the relationship between the auriferous veins and granite intrusions, the granite emplaced in contact with the Beaver Dam gold deposit is analyzed using U-Pb zircon dating, to compare the Re-Os arsenopyrite ages of the Beaver Dam deposit. According to the previous different Re-Os arsenopyrite ages, there were multiple hydrothermal events in the Meguma terrane (Morelli et al., 2005). The backscattered SEM images showing the crystal textures are used to examine the over-crystallization of the vein host arsenopyrite. In this study, the Re-Os arsenopyrite geochronology data is combined with regional structure, U-Pb zircon dating of local granites, and SEM mapping, to obtain a comprehensive understanding of gold ore forming stages in the Meguma terrane.

2.0 Geology Background:

2.1 Tectonic Background

The northeastern Appalachian orogenic belt is composed of several Neoproterozoic to early Paleozoic exotic crustal domains, one of which is the Meguma terrane. The domains separated from Gondwana during Cambrian to Ordovician time, opening the Rheic Ocean and closing the Iapetus Ocean. After this separation in the early Paleozoic, the domains moved to Laurentia during the Ordovician and Silurian, leading to the closure of the Rheic Ocean (Pollock et al., 2012). Then from Devonian to Carboniferous time, this assemblage converged with Gondwana, forming Pangaea (Murphy and Keppie, 2005; Pollock et al., 2012, Fig 2.3 A, B).

Based on the stratigraphy, paleontology, geochemistry and geochronology of the Meguma terrane, the original source of sediments in the Meguma terrane is believed to be the West Africa Craton (Schenk 1997; White and Barr 2010). The latest detrital zircon data supports the idea that the Meguma terrane was located in the rift system between Avalonia and West Africa in Cambrian time (Waldron et al., 2011, Fig 2.2). The U-Pb zircon ages of 460.0 ± 3.4 Ma (Dunn Point Formation) and 454.5 ± 0.7 Ma (McGillivray Brook Formation) from Avalonia (Murphy et al., 2012) implies that Avalonia probably accreted to Baltica in the Ordovician. The travel path of the Meguma terrane after rifting from Gondwana is undocumented, but U-Pb ages of 442 ± 4 Ma, $439\ ^{+4}_{-3}$ Ma, 438^{+3}_{-2} Ma of volcanic rocks (White Rock Formation) from the west Meguma Terrane imply that the Meguma terrane underwent some tectonic events when moving towards Laurentia in Early Silurian (Keppie and Krogh, 2000; MacDonald et al., 2002). The collision of the Meguma terrane and the Avalon terrane started during the Acadian orogeny in early

Devonian at 410-400 Ma followed by widespread post-tectonic magmatic intrusions at 380-370 Ma (Clarke and Halliday, 1980; Bradley, 1983; Keppie and Dallmeyer, 1987; Eberz et al., 1991; Murphy and Keppie, 1998; 2005).

2.2 Regional Geologic Setting

The Meguma terrane, outboard of the northern Appalachian orogen, was accreted to the Avalon Terrane along the Cobequid-Chedabucto Fault during Devonian time (Mawer and White, 1987). The exposed Meguma terrane, a 480 km long by 120 km wide (maximum) wedge, consists of Cambro-Ordovician turbidite successions (known as Meguma supergroup from old literature): a basal metasandstone-dominated Goldenville Group and the conformably overlying metasiltstone-dominated Halifax Group (Sangster and Smith, 2007, Fig 2.1). These sequences were deformed into upright, doubly plunging, northeast- southwest to east-west trending folds and regionally metamorphosed to greenschist and amphibolite facies during the Acadian orogeny at ca. 410-400 Ma (Keppie and Dallmeyer, 1987; Hicks et al., 1999; Kontak and Horne, 2010). An extensive suite of peraluminous granites intruded the package at ca. 380-370 Ma, truncating regional fold patterns and cleavages (Clarke and Halliday, 1980; Reynolds et al., 1981; 1987; Clarke et al., 1993; Keppie et al., 1993; 1999; Kontak et al., 1990b; 1993; 2004). The post-tectonic central granitoid plutons, such as the South Mountain Batholith, are predominantly unfoliated and are emplaced into low grade metamorphic country rocks. Some peripheral foliated granitoid bodies intruded with syn-plutonic mafic dykes (Clarke et al., 1997). In the northwestern Meguma terrane, the Lower Paleozoic metasedimentary rocks are overlain by a succession of Late Ordovician to Early Devonian sedimentary and volcanic rocks of the White Rock, Kentville,

New Canaan and Torbrook Formations, which were also deformed during the Acadian orogeny and covered by Mesozoic successions (Keppie and Dallmeyer, 1987, Fig 2.1, 2.5). A few U-Pb zircon ages 442 ± 4 Ma, 439 $^{+4}_{-3}$ Ma, 438 $^{+3}_{-2}$ Ma of volcanic rocks from the White Rock Formation indicate the magma intrusion event occurred at ca. 440 Ma (Keppie and Krogh, 2000; MacDonald et al., 2002; Pollock et al., 2012). A suite of ca. 360 Ma greisen-contacted granites (Clayton Hill pluton) occurs to the northwest corner of the South Mountain Batholith (Kontak et al., 2013). In the northern Meguma terrane, adjacent to the Cobequid-Chedabucto Fault, the meta-sedimentary successions are unconformably overlain by Carboniferous sedimentary rocks. The Liscomb Complex (see Fig 2.1, LC), consisting of post-Acadian (ca. 370 Ma, $^{40}Ar/^{39}Ar$ age, Rb-Sr age) granite and gabbro intrusions and associated coeval high grade gneiss, is emplaced in the northeast (Eberz et al., 1991; Clarke et al., 1993; Kontak and Reynolds, 1994).

2.3 Geology and Geochronology of Meguma Gold Deposits

There are over 300 gold occurrences and 60 gold deposits hosted by the Cambro-Ordovician metasedimentary rocks of the Meguma terrane, predominantly within the upper Goldenville Formation (Ryan and Smith, 1998). The total tonnage and grade of the gold deposits is unavailable. However the Goldenville district, the largest producer in the Meguma Terrane, has produced 6,535,730 g of gold (Sangster and Smith, 2007). About 808,600 g of gold was produced from the Touquoy Zone of the Moose River gold deposit in the past (Bierlein and Smith, 2003).

The gold deposits can be divided into two main categories: dominant high-grade vein-hosted gold and locally low-grade disseminated gold deposits. Gold occurs in both concordant and discordant auriferous quartz veins, typically at anticlinal fold hinges or the steeper limb of

folds (Kontak et al., 1990b; Ryan and Smith, 1998; Horne and Culshaw, 2001). Disseminated gold deposits are present in specific districts, including the Moose River deposit (Touquoy zone) hosted by slate, and the North Brookfield district hosted by meta-sandstone for instance (Sangster and Smith, 2007). The concordant or stratabound quartz veins, the most important gold producer, consist of bedding-parallel, saddle-reef, buckled and en-echelon vein types (Fig 2.6). On the other hand, the discordant veins include angular and crosscutting types (Kontak and Horne, 2010; Kontak et al., 2011). Veins, centimeters to meters thick and meters to hundreds of metres in strike length, are emplaced at brittle-ductile shear zones, and all vein types contain visible gold (Kontak, 1990; Ryan and Smith, 1998; Horne and Culshaw, 2001; Kontak and Horne, 2010). The gold mineralization occurs primarily as fine films along vein-wall rock contacts, at the intersections of discordant and concordant veins or as coarse grains within quartz veins (Ryan and Smith, 1998; Sangster and Smith, 2007). The dominated mineral assemblage of auriferous veins is quartz, carbonates, and Fe-As-S minerals. Less commonly Bi–Te–Ag–Hg phases, other sulfides (galena, sphalerite, molybdenite) and silicates are present (k-feldspar, plagioclase, muscovite, biotite, amphibole, tourmaline, garnet, and epidote) (Kontak and Smith 1993; Kontak et al., 2011). Vein forming conditions are constrained to be 350–500°C and 2–3 kbars based on the mineralogy, fluid inclusions, and stable isotope studies (Graves and Zentilli, 1982; Kontak et al., 1993; 2011). Arsenopyrite is the most abundant sulfide associated with gold mineralization, and is present in all gold districts. Arsenopyrite is found both in wall rocks and veins, closely related to the gold distribution, together with minor galena, pyrrhotite, pyrite and chalcopyrite. Visible gold usually contacts arsenopyrite grains, occurring as coatings on grain boundaries or infillings in cracks (Graves and Zentilli, 1982; Sangster and Smith, 2007; Morelli et al., 2005, Fig 2.8). Wall rock alteration consists of carbonitization, sulfidization, silicification and sericitization (Ryan and Smith, 1998; Bierlein and Smith, 2003).

In addition to lode gold, the Touquoy zone of the Moose River gold district is dominated by disseminated gold at grades of 2 g/t, and has historically produced 8 Mt Au (Malcolm, 1929; Bierlein and Smith, 2003; Sangster and Smith, 2007). The ore zone occurs in altered meta-siltstone beds in the hinge zone of a regional anticline where present one centimeter- to a few centimeter- thick quartz veins. The gold is found disseminated in the meta-siltstone and also from narrow quartz veins, associated with secondary Fe carbonate and sulfide minerals (dominant arsenopyrite) (Bierlein and Smith, 2003; Morelli et al., 2005; Kontak et al., 2010).

Several gold deposit genetic models have been proposed, based on the time of the vein emplacement with respect to the regional deformation. An early theory was put forward as a syn-genetic origin for quartz veins within meta-sedimentary rocks (Hunt 1868; McBride, 1978), supported by publications suggesting that the veins were pre- to syn- folding origin, with the gold pre-concentrated within the enclosing host rocks and mobilized later by regional metamorphic fluids to form the gold (Graves and Zentilli, 1982, 1988; Henderson and Henderson, 1986; Sangster, 1990, 1992). Another syn-genetic water sill hypothesis was proposed that auriferous veins formed during compaction-related dewatering rather than tectonic shortening-related (Henderson and Henderson, 1990). However, some structure features argued against the syn-sedimentary origin for the veins (Mawer, 1987). Moreover, the isotopic data of fluid inclusions disagreed the host rock as the gold reservoir, indicating that the source reservoir of fluids was not Goldenville or Halifax Group (host rock), with some contamination from the sedimentary host rock as a result of fluid-rock interaction (Morelli et al., 2005; Kontak and Horne, 2010). The syn-tectonic model was firstly proposed based on the early field observations (Faribault 1899), modernly supported by the metamorphic features from vein inclusions and the observations that the veins cut the cleavage and are confined to the hinge of regional folds (Keppie, 1976; Mawer,

1987). A late-folding theory that the origin of the veins was related to post-tectonic magmatism was advocated by Newhouse (1936) and was supported by $^{40}Ar/^{39}Ar$ vein-fill mica ages of 367 Ma to 382 Ma from several deposits (Kontak et al., 1990). However, from vein fluid oxygen and salinity analyses, a metamorphic source was suggested (Kontak et al., 2011). Therefore a proposal was forwarded that vein materials were derived from lower crust or mantle, mobilized by syn-folding deep crustal metamorphic fluids driven by post-folding magmatic heat (Kontak et al., 1990; 1993; 1998). More recently, Morelli et al. (2005) published the absolute Re-Os arsenopyrite ages of two deposits: 380 ± 3 Ma for saddle-reef concordant veins from the Dufferin deposit, similar to the $^{40}Ar/^{39}Ar$ vein mineral dating and granite intrusion ages, and 407 ± 4 Ma for a discordant vein from the Ovens deposit, the same as the regional metamorphic age, arguing that there are at least two stages of gold mineralization over the time span of 30 Ma (Kontak et al., 1990; Keppie and Dallmeyer, 1995; Morelli et al., 2005). Based on geochronology study, combining with fluid inclusion geochemical analyses, Kontak and Horne (2010) proposed a two-stage orogenic and intrusion-related gold mineralization model.

2.4 Geology and Sampling of the Beaver Dam and the Moose River Gold Deposits

Arsenopyrite samples were collected from quartz veins in drill cores from the Beaver Dam deposit (Drill Core BD 09-141, Sample LC-12-15/16/17) and the Moose River deposit (Drill Core MR 05-110, Sample LC-12-01/02). Host rock samples were sampled from the Beaver Dam deposit (Drill Core BD 09-140, Sample LC-12-10/11/12/13/14).

2.4.1 Geology and Sampling from the Beaver Dam Deposit

The Beaver Dam deposit is located in the eastern part of the Meguma terrane, occurring within a package of turbidite sediment sequences (Goldenville Formation) at the southern limb of a major northeast-trending anticline, which is cut by the Mud Lake fault system (Fig 2.1). The deposit is hosted by psammitic and pelitic rocks metamorphosed to greenschist facies. Some high-grade metamorphic mineral assemblages in the deposit area appear to be spatially related to the closest River Lake granite intrusion, which is approximately 1 km is to the west of the deposit (Kontak et al., 1993, 1995, Fig 2.1, 2.4; Horne and Pelley, 2007). Bedding-parallel veins are the most common vein type in the Beaver Dam deposit with various thickness from 0.5 cm to 3 m (some with the characteristic crack-seal or ribbon texture), but the discordant quartz veins also occur. Major minerals in the veins are quartz (>90%), sulfide (mainly arsenopyrite), laminated carbonates and silicates (Kontak and Smith, 1993). Ages of vein-fill minerals (Hbl, Ms, Bt) (367-374 Ma) and whole rock (382 Ma) were provided by $^{40}Ar/^{39}Ar$ dating (Kontak et al., 1990, Table 5.1).

The arsenopyrite sample LC-12-15 was collected from Drill Core BD 09-141 (0521319E, 4990700 N, UTM NAD83, Zone 20) from the Beaver Dam deposit at the depth of 57.0 m (Table 2.1). A narrow quartz vein, parallel to the meta-sandstone bed, was occupied by arsenopyrite crystals with diameters of 1-3 cm (Fig 2.7 C, D). From thin section observation, the host rock and quartz vein displayed metamorphic features such as alignment of minerals and metamorphic mica (Fig 2.11 A, C). Thin pyrrhotite and calcite rims occurred on the exterior of arsenopyrite in the quartz vein (Fig 2.11 A, B, F). Biotite was also observed in quartz veins (Fig 2.11 A). Inside the arsenopyrite crystal, inclusions were concentrated in the core of the arsenopyrite crystal (Fig 2.11 D, E) and gold grains were observed (Fig 2.15 A).

The Beaver Dam coarse arsenopyrite sample LC-12-16 (d = 5 cm) was sampled at the depth of 64.6 m from the same drill core as LC-12-15 (Table 2.1, Fig 2.7 E). The arsenopyrite was present in a very thin calcite vein, close to the black mudstone host rock (Fig 2.12 A, B). Within the calcite vein there were dominantly (90%) large arsenopyrite crystals, associated with tiny pyrrhotite and pyrite grains (Fig 2.12 D). Pyrrhotite inclusions appeared along the cracks in the arsenopyrite crystal (Fig 2.12 D, Fig 2.15 C) and several gold grains were found in the arsenopyrite (Fig 2.15 B, C).

Sample LC-12-17 (d = 3 cm) was collected from the same drill core as the above two samples, at the depth of 66.0 m. The arsenopyrite was collected from a bedding-concordant quartz vein in the black shale host rock (Table 2.1, Fig 2.7 F), surrounded by a thin calcite rim (Fig 2.13 A, B). Pyrrhotite inclusions were found in the arsenopyrite crystal (Fig 2.13 D). A small amount of pyrrhotite and chalcopyrite also occur within the quartz vein.

Host rock samples LC-12-10/11/12/13/14 were collected from vein-poor areas with low Au concentration in the Beaver Dam deposit, in order to investigate the black shale Re-Os system and constrain any possible relationships with the quartz veins or sulfides (Table 2.2). All five samples were dark colored meta-sedimentary rocks, sampled from Drill Dore BD 09-140 (0521319E, 4990700 N, UTM NAD83, Zone 20), varying from 37.5 m to 100 m deep (Fig 2.8 A, B) (samples LC-12-10/11/12/14 were black shales, sample LC-12-13 was a dark sandstone-siltstone).

2.4.2 Geology and Sampling from the Moose River Deposit

The Moose River gold district is located ~80 km northeast of Halifax, at the junctions of the Fifteen Mile Stream and the Beaver Dam anticlines (Fig 2.1; Malcolm, 1929; Kontak et al.,

1990b; Bierlein and Smith, 2003). In the northeast Moose River gold district, the Touquoy Zone deposit occurs (also known as the Moose River deposit in this thesis), which is proximal to the historically mined Higgins and Lawler deposits (Malcolm, 1929; Morelli et al., 2005). The Touquoy Zone is dominated by carbonate rich argillites, inter-bedded meta-mudstone, meta-siltstone and greywacke, with few quartz veins but more disseminated gold and sulfides comparing to other gold deposits in the Meguma terrane (Ryan and Smith., 1998). The gold occurs in both meta-sedimentary host rocks and narrow quartz veins. Arsenopyrite and pyrite are the most abundant sulfide phases, and arsenopyrite is usually closely associated with gold mineralization (Bierlein and Smith, 2003). The $^{40}Ar/^{39}Ar$ whole rock and vein mica cooling ages (370 Ma to 384 Ma) were determined by Kontak (1990, 1993). Re-Os dating of disseminated arsenopyrite from Touquoy was attempted by Morelli et al. (2005) but failed to obtain a successful isochron age (457 Ma ± 110 Ma, MSWD = 27), considered to be owing to the host-rock Re/Os influence or the multiple origins of the arsenopyrite. Recently, the availability of new drill cores at the Moose River deposit makes it feasible to collect arsenopyrite samples from quartz veins, instead of disseminated from within host-rocks.

For this study, the arsenopyrite sample LC-12-01 was collected from a narrow quartz vein in the Drill Core MR 05-110 (44º58′57.5″ N, 62º56′39.9″ W) from the Moose River deposit at depth of 14.9-15.0 m (Table 2.1). In the fissile shale host-rock, the buckled thin quartz vein, around 1-2 cm wide, was filled by small arsenopyrite crystals (d = 0.3-0.5 cm, Fig 2.7 A). From petrographic observations, the only opaque mineral in the quartz vein was arsenopyrite (Fig 2.9 A, C, D). In the arsenopyrite crystal, inclusions were concentrated in the core (Fig 2.9 B). Tiny gold grains and sphalerite inclusions occurred in the arsenopyrite crystal (Fig 2.15 D).

The arsenopyrite sample LC-12-02 was collected from the same drill core with sample LC-12-01, at depth of 30.1 m (Table 2.1). Quartz veins were emplaced in the fissile shale host rock. Within the quartz vein, arsenopyrite (d = 1 cm) occupied 60% of the vein, associated with some pyrite, small chalcopyrite and calcite (Fig 2.7 B; Fig 2.10 A, C, D, F). The pyrite rim grew out of the arsenopyrite (Fig 2.10 B) and sphalerite inclusions were found in the arsenopyrite crystal (Fig 2.10 E).

Table 2.1 Location and description of arsenopyrite samples used for Re-Os analysis

Sample Name	Deposit Name	Drill Core	Location	Depth	Specimen Description (arsenopyrite size, associated minerals observed from thin sections, host rock)
LC-12-01	Touquoy (Moose River)	MR 05-110	44º58′57.5″ N, 62º56′39.9″ W	14.9-15.0m	0.3-0.5 cm, Aspy in clean Qtz vein, HR: black shale (sandy, fissile)
LC-12-02	Touquoy (Moose River)	MR 05-110		30.1m	1.0 cm, little Py at the rim of Aspy, tiny cpy, HR: mudstone (thin layer)
LC-12-15	Beaver Dam	BD 09-141	0521319E, 4990700 N, UTM NAD83, Zone 20	57.0m	1-3 cm, little Pyr and Cal at the Aspy rim, HR: "Millet Seeds" sandstone
LC-12-16	Beaver Dam	BD 09-141		64.6m	3-5 cm (huge crystal), tiny Pyr, HR: black shale
LC-12-17	Beaver Dam	BD 09-141		66.0m	3 cm, calcite rim out of Aspy crystal, tiny Pyr, Cpy, HR: black mudstone

Table 2.2 Location and description of host rock samples used for Re-Os analysis

Sample Name	Sample Category	Deposit Name	Location	Drill Core	Depth	Description
LC-12-10	Host Rock	Beaver Dam	0521319E, 4990700 N, UTM NAD83, Zone 20	BD 09-140	100.0m	"Austen" unit, black shale, Au assay <0.025g/t
LC-12-11	Host Rock	Beaver Dam		BD 09-140	73.5m	"Papke" unit, black shale, Au assay <0.025g/t
LC-12-12	Host Rock	Beaver Dam		BD 09-141	37.5m	"Papke" unit, black shale, Au assay <0.05g/t
LC-12-13	Host Rock	Beaver Dam		BD 09-141	50.0m	"Millet seeds" unit, sandstone, Au assay <0.05g/t
LC-12-14	Host Rock	Beaver Dam		BD 09-141	93.1m	"Austen" unit, black shale, Au assay <0.05g/t

2.5 Sampling of Granite from the River Lake Pluton

Two granite samples LC-12-05 and LC-12-06 were collected from outcrops of the River Lake intrusion (45°00.764′N, 62°44.567′W; 45°00.703′N, 62°44.343′W, Fig 2.4; Table 2.3), ~1 km west of the Beaver Dam deposit, to determine the U-Pb zircon age, in order to compare with the mica $^{40}Ar/^{39}Ar$ River Lake pluton age (371-378 Ma, Kontak et al., 1990b) and the gold mineralization age.

Sample LC-12-05 is a white color granite, with the mineral composition of: quartz (25%), plagioclase (30%), orthoclase (32%), biotite (5%) and muscovite (8%) (Fig 2.14 A, B).

Sample LC-12-06 is a relatively biotite-rich granite (Fig 2.8 C), consisting of: quartz (30%), plagioclase (23%), orthoclase (30%), biotite (10%) and muscovite (7%) (Fig 2.14 C, D).

Table 2.3 Location and description of granite samples used for U-Pb analysis

Sample Name	Sample Category	Pluton Name	Location	Description
LC-12-05	Granite	River Lake Intrusion	45°00.764′N,62°44.567′W,103m	Coarse crystal, equigranular, Qtz, Fsp, Bt, Ms, pale color
LC-12-06	Granite	River Lake Intrusion	45°00.703′N,62°44.343′W,113m	Coarse crystals, equigranular Qtz, Fsp, Bt, Ms, more dark minerals

3.0 Methods:

3.1 Sample Preparation

All sulfide minerals (arsenopyrite) from quartz veins and zircons from granites were selected, prepared and analyzed at the University of Alberta.

Thin sections were made in the Rock Crushing and Mineral Separation Laboratory at the University of Alberta.

For Re-Os sulfide analysis, coarse-grained (d>1 cm) arsenopyrite crystals from the quartz veins were cut into subdivisions with a fine saw and were polished using a diamond mill (each subdivision is a separate sample). To obtain the pure arsenopyrite samples, individual crystal subdivisions (probably with quartz) were crushed in an agate mortar by hand into smaller size (1-3 mm) and a final hand picking under a binocular microscope was performed. The hand-picked arsenopyrite was leached by 2N HCl overnight and dried, to removal calcite and other minerals (e.g. pyrrhotite, galena if present). Small arsenopyrite crystals (d<1 cm) were cut with quartz veins and wall rocks into subdivisions as well (each subdivision is a separate sample). But because the arsenopyrite was too small to be separated by handpicking, mineral separation procedures were performed to get pure arsenopyrite. The samples were crushed to approximately 100 μm size and were sieved to obtain the desired-size fractions between 70-mesh and 200-mesh (~100 μm). Then magnetic Frantz Isodynamic separation and heavy liquid separation (MI) were performed to separate the unwanted sulfide, quartz and wall rocks from arsenopyrite (Table 3.1).

For Re-Os wall rock (black shale) analysis, the whole rock samples (collected far away from the arsenopyrite in drill cores) were cut by thin saw, polished and crushed into fine powder (~30 μm) in the Rock Crushing and Mineral Separation Laboratory at the University of Alberta.

Zircons for U-Pb analysis were separated and selected from two granite samples. The samples were firstly crushed and milled by pre-cleaned Jaw Crusher and Disk Mill. After the Wilfley table separation, Frantz magnetic separation and heavy liquid separation (MI), about 100-200 zircons for each sample were hand selected under a binocular microscope, mounted in the epoxy mounts and polished. Cathodoluminescence images were taken before LA-ICP-MS in-situ analysis. All procedures were completed at the University of Alberta.

Table 3.1 Sample divisions preparation before analysis

Moose River: LC-12-01				
Sample Name	Hand Picking under microscope	Leaching with HCl	Frantz	Heavy liquid
LC-12-01-A1	Hand picked, pure crystal	N/A	N/A	N/A
LC-12-01-A2	Hand picked, pure crystal	N/A	N/A	N/A
LC-12-01-C	Hand picked, pure crystal	N/A	N/A	N/A
LC-12-01-B1	Hand picked, pure crystal	leached with 2 N HCl	N/A	N/A
LC-12-01-B2	Hand picked, pure crystal	leached with 2 N HCl	N/A	N/A
LC-12-01-B3	Hand picked, pure crystal	leached with 2 N HCl	N/A	N/A
LC-12-01-B4	Hand picked, pure crystal	leached with 2 N HCl	N/A	N/A
LC-12-01-B5	Hand picked, pure crystal	leached with 2 N HCl	N/A	N/A
LC-12-01-B6	Hand picked, pure crystal	leached with 2 N HCl	N/A	N/A
LC-12-01-B7	Hand picked, pure crystal	leached with 2 N HCl	N/A	N/A

Moose River: LC-12-02				
Sample Name	Hand Picking under microscope	Leaching with HCl	Frantz	Heavy liquid
LC-12-02-2	N/A	N/A	Y	N/A
LC-12-02-04’	N/A	N/A	Y	Y
LC-12-02-5’	N/A	N/A	Y	Y
LC-12-02-06’	N/A	N/A	Y	Y
LC-12-02-09	N/A	N/A	Y	Y
LC-12-02-A	Hand picked, pure crystal	N/A	N/A	N/A
LC-12-02-B	Hand picked, pure crystal	N/A	N/A	N/A
LC-12-02-C	Hand picked, pure crystal	N/A	N/A	N/A
LC-12-02-1	Hand picked, pure crystal	N/A	N/A	N/A

LC-12-02-08’	N/A	N/A	Y	Y
LC-12-02-leached	Hand picked, pure crystal	leached with 2N HCl	N/A	N/A

Beaver Dam: LC-12-15				
Sample Name	Hand Picking under microscope	Leaching with HCl	Frantz	Heavy liquid
LC-12-15-A1	Hand picked, pure crystal	leached with 2N HCl	N/A	N/A
LC-12-15-A2	Hand picked, pure crystal	leached with 2N HCl	N/A	N/A
LC-12-15-B1	Hand picked, pure crystal	leached with 2N HCl	N/A	N/A
LC-12-15-B2	Hand picked, pure crystal	N/A	N/A	N/A
LC-12-15-B3	Hand picked, pure crystal	N/A	N/A	N/A
LC-12-15-B2'	Hand picked, pure crystal	leached with 2N HCl	N/A	N/A
LC-12-15-B3'	Hand picked, pure crystal	leached with 2N HCl	N/A	N/A
LC-12-15-B4'	Hand picked, pure crystal	leached with 2N HCl	N/A	N/A

Beaver Dam: LC-12-16				
Sample Name	Hand Picking under microscope	Leaching with HCl	Frantz	Heavy liquid
LC-12-16-01'	Hand picked, pure crystal	N/A	N/A	N/A
LC-12-16-02'	Hand picked, pure crystal	N/A	N/A	N/A
LC-12-16-03	Hand picked, pure crystal	N/A	N/A	N/A
LC-12-16-04	Hand picked, pure crystal	N/A	N/A	N/A
LC-12-16-05	Hand picked, pure crystal	N/A	N/A	N/A
LC-12-16-06'	Hand picked, pure crystal	N/A	N/A	N/A
LC-12-16-07	Hand picked, pure crystal	N/A	N/A	N/A
LC-12-16-08	Hand picked, pure crystal	N/A	N/A	N/A
LC-12-16-A1	Hand picked, pure crystal	leached with 0.2 N HCl	N/A	N/A
LC-12-16-B1	Hand picked, pure crystal	leached with 0.2 N HCl	N/A	N/A
LC-12-16-A2	Hand picked, pure crystal	leached with 2 N HCl	N/A	N/A
LC-12-16-B2'	Hand picked, pure crystal	leached with 2 N HCl	N/A	N/A

Beaver Dam: LC-12-17				
Sample Name	Hand Picking under microscope	Leaching with HCl	Frantz	Heavy liquid
LC-12-17-A	Hand picked, pure crystal	leached with 2 N HCl	N/A	N/A
LC-12-17-B	Hand picked, pure crystal	leached with 2 N HCl	N/A	N/A
LC-12-17-A3	Hand picked, pure crystal	N/A	N/A	N/A
LC-12-17-C2	Hand picked, pure crystal	N/A	N/A	N/A
LC-12-17-C3	Hand picked, pure crystal	N/A	N/A	N/A
LC-12-17-A3'	Hand picked, pure crystal	leached with 2 N HCl	N/A	N/A

3.2 Re-Os Analytical Procedure

3.2.1 Sulfide Re-Os Chemistry

Approximately 200 - 400 mg of arsenopyrite was weighed and transferred to a Carius tube with a known amount of ^{185}Re + ^{190}Os spike. A combination of 2 mL of 10N HCl and 6 mL of 16N HNO_3, which produced inverse aqua regia, was added to the carius tube to dissolve the sample, and was frozen immediately using dry ice/ethanol. The tube was sealed by a glassblowing torch and then was heated to 220 ºC for at least 24 hours to equilibrate the Re and Os from the sample and the spike. After equilibration the sample was cooled down to room temperature and subsequently frozen using dry ice/ethanol to prevent the loss of Os. Chloroform was then added to the frozen solution in three aliquots of 3.5 mL, in order to separate the Re from the Os. The Os was extracted into the chloroform layer, but the Re remained dissolved in the inverse aqua regia layer.

The chloroform portion containing Os was transferred to a pre-cleaned 22 mL glass vial with 3 mL of 9N HBr, tightly capped and rotated overnight, to back-extract the Os from chloroform to the HBr. The HBr solution was removed to a Teflon taped watch glass and dried down on the cap of a Savillex concial 3 mL vial for the next procedure: micro distillation. To purify the Os, a 7N H_2SO_4 solution containing 0.08 g/mL of CrO_3 was added to the dried HBr spot and was incubated at ~70 ºC in a sealed Savillex concial 3 mL vial ("Tri-Star"), in which the Os was distilled into 20 µL of 9N HBr held by surface tension in the vial tip (Birck et al., 1997). The micro distillation was repeated once more to guarantee the purity of Os. (Shirey and Walker, 1995; Selby and Creaser, 2001a, b; Creaser et al., 2002; Hnatyshin, Unpublished master thesis, 2012)

The Re-bearing inverse aqua regia was dried in the clean 22 mL glass vial at 80 ^{o}C and purified by the following anion exchange chromatography procedure:

1). The dried sample was dissolved in 3 mL of 0.2N HNO_3 and loaded into prepared anion columns.

2). To remove impurities, the columns went through two washes of 0.5 mL 0.2N HNO_3, two washes of 1.0 mL 0.2N HNO_3, two washes of 1.0 mL 0.2N HCl, and one wash of 2.0 mL 6.0N HNO_3.

3). Collected the Re solution into a clean polymethylpentene beaker by washing the columns with 4.0 mL of 6.0N HNO_3.

After drying down the Re solution, it was further purified by single bead anion extraction. The dried Re fraction was re-dissolved using 200 μL of 0.05N HNO_3 and transferred to a 1mL centrifuge tube containing a single DOWEX AGI-X8 < 20 mesh anion bead, which absorbed Re. The centrifuge tube was rotated for at least 6 hours. The anion bead was then washed and moved to a 1 mL centrifuge tube containing 1 mL of 6N HNO_3, which could strip the Re from the anion bead over a period of 6 hours. Once stripped, the 6N HNO_3 solution was dried in a clean beaker, and sent to the mass spectrometry lab for analysis. (Selby and Creaser, 2003; Hnatyshin, Unpublished master thesis, 2012)

3.2.2 Host Rock Re-Os Chemistry (Black Shale)

One gram of black shale power was weighed and added to the Carius tubes with a calculated amount of ^{185}Re + ^{190}Os spike. The chemistry procedures were performed the same as the procedures for arsenopyrite samples described above, except that the sealed Carius tube needed to be incubated at 220 ºC at least 48 hours to dissolve the sample (Selby and Creaser, 2003; Kendall et al., 2004).

3.2.3 Mass Spectrometry

Isotopic compositions of Re and Os were determined using the negative thermal ionization mass spectrometry (NTIMS; Creaser et al., 1991). The distilled Os sample was loaded onto a Pt filament and activated by a saturated solution of $Ba(OH)_2$ in 1N NaOH. The OsO_3^- signal was obtained by a single collector peak-hopping using an ETP electron multiplier in pulse-counting mode. The dried pure Re fraction was loaded onto a Ni filament and activated using a saturated $Ba(NO_3)_2$ water solution. The ReO_4^- beam was collected by Faraday cup detectors in static mode. Approximately 100 measurements were performed for each isotope, to guarantee good counting statistics.

3.2.4 Data Correction

Procedure blanks using the normal purged TMG nitric acid was higher than the double purged nitric acid, with an average Re content of 0.89 ± 0.39 pg (1σ; n=4), a mean Os content of 0.19 ± 0.13 pg (1σ; n=4) and an average ^{187}Os / ^{188}Os value of 0.27 ± 0.10. The biggest blank contribution was to the ^{188}Os isotope and could reach up to 20% of an analysis. However, the Os blanks decreased significantly by using the double purged nitric acid, with a mean Os content of 0.03 ± 0.01 pg (1σ; n=4) and a mean ^{187}Os / ^{188}Os ratio of 0.33 ± 0.16, and the Os blank was just responsible for less than 5% of ^{188}Os. All blanks values were used to correct the raw data. The abundances of ^{185}Re and ^{190}Os in the mixed spike were calibrated using Re and Os standard solutions (Creaser et al., 2002), and the spike unmixing regressions were calculated during the data processing (Further details see Morelli et al., 2005, 2010). Re and Os standards were used to monitor the reproducibility of Re and Os analyses. For Re, 130 analyses over 6 years yielded an average 185/187 ratio of 0.59839 ± 0.00068, close to the value determined by Gramlich et al.

(1973) of 0.59738 ± 0.00039. For Os, the in-house AB2 standard yielded an average 187/188 ratio of 0.10684 ± 0.00006. All isochron ages were calculated by Isoplot (Ludwig, 1980, 2012) and reported with 2 sigma uncertainties.

3.3 SEM and Major Element Analysis

The backscattered SEM images and major element (As, S, Fe, reported as mass percentage) analyses were conducted by the Zeiss EVO MA 15 equipped with a Bruker Silicon Drift Detector in the Scanning Electron Microscope Lab at the University of Alberta. Thin sections were coated with carbon using Leica EM SCD005 evaporative carbon coater before analyses. To observe the overgrowth zoning of arsenopyrite crystals, the contrast was lowered during analyses. The error of the element concentration was given to 1wt% (1σ).

3.4 U-Pb In-situ LA-ICP-MS Dating

In-situ U-Pb isotopic analyses of zircons were conducted by a Nu-Plasma multi-collector inductively coupled plasma-mass spectrometer coupled to a New Wave Research UP-213 nm laser ablation system (LA-MC-ICP-MS) located at the Radiogenic Isotope Facility at the University of Alberta. Analyses were performed using a 30 μm spot-size, with a repetition rate of 4 Hz and energy densities of 2-3 J/cm^2. The well-calibrated international zircon standard GJ-1-32 was used as the external standard, along with the homogeneous zircon LH94-15 as the internal standard, to normalize the U/Pb values and verify the $^{207}Pb/^{206}Pb$ values (Simonetti et al., 2005, 2006). Analytical protocols were described in detail by Simonetti et al. (2005). The U decay

constants $^{238}U/^{235}U$ ratio of 137.88 was used for calculation (Ludwig, 2012). Concordia ages were calculated using Isoplot/Ex (Ludwig, 2012)

4.0 Results:

4.1 Re-Os Results

In total, 57 Re-Os isotopic analyses have been completed; 26 from 3 separate arsenopyrite samples (LC-12-15/16/17) from the Beaver Dam deposit, 21 from 2 separate arsenopyrite samples (LC-12-01/02) from the Moose River deposit, and 10 from 5 host rock samples (LC-12-10/11/12/13/14) from the Beaver Dam deposit. Isochron diagrams were constructed by plotting $^{187}Re/^{188}Os$ vs. $^{187}Os/^{188}Os$ using Isoplot 3.75 (Ludwig, 2012), with uncertainties given to 2σ. The Re-Os analytical results are reported in Table 4.1 and 4.2.

4.1.1 Re-Os Result of the Beaver Dam Deposit

Sample LC-12-15 has Re content variation from ~1 ppb to ~8 ppb and Os from ~10 ppt to ~39 ppt (radiogenic ^{187}Os: ~4-33 ppt). Therefore the $^{187}Re/^{188}Os$ ratios indicate a large range from ~800 to ~8300 (Table 4.1), and Os is intermediately to highly radiogenic. An eight-point Model 3 regression corresponds to an age of 434 ± 18 Ma (MSWD = 18, Fig 4.1) with high uncertainty for the initial $^{187}Os/^{188}Os$ ratio of 1.5 ± 1.6. However, the 8 points appear to fall into two linear groups; three of the eight analyses (15-A1, 15-A2, 15-B1) appear to be close to one regression line, and the alternate 5 points trend another regression line. When plotting the eight sample divisions separately as these two groups, they yield two Model 1 isochron ages. Three data produce the isochron age of 456.0 ± 2.8 Ma (MSWD = 0.90, Fig 4.2A) and initial $^{187}Os/^{188}Os$ ratio of 0.796 ± 0.064, and the other five analyses provide another isochron age of 446 ± 13 Ma (MSWD = 0.66, Fig 4.2B) with an imprecise initial $^{187}Os/^{188}Os$ ratio of = -0.1 ± 1.2.

The two data groups and ages will be discussed in detail in Discussion chapter together with SEM results (Fig 4.11 E, Fig 4.13; Table 4.8).

The Re concentrations of the arsenopyrite sample LC-12-16 range from ~2 ppb to ~5 ppb, and Os concentrations vary from ~15 ppt to ~35 ppt (radiogenic ^{187}Os: ~11-21 ppt, Table 4.1). The range of ^{187}Re/^{188}Os ratios from ~1500 to ~5700 allows the calculation of precise isochron age. Regression of the Re-Os data (n = 12) yields a Model 1 isochron age of 461.3 ± 2.9 Ma (MSWD = 1.3, Fig 4.3) with initial ^{187}Os/^{188}Os ratio of 0.24 ± 0.12.

For sample LC-12-17, due to the low Re and Os content (Re: ~0.1-0.5 ppb, Os: ~4-7 ppt, ^{187}Os: ~1-3 ppt, Table 4.1) and small ^{187}Re/^{188}Os variation (~200-1000), the 6-point regression yields a Model 3 isochron age with relatively larger uncertainties: 464 ± 26 Ma (MSWD = 6.4, Fig 4.4) and an initial ^{187}Os/^{188}Os ratio of 0.51 ± 0.28.

4.1.2 Re-Os Results of the Moose River Deposit

Ten arsenopyrite samples of LC-12-01 are analyzed and yield relatively scattered data on a Re-Os isochron diagram. The 10 points are distributed around a regression line having an age of 408 ± 25 Ma, with high MSWD of 32 (Fig 4.5). Because the percentage of radiogenic ^{187}Os in the 10 sulfide analyses is extremely high (mostly >97%, only one sample below 95%, Table 4.2), precise single analysis model ages can be calculated, by assuming an initial ^{187}Os/^{188}Os ratio of 0.5. The reason why the ^{187}Os/^{188}Os initial value of 0.5 is used will be discussed in the Discussion chapter. Model ages of the 10 analyses vary from ~400 Ma to ~440 Ma (Table 4.2, Fig 4.6).

Similar to sample LC-12-01, 11 analyses of sample LC-12-02 from a different vein of the same deposit scatter around a regression line. The analyses exhibit varied Re (~3-6 ppb) and Os

(~22-35 ppt) concentrations and highly radiogenic ^{187}Os compositions (mostly over 98%, Table 4.2). When plotting the 11 points on an isochron diagram, they clearly represent two trends (Fig 4.7A). Eight of the analyses are close to a regression line defining a Model 3 isochron age of 437.6 ± 8.2 Ma (MSWD = 6.4, 2σ, Fig 4.7B), and the other three fall on a regression line yielding a Model 1 isochron age of 380.3 ± 4.0 Ma (MSWD = 1.15, 2σ, Fig 4.7C). These data suggest that the arsenopyrite samples from the Moose River deposit are not isotopically or geochronologically homogeneous. These ages are discussed in detail below.

4.1.3 Re-Os Results of the Host Rock Samples

Nine analyses from the five host rocks show extremely low Re concentration and low radiogenic ^{187}Os content (Table 4.3). With such low ^{187}Re and ^{187}Os concentration, the Re-Os isochron age is highly imprecise at 520 ± 330 Ma with MSWD of 67. From the regression line, the initial $^{187}Os/^{188}Os$ ratio of host rocks is 0.653 ± 0.099 (Fig 4.8). Comparing the host-rock Re-Os characteristics to the above arsenopyrite Re-Os results, the low Re/Os ratio and Re and Os abundances from host rocks contrast strongly to the sulfide Re-Os system. Details will be discussed in the next chapter.

Table 4.1 Re-Os isotope data of arsenopyrite from the Beaver Dam deposit

Sample No.	Sample wt (g)	Total Re (ppb)	± 2σ	Total Os (ppt)	± 2σ	187Re/188 Os	± 2σ	187/188 Os	± 2σ	rho	187Re (ppb)	± 2σ	187Os* (ppb)	± 2σ	% Re blank	%^{187}Os blk	%^{188}Os blk	Model Age (Ma)	± 2σ (Ma)
LC-12-15																			
15-A1	0.393	0.84	0.01	9.55	0.10	805	13	6.93	0.10	0.907	0.53	0.00	0.004	0.000	0.30	0.07	1.43	478	3
15-A2	0.396	4.49	0.02	26.88	0.51	4461	72	34.91	0.58	0.898	2.82	0.01	0.022	0.000	0.06	0.01	1.48	461	3
15-B1	0.408	4.46	0.02	27.45	0.42	3818	52	29.86	0.41	0.897	2.80	0.01	0.022	0.000	0.05	0.01	1.24	460	3
15-B2	0.318	3.89	0.02	22.34	0.62	4486	104	33.42	0.84	0.889	2.45	0.01	0.018	0.000	0.08	0.02	2.14	439	5
15-B3	0.312	6.34	0.03	34.90	0.88	5755	112	42.83	0.97	0.824	3.99	0.02	0.029	0.000	0.05	0.01	1.72	440	6
15-B2'	0.267	7.62	0.03	38.61	1.46	7296	197	53.72	1.82	0.776	4.60	0.02	0.034	0.001	0.05	0.01	2.20	436	9
15-B3'	0.258	7.13	0.03	37.66	1.43	8286	238	62.11	1.96	0.890	4.48	0.02	0.033	0.000	0.05	0.01	2.66	445	6
15-B4'	0.265	6.19	0.03	33.59	1.14	6289	161	46.74	1.40	0.830	3.89	0.02	0.029	0.000	0.06	0.02	2.27	440	7
LC-12-16																			
16-1'	0.355	3.17	0.01	20.83	3.01	2785	379	21.59	2.95	0.997	1.99	0.01	0.015	0.000	0.08	0.12	9.59	453	5
16-2'	0.344	3.62	0.02	21.64	4.70	4256	798	32.93	6.18	0.998	2.28	0.01	0.017	0.000	0.07	0.11	13.21	456	6
16-3	0.339	3.61	0.02	20.72	5.97	5343	1281	41.29	9.91	0.999	2.27	0.01	0.017	0.000	0.07	0.11	16.91	457	5
16-4	0.326	3.80	0.02	23.60	4.07	3494	541	27.01	4.19	0.999	2.39	0.01	0.018	0.000	0.07	0.11	10.93	454	4
16-5	0.372	4.38	0.02	34.98	1.64	1555	82	12.22	0.64	0.995	2.75	0.01	0.021	0.000	0.05	0.08	3.70	451	3
16-6'	0.336	3.83	0.02	22.77	5.35	4671	931	36.62	7.31	0.999	2.41	0.01	0.019	0.000	0.07	0.10	14.06	462	5
16-7	0.335	3.59	0.02	21.69	4.76	4173	794	32.53	6.19	0.999	2.26	0.01	0.017	0.000	0.07	0.11	13.42	459	3
16-8	0.326	2.27	0.01	15.15	3.18	2688	536	21.04	4.20	0.999	1.42	0.01	0.011	0.000	0.12	0.18	14.07	457	4
16-A1	0.324	5.39	0.02	30.83	0.92	5664	126	43.97	1.19	0.792	3.39	0.01	0.026	0.000	0.06	0.01	1.92	459	8
16-B1	0.328	2.37	0.01	16.27	0.33	2445	48	19.18	0.38	0.937	1.49	0.01	0.011	0.000	0.13	0.03	1.86	457	3
16-A2	0.310	3.69	0.02	24.47	0.38	2736	41	21.32	0.32	0.925	2.32	0.01	0.018	0.000	0.09	0.02	1.41	455	3
16-B2'	0.098	2.82	0.02	17.15	1.69	3931	337	30.50	2.65	0.982	1.77	0.01	0.014	0.000	0.36	0.09	8.40	456	8
LC-12-17																			
17-A1	0.425	0.13	0.00	4.15	0.04	193	6	2.04	0.04	0.599	0.08	0.00	0.001	0.000	1.75	0.33	2.01	476	13
17-B1	0.403	0.40	0.00	3.91	0.12	1059	43	8.82	0.35	0.958	0.25	0.00	0.002	0.000	0.61	0.14	3.85	470	6
17-A3	0.422	0.35	0.00	5.45	0.07	460	11	3.98	0.10	0.752	0.22	0.00	0.002	0.000	0.68	0.15	1.86	452	9
17-C2	0.425	0.31	0.00	5.04	0.09	455	13	4.14	0.14	0.681	0.22	0.00	0.002	0.000	0.75	0.16	2.02	478	14
17-C3	0.393	0.49	0.00	5.34	0.11	831	23	6.83	0.20	0.884	0.31	0.00	0.002	0.000	0.51	0.12	2.54	455	7
17-A3'	0.195	0.54	0.01	6.80	0.17	661	27	5.66	0.22	0.912	0.34	0.00	0.003	0.000	0.94	0.22	3.69	467	8

Table 4.2 Re-Os isotope data of arsenopyrite from the Moose River deposit

Sample No.	Sample wt (g)	Total Re (ppb)	± 2σ	Total Os (ppt)	± 2σ	187Re/188 Os	± 2σ	187/188 Os	± 2σ	rho	187Re (ppb)	± 2σ	187Os* (ppb)	± 2σ	% Re blank	%^{187}Os blk	%^{188}Os blk	Model Age (Ma)	± 2σ (Ma)
LC-12-01																			
01-A1	0.251	2.20	0.01	14.21	0.42	2622	76	19.42	0.56	0.970	1.38	0.01	0.010	0.000	0.18	0.05	2.81	432	3
01-A2	0.274	2.00	0.01	19.41	0.19	994	13	7.79	0.11	0.776	1.26	0.01	0.009	0.000	0.18	0.05	1.07	438	4
01-C	0.266	3.85	0.02	22.78	0.50	3307	67	23.63	0.49	0.934	2.42	0.01	0.017	0.000	0.10	0.03	1.91	418	3
01-B1	0.267	3.13	0.01	24.91	0.25	1519	18	11.70	0.14	0.872	1.97	0.01	0.015	0.000	0.12	0.03	1.07	441	3
01-B2	0.269	2.42	0.01	15.08	0.43	2815	76	20.39	0.58	0.929	1.97	0.01	0.011	0.000	0.15	0.04	2.55	423	5
01-B3	0.265	3.25	0.01	22.84	0.35	2095	33	15.88	0.26	0.880	2.04	0.01	0.015	0.000	0.12	0.03	1.43	439	4
01-B4	0.265	2.12	0.01	14.22	0.41	2014	53	13.98	0.49	0.728	1.33	0.01	0.009	0.000	0.18	0.05	2.12	401	10
01-B5	0.254	3.04	0.01	33.70	0.16	780	6	6.22	0.05	0.705	1.91	0.01	0.014	0.000	0.13	0.03	0.60	438	3
01-B6	0.281	2.76	0.01	16.54	0.42	2917	69	20.27	0.52	0.900	1.73	0.01	0.012	0.000	0.13	0.04	2.22	406	5
01-B7	0.271	3.64	0.02	23.84	0.35	2378	36	17.26	0.25	0.946	2.29	0.01	0.016	0.000	0.10	0.03	1.42	422	2
LC-12-02																			
02-2	0.170	3.65	0.02	23.82	4.80	2303	471	16.40	3.37	0.995	2.29	0.01	0.016	0.000	0.14	0.24	14.40	413	9
02-4'	0.257	5.51	0.02	27.87	14.36	10318	4125	75.46	30.18	1.000	3.46	0.01	0.025	0.000	0.06	0.10	28.21	435	4
02-5'	0.096	5.35	0.02	34.89	9.31	2458	649	17.96	4.75	0.998	3.36	0.01	0.024	0.000	0.17	0.28	18.60	425	9
02-6'	0.251	4.74	0.02	24.55	11.63	8169	3073	59.73	22.47	1.000	2.98	0.01	0.022	0.000	0.08	0.12	26.54	434	4
02-9	0.263	5.97	0.02	30.59	12.12	8941	2788	65.31	20.37	1.000	3.75	0.02	0.027	0.000	0.06	0.09	22.00	434	3
02-A	0.255	3.90	0.02	22.48	0.70	4323	116	32.06	0.89	0.945	2.45	0.01	0.018	0.000	0.10	0.03	2.56	437	4
02-B	0.263	4.20	0.02	21.86	1.12	7572	312	55.16	2.27	0.989	2.64	0.01	0.019	0.000	0.09	0.02	4.04	432	3
02-C	0.263	4.23	0.02	22.30	0.92	6219	211	44.61	1.53	0.975	2.66	0.01	0.019	0.000	0.09	0.02	3.30	424	3
02-1	0.101	4.78	0.02	25.31	11.67	3745	1590	24.01	10.20	0.999	3.00	0.01	0.019	0.000	0.18	0.34	29.94	376	7
02-8'	0.267	5.70	0.03	26.65	7.99	6865	1700	43.53	10.79	0.999	3.58	0.02	0.022	0.000	0.06	0.11	17.46	375	4
02-L	0.216	3.08	0.01	31.06	1.26	780	50	4.97	0.32	0.986	1.94	0.01	0.011	0.000	0.13	0.25	4.53	343	5

Table 4.3 Re-Os analytical results of host rock (black shale) from the Beaver Dam deposit and a single test from the Moose River deposit

Sample No.	Sample wt (g)	Total Re (ppb)	± 2σ	Total Os (ppt)	± 2σ	187Re/188 Os	± 2σ	187/188 Os	± 2σ	rho	187Re (ppb)	± 2σ	187Os* (ppb)	± 2σ	% Re blank	$\%^{187}$Os blk	$\%^{188}$Os blk	Model Age (Ma)	± 2σ (Ma)
10-01	1.053	0.085	0.001	16.3	0.1	27	1	0.81	0.02	0.737	0.054	0.001	0.001	0.000	0.99	0.39	1	678	28
10-02	0.982	0.081	0.001	14.6	0.1	30	1	0.93	0.02	0.836	0.051	0.001	0.001	0.000	1.12	0.41	1	866	26
11-01	0.935	0.005	0.001	9.0	0.1	3	0	0.60	0.02	0.185	0.003	0.001	0.000	0.000	17.55	1.04	2	1961	483
11-02	0.939	0.010	0.001	8.9	0.1	6	1	0.69	0.03	0.324	0.006	0.001	0.000	0.000	10.03	0.93	2	2026	282
12-01	1.093	0.010	0.001	10.5	0.1	5	0	0.7	0.0	0.286	0.006	0.000	0.000	0.000	8.24	0.66	2	2519	264
12-02	0.990	0.009	0.001	11.3	0.1	4	0	0.70	0.02	0.252	0.006	0.001	0.000	0.000	9.94	0.69	2	2814	327
13-01	1.062	0.030	0.001	13.2	0.1	12	0	0.88	0.02	0.594	0.019	0.000	0.001	0.000	2.85	0.45	1	1911	78
14-01	0.968	0.050	0.001	14.4	0.1	18	0	0.75	0.02	0.703	0.031	0.001	0.000	0.000	1.86	0.52	1	821	44
14-02	0.971	0.052	0.001	11.1	0.1	25	1	0.93	0.03	0.811	0.033	0.001	0.001	0.000	1.77	0.56	2	1013	42
Moose River host rock sample is close to the quartz vein where the arsenopyrite is collected																			
LC1202WR	0.226	0.069	0.002	4.8	0.2	77	9	0.97	0.14	0.828	0.044	0.001	0.000	0.000	4.28	10.60	36.90	370	75

4.2 U-Pb Zircon Results

For granite sample LC-12-05 and LC-12-06, 40-50 euhedral zircons were selected respectively for analyses. Under cathodoluminescence (CL) imaging of these zircons, magmatic oscillatory zoning sometimes surrounding bright CL core was observed (Fig 4.9). For each granite sample, approximately 40 laser ablation analyses were performed using a 30 μm spot-size on those zircons with clear magmatic oscillatory zoning (from CL image, Fig 4.9). The in-house zircon standard LH 94-15 was analyzed several times within 10 years by LC-ICP-MS and TIMS, yielded an average age of 1830 Ma (common Pb corrected, Simonetti et al., 2005). The U-Pb results of standard LH 94-15 was presented in Table 4.4. For the granite samples LC-12-05 and LC-12-06, data of zircons without inherited cores were presented in Table 4.5, 4.6, given the magmatic intrusion age. From the Tera-Wasserburg diagrams (Fig 4.10), analyses of both samples fell on a discordia line, yielded a lower intercept age of 382.2 ± 2.9 Ma (2σ) for LC-12-05 and 383.2 ± 2.3 Ma (2σ) for LC-12-06. Data of zircons with inherited cores were presented in Table 4.7, given inherited ages.

Table 4.4 LA-ICPMS U-Pb isotope data for standard LH 94-15 (not common Pb corrected)

Standard Grain No.	^{206}Pb (cps)	^{204}Pb (cps)	$^{207}Pb/^{206}Pb$	±2σ(abs)	$^{207}Pb/^{235}U$	±2σ(abs)	$^{206}Pb/^{238}U$	±2σ(abs)	Rho	$^{207}Pb/^{206}Pb$ age (Ma)	±2σ (Ma)
LH9415-1	683532	92	0.11168	0.00090	5.14260	0.20137	0.33397	0.01280	0.979	1827	15
LH9415-2	487635	149	0.11176	0.00092	5.21645	0.27479	0.33853	0.01761	0.988	1828	15
LH9415-3	613842	102	0.11095	0.00089	5.11140	0.20961	0.33414	0.01344	0.981	1815	14
LH9415-4	583663	273	0.11109	0.00090	4.90889	0.20395	0.32049	0.01306	0.981	1817	15
LH9415-5	546427	30	0.11172	0.00093	4.83534	0.19293	0.31389	0.01225	0.978	1828	15
LH9415-6	438171	21	0.11180	0.00111	4.83578	0.17148	0.31370	0.01068	0.960	1829	18
LH9415-7	855267	13	0.11084	0.00109	5.17567	0.19503	0.33865	0.01232	0.966	1813	18
LH9415-8	565251	3	0.11111	0.00111	5.03881	0.15757	0.32891	0.00975	0.948	1818	18
LH9415-9	1151312	1	0.11084	0.00112	4.96784	0.19866	0.32506	0.01258	0.967	1813	18
LH9415-10	693788	0	0.11101	0.00111	4.97040	0.18002	0.32473	0.01130	0.961	1816	18
LH9415-11	614043	0	0.11139	0.00111	4.91954	0.16084	0.32032	0.00998	0.953	1822	18
LH9415-12	767007	0	0.11096	0.00111	4.98716	0.18614	0.32598	0.01172	0.963	1815	18
LH9415-13	617573	0	0.11149	0.00109	4.88541	0.16942	0.31779	0.01057	0.959	1824	18

Table 4.5 LA-ICPMS U-Pb isotope data for zircons of granite LC-12-05 from the River Lake granite intrusion (not common Pb corrected)

Sample name	^{206}Pb (cps)	^{204}Pb (cps)	^{207}Pb/^{206}Pb	±2σ(abs)	^{207}Pb/^{235}U	±2σ(abs)	^{206}Pb/^{238}U	±2σ(abs)	Rho	^{207}Pb/^{206}Pb age (Ma)	±2σ (Ma)
LC1205-1	246704	226	0.0553	0.0007	0.4738	0.0186	0.0621	0.0023	0.954	424	26
LC1205-2	264736	170	0.0548	0.0005	0.4580	0.0166	0.0606	0.0021	0.972	405	19
LC1205-3	488184	180	0.0546	0.0006	0.4566	0.0181	0.0606	0.0023	0.959	397	25
LC1205-4	276894	222	0.0547	0.0006	0.4641	0.0220	0.0616	0.0028	0.973	398	24
LC1205-5	243382	225	0.0543	0.0005	0.4592	0.0165	0.0613	0.0021	0.970	385	19
LC1205-8	180796	89	0.0542	0.0005	0.4633	0.0161	0.0620	0.0021	0.969	379	19
LC1205-9A	465426	94	0.0538	0.0005	0.4613	0.0200	0.0622	0.0026	0.980	363	19
LC1205-11	423733	113	0.0540	0.0005	0.4614	0.0212	0.0620	0.0028	0.982	371	19
LC1205-12	300915	213	0.0569	0.0014	0.4808	0.0233	0.0613	0.0025	0.853	487	55
LC1205-13	488369	195	0.0543	0.0005	0.4584	0.0201	0.0613	0.0026	0.977	382	21
LC1205-14	821223	740	0.0560	0.0011	0.4776	0.0196	0.0618	0.0023	0.888	454	41
LC1205-15	381461	325	0.0578	0.0007	0.4741	0.0191	0.0595	0.0023	0.950	522	27
LC1205-16	479189	230	0.0544	0.0006	0.4547	0.0180	0.0607	0.0023	0.956	385	26
LC1205-17	167272	192	0.0547	0.0007	0.4559	0.0163	0.0604	0.0020	0.934	401	28
LC1205-18	235569	164	0.0541	0.0005	0.4546	0.0189	0.0609	0.0025	0.975	375	21
LC1205-19	283901	168	0.0542	0.0005	0.4507	0.0166	0.0603	0.0022	0.971	381	20
LC1205-20	188798	231	0.0544	0.0005	0.4598	0.0164	0.0613	0.0021	0.967	389	20
LC1205-22	195402	82	0.0564	0.0006	0.4720	0.0165	0.0607	0.0020	0.960	469	22
LC1205-25	121817	6	0.0581	0.0006	0.4911	0.0180	0.0613	0.0022	0.957	534	23
LC1205-26	78715	14	0.0563	0.0008	0.4747	0.0193	0.0611	0.0024	0.945	465	29
LC1205-28	184236	17	0.0547	0.0006	0.4613	0.0156	0.0612	0.0020	0.950	398	24
LC1205-30	409660	21	0.0540	0.0006	0.4589	0.0161	0.0617	0.0021	0.952	370	24
LC1205-31	151096	32	0.0561	0.0015	0.4738	0.0232	0.0613	0.0025	0.844	456	57
LC1205-34	991397	112	0.0536	0.0004	0.4499	0.0150	0.0608	0.0020	0.970	355	18
LC1205-35	351115	137	0.0541	0.0004	0.4551	0.0193	0.0611	0.0025	0.982	373	18
LC1205-36	251487	178	0.0549	0.0005	0.4542	0.0171	0.0600	0.0022	0.971	408	20
LC1205-37	292961	147	0.0542	0.0005	0.4513	0.0181	0.0603	0.0024	0.977	381	19
LC1205-38	904139	341	0.0547	0.0005	0.4556	0.0157	0.0604	0.0020	0.965	400	20
LC1205-39	221033	332	0.0594	0.0021	0.5013	0.0247	0.0612	0.0021	0.694	581	75

Table 4.6 LA-ICPMS U-Pb data for zircons of granite LC-12-06 from the River Lake granite intrusion (not common Pb corrected)

Sample name	^{206}Pb (cps)	^{204}Pb (cps)	^{207}Pb/^{206}Pb	±2σ(abs)	^{207}Pb/^{235}U	±2σ(abs)	^{206}Pb/^{238}U	±2σ(abs)	Rho	^{207}Pb/^{206}Pb age (Ma)	±2σ (Ma)
LC1206-1	157224	0	0.0573	0.0014	0.4737	0.0349	0.0600	0.0042	0.940	503	54
LC1206-2B	508992	174	0.0593	0.0029	0.5049	0.0294	0.0617	0.0020	0.550	580	102
LC1206-3	210535	13	0.0612	0.0011	0.5062	0.0179	0.0600	0.0018	0.849	646	40
LC1206-4	290503	0	0.0542	0.0006	0.4681	0.0136	0.0626	0.0017	0.936	380	23
LC1206-5	218561	83	0.0707	0.0023	0.5932	0.0329	0.0608	0.0028	0.814	950	65
LC1206-6	240613	0	0.0553	0.0006	0.4690	0.0147	0.0616	0.0018	0.929	422	26
LC1206-7	615941	93	0.0554	0.0009	0.4614	0.0156	0.0604	0.0018	0.871	430	37
LC1206-9	670046	737	0.0573	0.0010	0.4888	0.0179	0.0619	0.0020	0.876	502	38
LC1206-10	606769	1046	0.0826	0.0049	0.6966	0.0442	0.0612	0.0013	0.338	1259	113
LC1206-12	387137	0	0.0540	0.0006	0.4590	0.0145	0.0617	0.0018	0.947	371	23
LC1206-13	511366	8	0.0569	0.0007	0.4809	0.0163	0.0613	0.0019	0.932	489	27
LC1206-14	717019	672	0.0585	0.0007	0.4957	0.0138	0.0615	0.0015	0.904	548	26
LC1206-15	338693	134	0.0591	0.0011	0.4926	0.0172	0.0605	0.0018	0.842	570	41
LC1206-18	307937	0	0.0551	0.0006	0.4717	0.0116	0.0621	0.0014	0.895	414	24
LC1206-19	365089	0	0.0563	0.0006	0.4733	0.0156	0.0609	0.0019	0.944	465	24
LC1206-21	482182	40	0.0602	0.0012	0.4974	0.0166	0.0599	0.0016	0.809	611	42
LC1206-22	209319	187	0.0705	0.0024	0.6025	0.0291	0.0620	0.0022	0.719	944	67
LC1206-23	335334	0	0.0542	0.0006	0.4610	0.0132	0.0617	0.0016	0.931	378	23
LC1206-24	392402	679	0.0544	0.0007	0.4524	0.0223	0.0603	0.0029	0.970	387	27
LC1206-25	200833	0	0.0576	0.0011	0.4830	0.0143	0.0608	0.0014	0.791	514	39
LC1206-26	285299	101	0.0554	0.0006	0.4661	0.0161	0.0611	0.0020	0.943	426	26
LC1206-27	272389	22	0.0652	0.0012	0.5481	0.0172	0.0610	0.0016	0.815	779	38
LC1206-28	217996	0	0.0549	0.0006	0.4661	0.0135	0.0616	0.0017	0.929	407	24
LC1206-29	268253	0	0.0543	0.0006	0.4575	0.0123	0.0611	0.0015	0.925	385	23
LC1206-31	304246	0	0.0556	0.0006	0.4756	0.0168	0.0621	0.0021	0.947	436	25
LC1206-32	698320	671	0.0743	0.0038	0.6295	0.0422	0.0615	0.0026	0.640	1050	100
LC1206-33	166502	0	0.0567	0.0006	0.4738	0.0133	0.0607	0.0016	0.921	478	24
LC1206-34	229535	0	0.0606	0.0014	0.5095	0.0187	0.0610	0.0018	0.793	624	48
LC1206-37	617602	40	0.0589	0.0013	0.4958	0.0185	0.0610	0.0019	0.822	564	46
LC1206-38	219242	1	0.0610	0.0007	0.5060	0.0135	0.0602	0.0015	0.912	640	23
LC1206-39	268863	0	0.0545	0.0006	0.4584	0.0149	0.0610	0.0019	0.944	392	24

Table 4.7 LA-ICPMS U-Pb data for zircons with inherited cores of granite LC-12-05 and LC-12-06 (not common Pb corrected)

Sample name	^{206}Pb (cps)	^{204}Pb (cps)	^{207}Pb/^{206}Pb	±2σ(abs)	^{207}Pb/^{235}U	±2σ(abs)	^{206}Pb/^{238}U	±2σ(abs)	Rho	^{207}Pb/^{206}Pb age (Ma)	±2σ (Ma)
LC1205-9B	828170	174	0.17514	0.00575	7.03978	1.28984	0.29152	0.05255	0.984	2607	54
LC1205-9C	844855	193	0.16466	0.00489	4.84225	0.66941	0.21329	0.02880	0.977	2504	49
LC1205-10	110128	59	0.05775	0.00073	0.65410	0.04446	0.08214	0.00549	0.982	520	28
LC1205-21	323002	1061	0.09732	0.00906	0.63891	0.06534	0.04762	0.00202	0.415	1573	165
LC1205-24	141762	76	0.06049	0.00067	0.46778	0.01741	0.05609	0.00199	0.955	621	24
LC1205-29	208678	15	0.06131	0.00069	0.76751	0.02641	0.09079	0.00295	0.945	650	24
LC1205-29B	153473	24	0.06012	0.00062	0.75904	0.02956	0.09157	0.00344	0.964	608	22
LC1205-32	236270	638	0.09046	0.00174	0.52376	0.02289	0.04199	0.00165	0.898	1435	36
LC1206-10	606769	1046	0.0826	0.0049	0.6966	0.0442	0.0612	0.0013	0.338	1259	113
LC1206-2	1568064	2513	0.08750	0.00297	0.87812	0.03985	0.07279	0.00219	0.663	1371	64
LC1206-11	360707	0	0.06121	0.00062	0.86924	0.02782	0.10299	0.00313	0.949	647	22
LC1206-20	227509	2	0.06783	0.00206	0.53777	0.02101	0.05750	0.00142	0.630	863	62
LC1206-30	269541	2	0.05924	0.00121	0.43076	0.01963	0.05274	0.00215	0.894	576	44
LC1206-35	305350	96	0.06518	0.00096	0.53495	0.01313	0.05952	0.00117	0.798	780	31
LC1206-36	519461	1579	0.06519	0.00211	0.52464	0.02314	0.05836	0.00175	0.679	781	67
LC1206-40	176299	327	0.08987	0.00553	0.62048	0.04225	0.05007	0.00147	0.430	1423	113

4.3 SEM and Major Element Results

For all the arsenopyrite samples used for Re-Os geochronology, LC-12-01/ 02 (Moose River deposit) and LC-12-15/16/17 (Beaver Dam deposit), backscattered scanning electron microscope (SEM) images and major element mapping were performed by Zeiss EVO MA 15. The data were collected under a beam of 20 kV and low contrast with detection limits at approximately 5000-10000 ppm for most elements.

4.3.1 SEM and Major Element Result of the Moose River Deposit

For sample LC-12-01 and LC-12-02 from the Moose River deposit, evidence of complex growth history of arsenopyrite is found, including clear compositional zoning, inclusion-rich core regions and inclusion-free overgrowth rims (Fig 4.11 A, C, D). In addition, for these two samples, Fe and S contents are enriched in the core, whereas As is more concentrated within the inclusion-free rim (Fig 4.12, Table 4.8).

4.3.2 SEM and Major Element Result of the Beaver Dam Deposit

Similar features appear in sample LC-12-15 from the Beaver Dam deposit, the boundary between inclusion-rich core and inclusion-free rims is clear (Fig 4.11 E) and major elements (Fe, As, S) distribution is comparatively different between the core and rim (Fig 4.13, Table 4.8). By contrast, there are no specific zoning or composition differences observed in sample LC-12-16 and LC-12-17 from the Beaver Dam deposit (Fig 4.11 G, H).

Table 4.8 Major element weight percentage of arsenopyrite analyzed by backscattered SEM

Analytical No.	S wt%	Fe wt%	As wt%
Sample	**Moose River deposit: LC-12-01, LC-12-02**		
Core			
02_5	18.40	34.03	46.56
02_2	18.57	34.46	45.87
01_10	18.68	34.07	46.13
01_8	18.93	34.28	45.70
01_6	18.85	34.43	45.54
Rim			
02_4	17.94	34.01	46.93
02_1	17.74	33.40	47.75
01_11	17.72	33.85	47.43
01_9	17.51	33.42	47.91
01_7	17.85	33.40	47.68
01_5	17.68	34.29	46.85
Sample	**Beaver Dam deposit: LC-12-15**		
Core			
15_19	19.36	35.01	45.63
15_16	19.14	34.69	46.17
15_15	19.53	34.63	45.84
15_12	19.44	34.68	45.88
15_11	19.50	34.50	46.00
Rim			
15_18	19.14	33.99	46.87
15_17	18.77	34.04	47.19
15_14	19.18	34.27	46.55
15_13	18.78	34.34	46.88
15_10	19.35	35.06	45.59
15_9	19.06	35.19	45.75

5.0 Discussion:

5.1 Re-Os Age Constraints for Sulfide and Gold Mineralization

The Re-Os analyses of arsenopyrite determined for the Moose River deposit and the Beaver Dam deposit yield multiple ages, indicating complex, multi-stage arsenopyrite growths between ca. 460 and 380 Ma. This is the first direct radiometric evidence that some Meguma Terrane gold occurrences may be pre-Acadian in age, forming prior to Acadian deformation at ca. 410 Ma.

5.1.1 Re-Os dating of the Beaver Dam deposit arsenopyrite

Re-Os analyses of arsenopyrite from veins at the Beaver Dam deposit provide Middle- to Late- Ordovician ages. Twelve analyses of sample LC-12-16 yield a precise $^{187}Re/^{188}Os$-$^{187}Os/^{188}Os$ isochron age of 461.3 ± 2.9 Ma (Fig 4.3). Gold grains are observed within this arsenopyrite (Fig 2.15 B, C). Consequently, the age of 461 ± 3 Ma represents the sulfide and gold formation age in the Beaver Dam deposit. The arsenopyrite sample was collected from calcite-bearing veins (Fig 2.12 A, B) and went through careful preparation procedures (described in Section 3.1, Table 3.1), to guarantee the purity of the sample in order to counter the potential problems of wall-rock incorporation put forward by Morelli et al. (2005). The arsenopyrite Re-Os system is unlikely to be influenced by the Goldenville Formation host-rocks because: (1) the sulfide is from the veins instead of directly from the host rock (cf. Morelli et al., 2005); (2) extremely low Re and Os concentrations characterize the wall rock Re-Os data (Fig 4.8).

The arsenopyrite sample LC-12-17 from the same drill core as LC-12-16 but different depth (Table 2.1) yields a similar age of 464 ± 26 Ma (Fig 4.4). The sample was collected from quartz-dominated veins (bedding-concordant) to avoid any possible host rock influence (Fig 2.13 A, B, C). The large uncertainty is due primarily to the much lower Re/Os ratios in this sample, some scatter around the regression line (MSWD = 6.4) and the low Re and Os concentrations in sample LC-12-17 (Table 4.1). From the SEM and thin section observation, there is no evidence for compositional zoning or multistage growth of arsenopyrite from samples LC-12-16 and LC-12-17 (Fig 2.12 C; Fig 2.13 D; Fig 4.11 G, H).

In contrast, apparent zoning of rim (paler BSE color, inclusion free) and core (darker BSE color, inclusion rich) is observed in both the SEM and the thin section images for sample LC-12-15, which was collected deeper in the same drill core (bedding concordant vein, Fig 2.11 D, E; Fig 4.11 E, F; Table 2.1). The major element SEM analytical results also show different element distribution patterns between the rim and the core of the crystal (Fig 4.13; Table 4.8). Regressing all the Re-Os data for sample LC-12-15 yields an age of 434 ± 18 Ma (MSWD = 18), which has significant scatter of the points around the regression line, and is imprecise, compared with the age of sample LC-12-16. However, if the overgrowth rim and the original core are with different ages or different initial $^{187}Os/^{188}Os$ ratios, the Re-Os characteristics will be different and the isochron age may be out of geological meaning. Unfortunately, owing to the technological limits, in-situ Re-Os dating or separately sampling along core-rim boundary cannot be performed (small crystal, see Fig 2.7 C, D). The only effort that could be made is to examine the data to see if different groups can be observed. For this sample, the eight points could be separated into two groups, yielding Re-Os ages of 456.0 ± 2.8 Ma (MSWD = 0.90, $^{187}Os/^{188}Os_i$ = 0.796 ± 0.064, n = 3, Fig 4.2A) and 446 ± 13 Ma (MSWD = 0.66, $^{187}Os/^{188}Os_i$ = -0.1 ± 1.2, n = 5, Fig 4.2B)

respectively. The former age is similar to the age results from LC-12-16 and LC-12-17, suggesting that the original stage of arsenopyrite growth may also have occurred at ca. 460 Ma. The latter age may reveal the existence of younger stage of arsenopyrite growth, but the timing of this growth is also pre-Acadian in age. However, this younger age of 446 ± 13 Ma remains to be confirmed, because possibly some sample analyses contain both rim and core portions. If this is the case, the actual rim overprinting age should be younger than current result of ca. 446 Ma. Gold grains also occur in the arsenopyrite (Fig 2.15 A), showing a close space and time relationship of the gold and arsenopyrite. Hence the age of arsenopyrite can represent the gold formation age.

5.1.2 Re-Os dating of the Moose River deposit arsenopyrite

Two arsenopyrite samples LC-12-01 and LC-12-02 were collected from quartz-bearing veins from the Moose River deposit (Table 2.1, Fig 2.7 A, B). Gold is found in the arsenopyrite (Fig 2.15 D). For both arsenopyrite samples, inclusion-rich cores and inclusion-free rims (Fig 4.11 A, B) are readily observed from the thin section observation and SEM BSE images. Moreover, clear zoning occurs in SEM images for both samples (Fig 4.11 C, D), and major element distribution varies from core to rim; arsenic concentration is higher within the rim, while Fe and S are enriched in the core (Fig 4.12, Table 4.8). In consequence, based on the SEM and thin section observation, the arsenopyrite samples from the Moose River deposit appear to have undergone more than one crystallization stage.

Eleven Re-Os analyses from sample LC-12-02 do not plot on a single regression line on a Re-Os isochron diagram (Fig 4.7 A). Like LC-12-15, if we assume that there is no core-rim mixed sample division, the eleven points may give two different ages, and the data clearly appear

to form two quite different linear arrays. Eight analyses can be regressed on one regression line, providing a Model 3 age of 437.6 ± 8.2 Ma (Fig 4.7 B), and another three analyses yield a younger Model 1 Re-Os age of 380.3 ± 4.0 Ma (Fig 4.7 C), again suggesting the multiple growth stages of arsenopyrite.

Sample LC-12-01 from the Moose River deposit has similar characteristics to LC-12-02: ten analyses scatter around a regression line that yields an imprecise age of 408 ± 25 Ma (Fig 4.5). Because the common Os is low in samples (over 97% of ^{187}Os is radiogenic), the model age is suggested to be used to determine the age of the arsenopyrite (Fig 4.6; Table 4.2). To calculate the model ages, an $^{187}Os/^{188}Os$ initial ratio (Os_i) must be assumed. Unfortunately from the isochron of LC-12-01, the imprecise Os_i of 1.04 ± 0.96 cannot be used with such large uncertainties (Table 5.3). Again, for sample LC-12-02 from the same deposit, the Os_i generated from two isochrons (0.017 ± 0.080 / -0.18 ± 0.90; Table 5.3) are not useful, because: (1) the unreasonable negative number and large uncertainties; (2) the Os_i cannot be lower than the mantle $^{187}Os/^{188}Os$ value of 0.125. Even though the present Os_i values from the Moose River deposit are useless for the calculation of model ages, Os_i values from other gold deposits in the Meguma terrane can be attempted as long as the source of the gold is the same. The Os_i values from the Beaver Dam (0.24 ± 0.12, 0.51 ± 0.28, 0.796 ± 0.064), the Dufferin (0.38 ± 0.16) deposit and the Ovens (0.83 ± 0.16) deposit are precise and all the deposits are believed to have the similar source reservoir (Morelli et al., 2005; Kontak et al., 2010, 2011; Table 5.3). As a result, the average Os_i value of the above data, namely $Os_i = 0.5$, is suggested for calculating model ages of sample LC-12-01 from the Moose River deposit. To show the possible model age range when using different assumptions of Os_i, we present different model ages based on the Os_i of 0.125 (lowest, mantle $^{187}Os/^{188}Os$ value), 0.5 (suggested value) and 1.0 (higher than all the

previous defined Os_i value in the Meguma terrane) respectively (Table 5.4; Fig 5.1). The model ages are ranging from ca. 385 Ma to 465 Ma within the realm of possibility.

After assuming an initial $^{187}Os/^{188}Os$ ratio of 0.5, samples 01-A2, 01-B1, 01-B3 and 01-B5 yield model ages from 438 Ma to 441 Ma (± 2σ within 4 Ma), similar as the isochron age of 437 Ma from sample LC-12-02. On the other hand, samples 01-B4 and 01-B6 yield model ages of 401 ± 10 Ma and 406 ± 5 Ma, which is similar to the Re-Os arsenopyrite isochron age of 407 ± 4 Ma from the Ovens deposit (Morelli et al., 2005) and in broad agreement with Acadian metamorphism ages (Hicks et al., 1999; Murphy and Keppie, 2005). Because the arsenopyrite crystal is too small to be sampled along the zoning boundary, bulk sample analyses likely contain both core and rim fragments. Therefore the result of mixed ages could exist. Model ages of ca. 418 Ma to ca. 432 Ma from four analyses may then represent mixed ages between older 440 Ma and younger 400-410 Ma ages (Table 4.2, Fig 4.6).

To evaluate any host-rock influence, a single mudstone Re-Os analysis was tested (the mudstone is close to the sulfide-bearing quartz vein from the Moose River deposit, data see table 4.3). The Re and Os concentrations are extremely low (Re < 0.1 ppb), as observed for wall rocks samples from Beaver Dam, again suggesting that unseen incorporation of wall rock into analyses would have negligible influence for the Re-Os sulfide analysis from the Moose River deposit.

From the Re-Os geochronology data, the original Re-Os system was not reset in the later metamorphic and magmatic events in arsenopyrite. The ca. 440 Ma age represents that the arsenopyrite primarily crystallized in early Silurian, and the young ages indicate sulfide overgrowth during syn- to post-Acadian hydrothermal events afterwards. Fluid inclusion and isotope analyses constrain the fluid temperature ranging from 350 ºC to 400 ºC (Kontak and

Horne, 2010). Based on the determined multiple Re–Os ages and on the temperature constraints, the closure temperature of Re-Os arsenopyrite chronometer is higher than 400 ºC, supporting the previous reported estimation of the minimum closure temperature at 400 ºC or higher (Morelli et al., 2010).

5.2 Implications for Complex Gold Metallogeny in the Meguma Terrane

5.2.1 Multi-stage Gold Metallogeny Model in the Meguma Terrane

From the isochron age data presented above, multiple generations of arsenopyrite occur in both the Beaver Dam and the Moose River deposit, yielding an age series of ca. 460 Ma, 450-440 Ma, 440 Ma and 380 Ma. Model ages of 440-400 Ma are determined in the Moose River deposit.

The Re-Os ages of 460 Ma and 450-440 Ma are determined from three arsenopyrite samples in the Beaver Dam deposit, which are much older that the previously reported $^{39}Ar/^{40}Ar$ ages of muscovite, biotite and from this deposit of 367-374 Ma (Table 5.1). This is reasonable because the blocking temperature for Ar diffusion in micas (~ 350 ºC) is much lower than the known blocking temperature for the Re-Os system in arsenopyrite of > 450 ºC (Morelli et al, 2010). The Ar-Ar ages reflect the last major thermal event regionally, whereas the Re-Os ages still retain evidence of older events.

The Re-Os ages of two vein-hosted arsenopyrite samples from the Moose River deposit yield isochron ages of ca. 440 Ma and 380 Ma, and model ages of 440 Ma and 410-400 Ma. Unlike the Beaver Dam deposit, and other vein-dominant gold deposits in the Meguma terrane, the Moose River district is a resource of disseminated gold (Bierlein and Smith, 2003). Re-Os

dating has been attempted on the arsenopyrite from auriferous host-rock siltstone, but high common Os and low $^{187}Re/^{188}Os$ precluded a precise isochron age, considering host-rock fragments within arsenopyrite crystals to be a possible reason. (Morelli et al., 2005; Age = 457 ± 110 Ma, MSWD = 27). However, from the host rock Re-Os test in the Moose River deposit and the analyses in the Beaver Dam deposit, the host-rock disturbance is neglected due to the very low Re and Os concentrations. Accordingly, a probable explanation is that the disseminated arsenopyrite samples are not homogeneous, the same as the vein-bearing samples in this thesis work (Morelli et al., 2005, Fig 5.2; Table 5.2), but more evidence is required for this assumption, such as thin section petrography and SEM mapping. The new Re-Os arsenopyrite age of 440 Ma is a previously undocumented mineralization age in the Meguma terrane, indicating there was active thermal fluid in southeastern Meguma at ca. 440 Ma. The model ages of 410-400 Ma are close to the Re-Os arsenopyrite isochron age of 407 ± 4 Ma reported for the the Ovens deposit (Morelli et al., 2005), The three point isochron age of ca. 380 Ma is equal to the ^{39}Ar-^{40}Ar vein mineral ages (Kontak et al., 1990; 1993, Table 5.1) and the Re-Os arsenopyrite age of the Dufferin deposit (Morelli et al., 2005, Table 5.2).

From previous studies of gold deposits in the Meguma terrane, the stratigraphic control of the auriferous quartz veins was considered to be the evidence supporting the syn-tectonic gold mineralization model (Mawer, 1987). In 1990s, absolute $^{39}Ar/^{40}Ar$ ages were produced from several gold deposits, and the gold mineralization age was commonly accepted to be ca. 365-380 Ma, coeval with post-Acadian granite emplacement in the Meguma terrane (Clarke and Halliday, 1980; Reynolds et al., 1981; Kontak and Smith., 1990b, 1993). Morelli et al. (2005) determined Re-Os arsenopyrite ages of two deposits in the Meguma terrane: 380 ± 3 Ma for the Dufferin deposit and 407 ± 4 Ma for the Ovens deposit, indicating that there were at least two gold

mineralization stages; synchronous with the Acadian regional deformation and post-folding coeval with magma intrusion respectively (Clarke and Halliday, 1980; Keppie and Dallmeyer, 1987; Hicks et al., 1999; Morelli et al., 2005).

In this study, however, the new Re-Os Ordovician age ca. 460 Ma and Silurian age ca. 440 Ma show that the gold-bearing arsenopyrite in the Beaver Dam deposit and the Moose River deposit originally formed prior to ca. 410 Ma Acadian deformation. Younger Re-Os ages determined here of 410-400 Ma and ca. 380 Ma are similar to previously constrained ^{39}Ar-^{40}Ar and Re-Os ages of hydrothermal mineralization (Kontak and Smith., 1990, 1993; Morelli et al., 2005). In addition to the complex Re-Os ages, from the oxygen and strontium isotope analyses of vein minerals (Fig 5.3, Kontak and Kerrich, 1995), the O and Sr isotope range is large in both the Beaver Dam and the Moose River deposit, possibly providing further support for a poly-phase origin of these deposits.

The gold formation type of deposits within the Meguma terrane has been generally accepted as orogenic gold deposits based on the tectonic, mineralogy, geochemistry work, and early geochronology results. The orogenic gold model (OGM) defined by Groves et al. (1998) comprises gold ores formed during compressional to transpressional metamorphism in deformed accretionary belts of collisional orogens. Most gold mineralization of OGM is mesothermal structurally controlled lode gold; orogenic disseminated gold also occurs (Groves et al., 1998; Goldfarb 2001; Bierlein and Maher, 2001). The previous constrained gold ages of ca. 410-400 Ma and 380 Ma (Kontak and Smith., 1990, 1993; Morelli et al., 2005) were syn- to post- Acadian orogeny, supporting the notion that the gold deposits in the Meguma terrane are OGM type. However, based on the Re-Os arsenopyrite dating presented here, gold mineralization in the Meguma terrane started at ca. 460 Ma, 50 Ma earlier than the onset of the Acadian orogeny, and

formed from multiple hydrothermal / tectonothermal events at 460 Ma, 440 Ma, 410-400 Ma and 380 Ma. The pre-Acadian ages and the large gold formation time span of ca. 80 Ma indicate that the gold deposits in the Meguma terrane are far more complex than being related to a single orogenic episode.

Table 5.1 Ar-Ar plateau age of the Beaver Dam and the Moose River deposit

Deposit	Whole Rock	Muscovite	Biotite	Reference
Beaver Dam	382 Ma	374 Ma	367, 374Ma	Kontak et al. 1990, 1993
Moose River-Touquoy	384 Ma	370, 380 Ma	-	Kontak et al. 1990, 1993

Table 5.2 Re-Os age of arsenopyrite from the Dufferin deposit, the Ovens deposit and the Moose River deposit (Touquoy) in the Meguma terrane (Morelli et al., 2005)

Deposit	Vein Type	$^{187}Re/^{188}Os$-$^{187}Os/^{188}Os$ Isochron Age	^{187}Re vs ^{187}Os Isochron Age	Model Age
Dufferin	Saddle reef	380 ± 3 Ma	381 ± 5Ma	~381 Ma
The Ovens	(Bedding concordant)	409 ± 5 Ma	405 ± 8 Ma	-
The Ovens	(Bedding-discordant)	407 ± 4 Ma		406 ± 2 Ma
Moose River-Touquoy	Disseminated arsenopyrite	Re-Os isochron age: 457± 110 Ma, MSWD = 27 (Scattered data on isochron)		

5.2.2 Host Rock Re-Os Data and Implications for the Metal Sources

Most of the gold-bearing veins in the Meguma Terrane are hosted by the Goldenville Group, consisting of greywacke and dark meta-siltstone to slate (Horen and Pelley, 2007, Fig 2.8 A, B). The black shale/siltstone host-rock was previously suspected as a physical contaminant for dating of disseminated arsenopyrite, owing to the Re and Os enrichment in hydrogenous organic rich shales (Morelli et al., 2005; Creaser et al., 2002). However, the Re-Os results from this study reveal that the Re and radiogenic Os contents are extremely low in the host rocks (Table 4.3; Fig 4.8), likely indicating a non-reducing depositional environment or later disturbance during metamorphism (Crusius et al., 1996; Morford et al., 2009). The effect of physical incorporation of wall rock into the Moose River Re-Os age reported by Morelli et al. (2005) is therefore likely to be small. Thus the imprecise Re-Os age of 457 ± 110 Ma determined from the disseminated gold in the Moose River deposit is not because of the wall rock influence as Morelli et al. (2005) considered, but might represent the true pre-Acadian gold mineralization age, albeit imprecise. A possible explanation of the large uncertainties is that the arsenopyrite is with multiple growths, similar to the two Moose River samples from this study.

Re-Os geochronology and the initial Os ratio of arsenopyrite samples can provide constraints of possible metal sources (Morelli et al. 2007). The $^{187}Os/^{188}Os$ initial ratios of arsenopyrite samples (Re-Os age of ca. 460Ma) from the Beaver Dam deposit vary from 0.24 ± 0.12 to 0.80 ± 0.06 (Table 5.3), similar to the arsenopyrite Os_i value of 0.83 ± 0.16 from the Ovens (ca. 408 Ma) deposit and 0.38 ± 0.16 from the Dufferin deposit (ca. 380 Ma) (Morelli et al., 2005), indicating a complex derivation of Os in the fluid. The Os_i yielded from the younger age regression line from sample LC-12-15 and from the multiple-age arsenopyrite from the Moose River deposit are imprecise, possibly because of the unclear rim-core mixed sampling (Table 5.3).

By calculating using equation below, the $^{187}Os/^{188}Os$ ratios of the Beaver Dam host rock

$$\left(\frac{^{187}Os}{^{188}Os}\right)_{460\,Ma} = \left(\frac{^{187}Os}{^{188}Os}\right)_{Present} - \frac{^{187}Re}{^{188}Os}\,(e^{\lambda t} - 1)$$

Re decay constant $\lambda = 1.666 \times 10{-}11\ yr{-}1$, t= 460 Ma

samples at 460 Ma can be obtained (Table 5.3); these range from 0.58 to 0.79. Comparing with the arsenopyrite Os_i from the same deposit: the arsenopyrite Os_i of 0.24 from LC-12-16 (461.3 ± 2.9 Ma) is the lowest, with the higher ratio from LC-12-17, the sample with large age uncertainties, (Os_i of 0.51, 464 ± 26 Ma) and the highest from LC-12-15 with younger overprinting (Os_i of 0.79, 456.0 ± 2.8 Ma). The possible reason for the large Os_i range from coeval samples in the Beaver Dam deposit is that the variable mixture has two components: the sample with lower Os_i contains more mantle-derived component (mantle $^{187}Os/^{188}Os$: 0.125, much lower than crust $^{187}Os/^{188}Os$ value) and the sample with higher Os_i might mainly contain crustal-derived component. The Os_i differences between the Beaver Dam deposit and the imprecise Os_i data of the Moose River deposit indicate a variation in the source of Os present in the mineralizing system. Comparing the various arsenopyrite Os_i data with the Beaver Dam host rock $^{187}Os/^{188}Os$ ratios at 460 Ma (Table 5.3), the Os in the arsenopyrite is not sourced from the meta-sedimentary host rocks. The arsenopyrite Os could be incorporated when interacting with the host rock during fluid transport, but the influence is small because of the low Os concentration in host rocks (Table 4.3; Fig 4.8).

Table 5.3 $^{187}Os/^{188}Os$ values of host rocks at the age of 460 Ma (Beaver Dam deposit, by calculation), comparing with $^{187}Os/^{188}Os$ initial ratio of arsenopyrite samples

Sample Name	Sample division	Host rock 187/188 Os values measured today	Host rock 187/188 Os at 460 Ma by calculation
LC-12-10	10-01	0.812	0.601
	10-02	0.930	0.702
LC-12-11	11-01	0.602	0.579
	11-02	0.690	0.647
LC-12-12	12-01	0.711	0.673
	12-02	0.700	0.668
LC-12-13	13-01	0.885	0.793
LC-12-14	14-01	0.749	0.610
	14-02	0.926	0.734
Sample Name	Re-Os age	Sulfide 187Os/188 Os initial	number of sample divisions (n)
Precise Os_i			
LC-12-15 old	456.0 ± 2.8 Ma	0.796 ± 0.064	3
LC-12-16	461.3 ± 2.9 Ma	0.24 ± 0.12	12
LC-12-17	464 ± 26 Ma	0.51 ± 0.28	6
Imprecise Os_i			
LC-12-15 young	446 ± 13 Ma	-0.1 ± 1.2	5
LC-12-01 mixed age	408 ± 25 Ma	1.04 ± 0.96	10
LC-12-02 young	380.3 ± 4.0 Ma	0.017 ± 0.080	3
LC-12-02 old	437.6 ± 8.2 Ma	-0.18 ± 0.90	9

Table 5.4 Different model ages when calculate using different $^{187}Os/^{188}Os$ initials, LC-12-01, Moose River

Sample division	Model Ages at Os_i of 0.5 (Suggested)	Model Ages at Os_i of 1.0 (Possible highest)	Model Ages at Os_i of 0.125 (Mantle ratio)
01-A1	431.6	420.3	440.2
01-A2	438.4	408.5	460.9
01-C	418.5	409.4	425.2
01-B1	440.9	421.3	455.6
01-B2	422.5	411.9	430.5
01-B3	439.1	424.9	449.7
01-B4	400.6	385.8	411.7
01-B5	438.4	400.3	467.1
01-B6	405.5	395.3	413.2
01-B7	421.6	409	430.9

5.2.3 Implications for Regional Tectonic Events and Paleocontinental Reconstruction

The pre-Acadian age of ca. 460 Ma is reported from all three arsenopyrite samples in the Beaver Dam deposit. No similar age is recorded in the Meguma terrane, but in northern Nova Scotia, U-Pb zircon ages of 460.0 ± 3.4 Ma (Dunn Point Formation) and 454.5 ± 0.7 Ma (McGillivray Brook Formation) are reported in the adjacent Avalon terrane (Murphy et al., 2012). The time of Avalonia separation from Gondwana is controversial: some researchers favor a Neoproterozoic-Cambrian separation (Landing 1996, 2005), whereas others prefer an Early Ordovician rifting (Prigmore et al., 1997; Pollock et al., 2012; Murphy et al., 2012). Based on detrital zircon ages, stratigraphy and fossil records of the Meguma terrane, the Avalon terrane and the Harlech Dome of North Wales, the Meguma was inferred to be originally located in a rift system between Avalonia and West Africa in Cambrian (Waldron et al. 2009, 2011, Fig 2.2). However, whether the Meguma terrane traveled accompanied with Avalonia or not is poorly constrained until the collision during the Acadian orogeny in Devonian. The ca. 460 Ma bimodal volcanic rocks from the Avalon terrane have been interpreted as a back-arc extensional environment, combining with the paleomagnetic and Nd isotope data, implying that Avalonia, drifting as a micro-continent, was accreted to a continent, probably Baltica, in middle-Ordovician time (Murphy et al., 2012; Waldron et al., 2014, Fig 2.3A). In this study, we report the first ca. 460 Ma age from the Meguma terrane, which might represent evidence that Meguma was affected by the same tectonomagmatic processes recorded in Avalonia at 460 Ma, if the similarity in ages is not coincidental. This may then imply a proximal relationship between these two terranes at ca. 460 Ma. In addition, the possibly mantle-derived component in the Beaver Dam hydrothermal fluid at 460 Ma is consistent with the coeval tectonic related magmatic intrusions

known from Avalonia. Therefore the Meguma micro-continent perhaps was located close to Avalonia domain in Middle Ordovician (Fig 2.3 A).

In the southern to southeast Meguma Terrane, there is a wide time gap between deposition of the basal Cambrian-Ordovician Goldenville and Halifax Group and Devonian Acadian metamorphism and the following magmatism. Geologic events such as magmatism or metamorphism prior to the ca. 410 Ma Acadian metamorphism are unknown in this area. In this study, we reported the vein-host arsenopyrite Re-Os isochron and model ages of ca. 440 Ma from the Moose River deposit (Fig 2.1). However, to the west of the Meguma terrane, in the Yarmouth area, zircons from felsic volcanic rocks from the White Rock Formation yielded U-Pb ages of $438\ ^{+3}_{-2}$ Ma and 442 ± 4 Ma (MacDonald et al., 2002, Fig 2.1, 2.5), and zircons of granite from the Brenton Pluton yielded U-Pb age of $439\ ^{+4}_{-3}$ Ma. The felsic rocks of the White Rock Formation and the Brenton Pluton are comagmatic with chemical characteristics of within-plate anorogenic granitic rocks (Keppie and Krogh, 2000, Fig 2.1, 2.5). More recently, in-situ electron microscope U-Pb work on monazite from metasedimentary rocks from south Meguma yields ages of ca. 430-450 Ma for the regional metamorphic rocks (T. Barresi and R. Jamieson, 2014, Unpublished data). These magmatic and metamorphic ages, combined with the arsenopyrite Re-Os age from the Moose River deposit, suggest that the regional hydrothermal and / or tectonothermal activity occurred at ca. 440 Ma, occurring more widely through the Meguma terrane than that was previously known. In addition, the rim growth age of LC-12-15 (ca. 446 Ma or younger) from the Beaver Dam deposit also suggests that there was an extensive thermal event in the Meguma terrane around 440 Ma. The magma intrusion or the regional metamorphism could be the source of the hydrothermal fluids, forcing the quartz vein emplacement, but the tectonic setting for generation of this magmatism and metamorphism remains enigmatic.

Re-Os model ages of 410-400 Ma yielded by arsenopyrite from the Moose River deposit are consistent with the Re-Os age of the Ovens deposit (ca. 407 Ma), suggesting the sulfide and gold mineralization corresponds to Devonian regional metamorphism during the Acadian orogeny (Keppie and Dallmeyer, 1987; Hicks et al., 1999; Morelli et al., 2005, Fig 2.3B).

A Re-Os ischron age of ca. 380 Ma yielded by arsenopyrite from the Moose River deposit is similar to ^{39}Ar-^{40}Ar vein mineral and whole rock ages (ca. 370-380 Ma, Kontak et al., 1993, 1995) and Re-Os arsenopyrite age from the Dufferin deposit (ca. 380 Ma, Morelli et al., 2005), which supports that the vein fluids were driven by post-tectonic magma intrusions (Reynolds et al., 1981; 1987; Clarke et al., 1993; Keppie et al., 1993; 1999). The syn- (ca. 410-400 Ma) and post-Acadian (ca. 380 Ma) deformation ages demonstrate that the late-stage vein formation and gold emplacement of the Moose River deposit occurred during Acadian orogeny, with a time span of 30-40 Ma.

5.3 Implications for U-Pb granite age

Zircon U-Pb ages of two granite samples from the River Lake pluton are 382.2 ± 2.9 Ma and 383.2 ± 2.3 Ma, similar to the U-Pb zircon and monazite TIMS age of the Musquodoboit Batholith (378 ± 1 Ma, Kontak et al., 2004) and the South Mountain Batholith (380 ± 1 Ma, Kontak et al., 2003) (Fig 2.4), indicating widespread post-orogenic granite intrusion in the Meguma terrane. The River Lake pluton is in contact with the Beaver Dam gold deposit (Fig 2.4) and vein minerals from the Beaver Dam deposit yielded ^{39}Ar-^{40}Ar ages of ca. 370-380 Ma (Kontak et al., 1990, 1993). Therefore the hydrothermal fluids of the Beaver Dam deposit at ca. 380 Ma is previously thought to be driven by the River Lake magma emplacement. However, the

new Re-Os data supports that the gold mineralization (ca. 460 Ma) is far earlier than the post-folding magma intrusion (ca. 380 Ma). Whether the River Lake intrusion contributed the multi-stage gold mineralization in the Beaver Dam deposit or not is uncertain. But the widespread granite emplacement at ca. 380 Ma in the Meguma terrane is closely related to the gold mineralization of several deposits, such as the Moose River deposit (isochron age of 380 Ma in this study) and the Dufferin deposit (Morelli et al., 2005).

6.0 Conclusions:

Re-Os arsenopyrite dating was undertaken from two gold deposits in the Meguma terrane; the Beaver Dam deposit and the Moose River deposit. Multi-stage growth of arsenopyrite is evidenced from thin sections and SEM images from both deposits. The Re-Os isotope data also yielded multiple ages: 461 Ma, 446 Ma for the Beaver Dam deposit; 437 Ma, 410-400 Ma, 380 Ma for the Moose River deposit, corresponding to several different tectonic or regional geological events respectively. The Ordovician and Silurian ages are the first reported in Meguma gold districts, providing evidence that the onset of gold mineralization is pre-Acadian in age. The ages of ca. 460 Ma and ca. 440 Ma are compared with magmatic ages known from elsewhere in the Meguma Terrane and in the adjacent Avalon Terrane, together with metamorphic ages of monazite from the Cambro-Ordovician turbidites. Collectively, these ages provide new clues to the pre-Acadian history of the Meguma terrane, and imply a closer link to Avalonia at 460 Ma than has been previously interpreted. The Devonian ages are related to syn- to post- Acadian metamorphic and magmatic events, consistent with previous Re-Os and ^{39}Ar-^{40}Ar age constraints, supporting the complex multi-stage gold mineralization model. The U-Pb age of the granite adjacent to the Beaver Dam deposit is 380 Ma, unrelated to the Ordovician arsenopyrite formation but coeval with other post-folding magma intrusions.

7.0 References:

Arne, D.C., Bierlein, F.P., Morgan, J.W., and Stein, H.J., 2001, Re-Os dating of sulfides associated with gold mineralization in central Victoria, Australia: Economic Geology, v. 96, p. 1455–1459.

Ayora, C., Ribera, F., and Cardellach, E., 1992, The genesis of the arsenopyrite gold veins from the Vall de Ribes District, eastern Pyrenees, Spain: Economic Geology, v. 87, p. 1877–1896.

Barresi, T., and Jamieson, R., 2014, Monazite Dating of Meguma Group Metamorphism: unpublished.

Bierlein, F., and Smith, P., 2003, The Touquoy Zone deposit: an example of " unusual" orogenic gold mineralisation in the Meguma Terrane, Nova Scotia, Canada: Canadian Journal of Earth Sciences, v. 40, p. 447–466.

Bradley, D.C., 1983, Tectonics of the Acadian orogeny in New England and adjacent Canada: The Journal of Geology, v. 91, p. 381–400.

Birck, J.L., Roy-Barman, M., and Capmas, F., 1997, Re-Os Isotopic Measurements at the Femtomole Level in Natural Samples. Geostandards newsletter, v. 21.1, p. 9-27.

Christie, A.B., Corner, N.G., Bierlein, F.P., Smith, P.K., Ryan, R.J., and Arne, D.C., 2000, Disseminated gold in turbidite-hosted gold deposits of Reefton (South Island, New Zealand), Victoria (Australia) and Nova Scotia (Canada): New Zealand, v. 29, p. 31.

Clarke, D.B., and Halliday, A.N., 1980, Strontium isotope geology of the South Mountain batholith, Nova Scotia: Geochimica et Cosmochimica Acta, v. 44, p. 1045–1058.

Clarke, D.B., Chatterjee, a. K., and Giles, P.S., 1993, Petrochemistry, tectonic history, and Sr-Nd systematics of the Liscomb Complex, Meguma Lithotectonic Zone, Nova Scotia: Canadian Journal of Earth …, v. 30, p. 449–464.

Clarke, D.B., Macdonald, M.A., and Tate, M.C., 1997, Late Devonian mafic-felsic magmatism in the Meguma Zone, Nova Scotia: Geological Society of America Memoirs, v. 191, p. 107–127.

Creaser, R.A., Papanstassiou, D.A., and Wasserburg, G.J., 1991, Negative thermal ion mass spectrometry of osmium, rhenium, and iridium: Geochimica et Cosmochimica Acta, v. 55, p. 397–401.

Creaser, R.A., Sannigrahi, P., Chacko, T., and Selby, D., 2002, Further evaluation of the Re-Os geochronometer in organic-rich sedimentary rocks: A test of hydrocarbon maturation effects in the Exshaw Formation, Western Canada Sedimentary Basin: Geochimica et Cosmochimica Acta, v. 66, p. 3441–3452.

Crusius, J., Calve, S., Pedersen, T., and Sage, D., 1996, Rhenium and molybdenum enrichments in sediments as indicators of oxic, suboxic and sulfidic conditions of deposition: Earth and Planetary Science Letters, p. 65–78.

Eberz, G., Clarke, D., Chatterjee, A.K., and Giles, P.S., 1991, Chemical and isotopic composition of the lower crust beneath the Meguma Lithotectonic Zone, Nova Scotia: evidence from granulite facies xenoliths: Contributions to Mineralogy and Petrology, v. 109, p. 69–88.

Faribault, E.R., 1899, On the gold measures of Nova Scotia and deep mining: Journal of the Canadian Mining Institute, v. 2, p. 119-128.

Fleetl, M.E., and Mumin, A.H., 1997, Gold-bearing arsenian pyrite and marcasite and arsenopyrite from Carlin Trend gold deposits and laboratory synthesis: American Mineralogist, v. 82, p. 182–193.

Goldfarb, R.J., Groves, D.I., and Gardoll, S., 2001, Orogenic gold and geologic time: a global synthesis: Ore Geology Reviews, v. 18, p. 1–75.

Gramlich, J.W., Murphy, T.J., Grrner, E.L., and Shields, W.R., 1973, Absolute isotopic Abundance Ratio and Atomic Weight of a Reference Sample of Rhenium: Journal of Research of the National Bureau of Standards - A Physics and Chemistry, v. 77, p. 691–698.

Graves, M.C., and Zentilli, M., 1982, A review of the geology of gold in Nova Scotia: Canadian Institute Mining and Metallurgy Special, v. 24, p. 233-242.

Graves, M.C., and Zentilli, M., 1988, The lithochemistry of metal-enriched coticules in the Goldenville-Halifax transition zone of the Meguma Group, Nova Scotia, Geological Survey of Canada, Paper 88-1B, p. 251-261.

Groves, D.I., Goldfarb, R.J., Gebre-Mariam, M., Hagemann, S.G., and Robert, F., 1998, Orogenic gold deposits: A proposed classification in the context of their crustal distribution and relationship to other gold deposit types: Ore Geology Reviews, v. 13, p. 7–27.

Henderson, M.N., and Henderson, J.R., 1986, Constraints on the Origin of Gold in the Meguma Zone, Ecum secum area, Nova Scotia: Marintime Sediments and Atlantic Geology, v. 22, p. 1–13.

Henderson, J.R., Henderson, M.N., and Wright, T.O., 1990, Water-sill hypothesis for the origin of certain veins in the Meguma Group, Nova Scotia, Canada: Geology, v. 18, p. 654–657.

Hicks, R.J., Jamieson, R. a., and Reynolds, P.H., 1999, Detrital and metamorphic 40Ar/39Ar ages from muscovite and whole-rock samples, Meguma Supergroup, southern Nova Scotia: Canadian Journal of Earth Sciences, v. 36, p. 23–32.

Hnatyshin, D., 2012, Geochronology and Trace Element Characteristics of Pyrite from Selected Carbonate Hosted Pb-Zn Ore Deposits: 138 p.

Hnatyshin, D., Creaser, R. a., Wilkinson, J.J., and Gleeson, S. a., 2015, Re-Os dating of pyrite confirms an early diagenetic onset and extended duration of mineralization in the Irish Zn-Pb ore field: Geology, v. 43, p. 143–146.

Horne, R., and Culshaw, N., 2001, Flexural-slip folding in the Meguma Group, Nova Scotia, Canada: Journal of Structural Geology, v. 23, p. 1631–1652.

Horne, R., and Pelley, D., 2007, Geological Transect of the Meguma Terrane from Centre Musquodoboit to Tangier: NS Mineral Resources Branch, Report of Activities, v. ME 2007-1, p. 71–89.

Hunt, T.S., 1968, Report on the gold region of Nova Scotia: Geological Survey of Canada, 48 p.

Kendall, B.S., Creaser, R. a., Ross, G.M., and Selby, D., 2004, Constraints on the timing of Marinoan "Snowball Earth" glaciation by 187Re–187Os dating of a Neoproterozoic, post-glacial black shale in Western Canada: Earth and Planetary Science Letters, v. 222, p. 729–740.

Keppie, J.D., 1976, Structural model for saddle reef and associated gold veins in the Meguma Group, Nova Scotia: Nova Scotia Department of Mines and Energy Paper 76-1, 34 p.

Keppie, J.D., and Dallmeyer, R.D., 1987, Dating Meguma-Avalon Terrane Accretion: An Example from the Meguma and Avalon Composite Terranes in the Northern Appalachians: Tectonics, v. 6, p. 831–847.

Keppie, J.D., Dallmeyer, R.D., Krogh, T.E., and Aftalion, M., 1993, Dating mineralization using several isotopic methods: an example from the South Mountain Batholith, Nova Scotia, Canada: Chemical Geology, v. 103, p. 251–270.

Kepple, J.D., and Dallmeyer, R.D., 1995, Late Paleozoic collision, delamination, short-lived magmatism, and rapid denudation in the Meguma Terrane (Nova Scotia, Canada): constraints from 40Ar/39Ar isotopic data: Canadian Journal of Earth Sciences, v. 659, p. 644–659.

Keppie, J.D., and Krogh, T.E., 1999, U - Pb Geochronology of Devonian Granites in the Meguma Terrane of Nova Scotia , Canada : Evidence for Hotspot Melting of a Neoproterozoic Source: The Journal of Geology, v. 107, p. 555–568.

Keppie, J.D., and Krogh, T.E., 2000, 440 Ma igneous activity in the Meguma terrane, Nova Scotia, Canada: Part of the Appalachian overstep sequence? Amerian Journal of Science, v. 300, p. 528–538.

Kontak, D.J., Smith, P.K., Kerrich, R., and Williams, P.F., 1990a, Integrated model for Meguma Group lode gold deposits, Mova Scotia, Canada: Geology, v. 18, p. 238–242.

Kontak, D.J., Smith, P., Reynolds, P., and Taylor, K., 1990b, Geological and 40 Ar/39 Ar geochronological constraints on the timing of quartz vein formation in Meguma Group lode-gold deposits, Nova Scotia: Atlantic Geology, v. 26, p. 201–227.

Kontak, D.J., and Smith, P.K., 1993, A metaturbidite-hosted lode gold deposit: the beaver dam deposit, Nova Scotia. Vein paragenesis and mineral chemistry: Canadian Mineralogist, v. 31, p. 471–522.

Kontak, D.J., and Reynolds, P.H., 1994, 40Ar/39Ar dating of metamorphic and igneous rocks of the Liscomb Complex, Meguma Terrane, southern Nova Scotia, Canada: Canadian Journal of Earth Sciences, v. 31, p. 1643–1653.

Kontak, D.J., and Kerrich, R., 1995, Geological and geochemical studies of a metaturbidite-hosted lode gold deposit; the Beaver Dam Deposit, Nova Scotia; II, Isotopic studies: Economic Geology, v. 90, p. 885–901.

Kontak, D.J., and Kerrich, R., 1997, An Isotopic(C, O, Sr) Study of Vein Gold Deposits in the Meguma Terrane, Nova Scotia: Implication for Source Reservoirs: Economic Geology, v. 92, p. 161–180.

Kontak, D.J., Horne, R.J., Sandeman, H., Archibald, D., and Lee, J.K.W., 1998, 40Ar/39Ar dating of ribbon-textured veins and wall-rock material from Meguma lode gold deposits, Nova Scotia: implications for timing and duration of vein formation in slate-belt hosted vein gold deposits: Canadian Journal of Earth Sciences, v. 35, p. 746–761.

Kontak, D.J., Ham, L.J., and Dunning, G., 2004, U-Pb dating of the Musquodoboit Batholith , southern Nova Scotia : evidence for a protracted magmatic-hydrothermal eventin a Devonian intrusion: Atlantic Geology, v. 40.

Kontak, D.J., and Horne, R.J., 2010, A Multi-stage Origin for the Meguma Lode Gold Deposits, Nova Scotia, Canada: A Possible Global Model for Slate Belt-hosted Gold Mineralization: Gold Metallogeny, p. 58–82.

Kontak, D.J., Horne, R.J., and Kyser, K., 2011, An oxygen isotope study of two contrasting orogenic vein gold systems in the Meguma Terrane, Nova Scotia, Canada, with implications for fluid sources and genetic models: Mineralium Deposita, v. 46, p. 289–304.

Kontak, D., Horne, R., Creaser, R., Petrus, J., and Archibald, D., 2013, A petrological and geochronological study of a 360 Ma metallogenic event in Maritime Canada with implications for lithophile-metal mineralization in the Canadian Appalachians: Canadian Journal of Earth Sciences, v. 50, p. 1147–1163.

Landing, E., and Westrop, S.R., 1996, Upper Lower Cambrian depositional sequence in Avalonian New Brunswick: Canadian Journal of Earth Sciences, v. 33, p. 404–417.

Landing, E., 2005, Early Paleozoic Avalon-Gondwana unity: An obituary - Response to "Palaeontological evidence bearing on global Ordovician-Silurian continental reconstructions" by R.A. Fortey and L.R.M. Cocks: Earth-Science Reviews, v. 69, p. 169–175.

Lin, S., and Corfu, F., 2002, Structural Setting and Geochronology of Auriferous Quartz Veins at the High Rock Island Gold Deposit, Northwestern Superior Province , Manitoba, Canada: Economic Geology, v. 97, p. 43–57.

Ludwig, K.R., 1980, Calculation of uncertainties of U-Pb isotope data: Earth and Planetary Science Letters, v. 46, p. 212–220.

Ludwig, K.R., 2012, A Geochronological Toolkit for Microsoft Excel: Berkeley Geochronology Center Special Publications, p. 1–75.

MacDonald, A.L., Barr, M.S., White, E.C., and Ketchum, W.F.J., 2002, Petrology, age, and tectonic setting of the White Rock Formation, Meguma terrane, Nova Scotia: evidence for Silurian continental rifting: Canadian Journal of Earth Sciences, p. 259–277.

Malcolm, W., 1929, Gold Fields of Nova Scotia: Geological Survey of Canada, Memoir 156, 253 p.

Mawer, C.K., 1987, Mechanics of formation of gold-bearing quartz veins, Nova Scotia, Canada: Tectonophysics, v. 135, p. 99–119.

Mawer, C.K., and White, J.C., 1987, Sense of displacement on the Cobequid–Chedabucto fault system, Nova Scotia, Canada: Canadian Journal of Earth Sciences, v. 24, p. 217–223.

McBride, D.E., 1978, Geology of the Ecum Secum Area, Halifax and Guysborough Counties, Nova Scotia: Nova Scotia Department of Mines, v. 78-1, p. 12.

Morelli, R.M., Creaser, R.A., Selby, D., Kontak, D.J., and Horne, R.J., 2005, Rhenium-Osmium Geochronology of Arsenopyrite in Meguma Group Gold Deposits, Meguma Terrane, Nova Scotia, Canada: Evidence for Multiple Gold-Mineralizing Events: Economic Geology, v. 100, p. 1229–1242.

Morelli, R.M., Creaser, R. a., Seltmann, R., Stuart, F.M., Selby, D., and Graupner, T., 2007, Age and source constraints for the giant Muruntau gold deposit, Uzbekistan, from coupled Re-Os-He isotopes in arsenopyrite: Geology, v. 35, p. 795.

Morelli, R.M., Bell, C.C., Creaser, R. A., and Simonetti, A., 2010, Constraints on the genesis of gold mineralization at the Homestake Gold Deposit, Black Hills, South Dakota from rhenium–osmium sulfide geochronology: Mineralium Deposita, v. 45, p. 461–480.

Morford, J.L., Martin, W.R., François, R., and Carney, C.M., 2009, A model for uranium, rhenium, and molybdenum diagenesis in marine sediments based on results from coastal locations: Geochimica et Cosmochimica Acta, v. 73, p. 2938–2960.

Muecke, G.K., P.Elias, and Reynolds, P.H., 1988, Hercynian/Alleghanian overprinting of an acadian terrane: 40Ar/39Ar studies in the Meguma zone, Nova Scotia, Canada: Chemical Geology, v. 73, p. 153–167.

Murphy, J.B., Oppliger, L.G., Brimhall, H.G.J., and Hynes, A., 1998, Plume-modified orogeny : An example from the western United States: Geology, v. 26, p. 731–734.

Murphy, J.B., and Keppie, J.D., 2005, The Acadian Orogeny in the Northern Appalachians: International Geology Review, v. 47, p. 37–41.

Murphy, J.B., Hamilton, M.A., and Leblanc, B., 2012, Tectonic significance of Late Ordovician silicic magmatism , Avalon terrane , northern Antigonish Highlands, Nova Scotia: Canadian Journal of Earth Sciences, v. 358, p. 346–358.

Ootes, L., Morelli, M.R., Creaser, A.R., Lentz, R.D., Falck, H., and Davis, J.W., 2011, The Timing of Yellowknife Gold Mineralization: A Temporal Relationship with Crustal Anatexis? Economic Geology, p. 713–720.

Pollock, J.C., Hibbard, J.P., and Staal, C.R. Van, 2012, A paleogeographical review of the peri-Gondwanan realm of the Appalachian orogen: Canadian Journal of Earth Sciences, v. 49, p. 259–288.

Prigmore, J.K., Butler, A.J., and Woodcock, N.H., 1997, Rifting during separation of Eastern Avalonia from Gondwana: Evidence from subsidence analysis: Geology, v. 25, p. 203–206.

Reynolds, P.H., Zentilli, M., and Muecke, G.K., 1981, K-Ar and 40Ar/39Ar geochronology of granitoid rocks from southern Nova Scotia: Its bearing on the geological evolution of the Meguma Zone of the Appalachians: Canadian Journal of Earth Sciences, v. 18, p. 386–394.

Reynolds, P.H., Elias, P., Muecke, G.K., and Grist, A.M., 1987, Thermal history of the southwestern Meguma zone , Nova Scotia , from an 40Ar / 39Ar and fission track dating study of intrusive rocks: Canadian Journal of Earth Sciences, v. 24, p. 1952–1965.

Ryan, R.J., and Smith, P.K., 1998, A review of the mesothermal gold deposits of the Meguma Group, Nova Scotia, Canada: Ore Geology Reviews, v. 13, p. 153–183.

Sangster, A.L., 1990, Metallogeny of the Meguma Terrane, Nova Scotia, Mineral Deposit Studies in Nova Scotia, Volume 1: Geological Survey of Canada, Paper 90-8, p. 115-162.

Sangster, A.L., 1992, Light stable isotope evidence for a metamorphogenic origin for bedding-parallel, gold-bearing veins in Cambrian flysch, Meguma Group, Nova Scotia, International Association on the Genesis of Ore Deposits, Eighth Quadrennial Symposium: Exploration and Mining Geology, v. 1, p. 69-79.

Sangster, A.L., and Smith, P.K., 2007, Metallogenic summary of the Meguma gold deposits, Nova Scotia: Mineral Deposits Division, p. 723–732.

Schenk, P.E., 1997, Sequence stratigraphy and proveance on Gondwana's margin: The Meguma Zone (Cambrian to Devonian) of Nova Scotia, Canada: Geological Society of American Bulletin, v. 109, p. 395–409.

Selby, D., and Creaser, R., 2001a, Late and mid-Cretaceous mineralization in the northern Canadian Cordillera: Constraints from Re-Os molybdenite dates: Economic Geology, v. 96, p. 1461–1467.

Selby, D., and Creaser, R., 2001b, Re-Os geochronology and systematics in molybdenite from the Endako porphyry molybdenum deposit, British Columbia, Canada: Economic Geology, v. 96, p. 197–204.

Selby, D., Creaser, R., and Hart, C., 2002, Absolute timing of sulfide and gold mineralization: A comparison of Re-Os molybdenite and Ar-Ar mica methods from the Tintina Gold Belt, Alaska: Geology, v. 30, p. 791–794.

Selby, D., and Creaser, R.A., 2003, Re–Os geochronology of organic rich sediments: an evaluation of organic matter analysis methods: Chemical Geology, v. 200, p. 225–240.

Shirey, S.B., and Walker, R.J., 1995, Carius Tube Digestion for Low-Blank Rhenium-Osmiun Analysis: Analytical Chemistry, v. 67, p. 2136–2141.

Simonetti, A., Heaman, L.M., Hartlaub, R.P., Creaser, R.A., Machattie, T.G., and Bo, C., 2005, U–Pb zircon dating by laser ablation-MC-ICP-MS using a new multiple ion counting Faraday collector array: The Royal Society of Chemistry, v. 20, p. 677–686.

Simonetti, A., Heaman, L.M., Chacko, T., and Banerjee, N.R., 2006, In situ petrographic thin section U–Pb dating of zircon, monazite, and titanite using laser ablation–MC–ICP-MS: International Journal of Mass Spectrometry, v. 253, p. 87–97.

Waldron, J.W.F., White, C.E., Barr, S.M., Simonetti, A., and Heaman, L.M., 2009, Provenance of the Meguma terrane, Nova Scotia: rifted margin of early Paleozoic Gondwana: Canadian Journal of Earth Sciences, v. 46, p. 1–8.

Waldron, J.W.F., Schofield, D.I., White, C.E., and Barr, S.M., 2011, Cambrian successions of the Meguma Terrane, Nova Scotia, and Harlech Dome, North Wales: dispersed fragments of a peri-Gondwanan basin? Journal of the Geological Society, v. 168, p. 83–98.

Waldron, J.W.F., Schofield, D.I., Murphy, J.B., and Thomas, C.W., 2014, How was the Iapetus Ocean infected with subduction? Geology, v. 42, p. 1095–1098.

White, C.E., and Barr, S.M., 2010, Lithochemistry of the Lower Paleozoic Goldenville and Halifax groups , southwestern Nova Scotia , Canada : Implications for stratigraphy , provenance , and tectonic setting of the Meguma terrane: Geological Society of America Memoir, v. 206, p. 347–366.

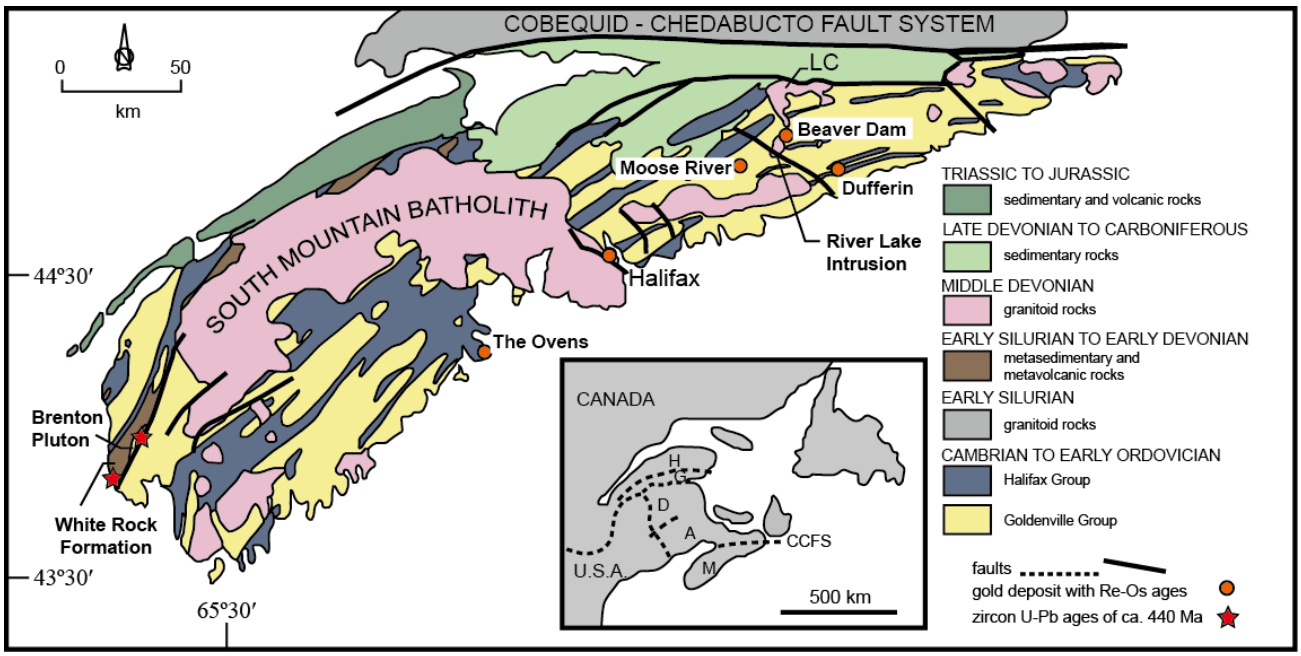

Figure 2.1: Regional geological map of the Meguma terrane, southern Nova Scotia, Canada, showing the location of Meguma gold deposits sampled for Re-Os dating: the Beaver Dam, Moose River; and previous Re-Os age constrained gold deposits: The Ovens, Dufferin. The Liscomb Complex (LC) and South Mountain batholith emplaced during the widespread Devonian magma events. The inset map shows the distribution of terranes in the Canadian part of the Appalachian orogen, including the Meguma terrane (MT), the Avalon (A), Dunnage (D) and Humber (H) terranes (modified from Kontak and Horne, 2010).

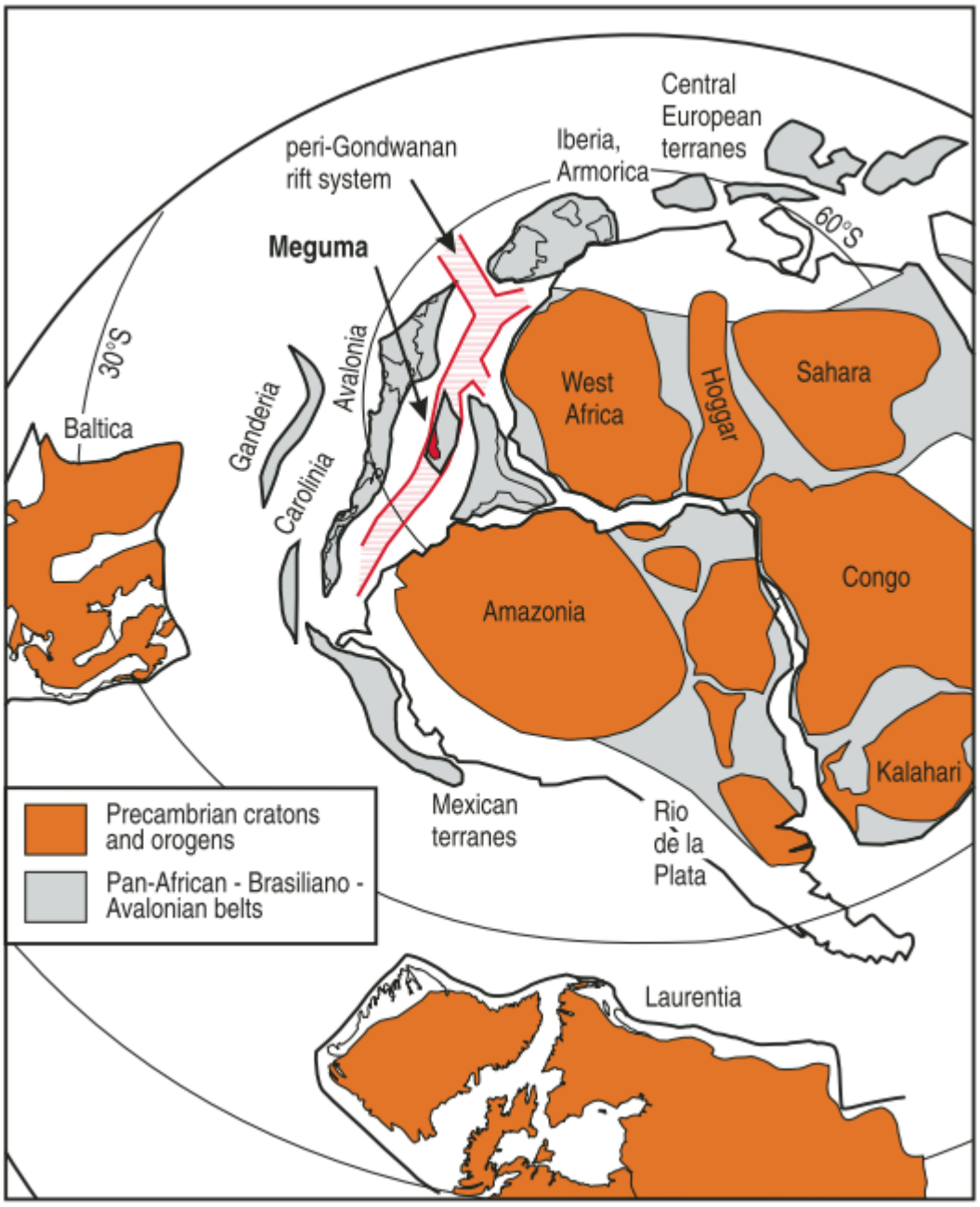

Figure 2.2: Possible Cambrian (ca. 500 Ma) continental reconstruction showing the location of Meguma (White and Barr (2010) modified from Waldron et al., 2009).

(A)

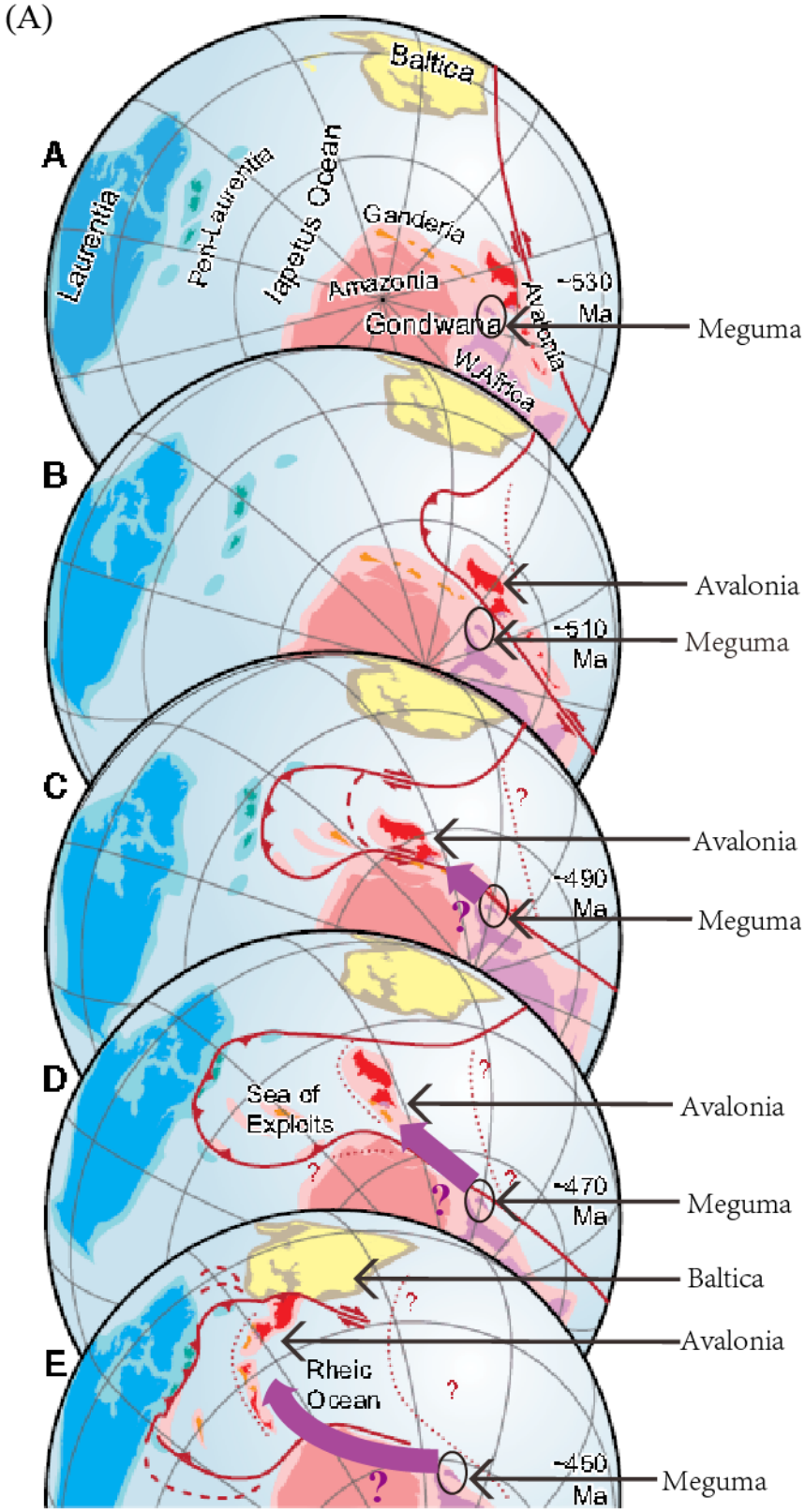
A
Baltica
Laurentia
Peri-Laurentia
Iapetus Ocean
Ganderia
Amazonia
Gondwana
W.Africa
Avalonia
~530 Ma
Meguma
B
Avalonia
~510 Ma
Meguma
C
Avalonia
~490 Ma
Meguma
D
Sea of Exploits
Avalonia
~470 Ma
Meguma
Baltica
E
Avalonia
Rheic Ocean
~450 Ma
Meguma

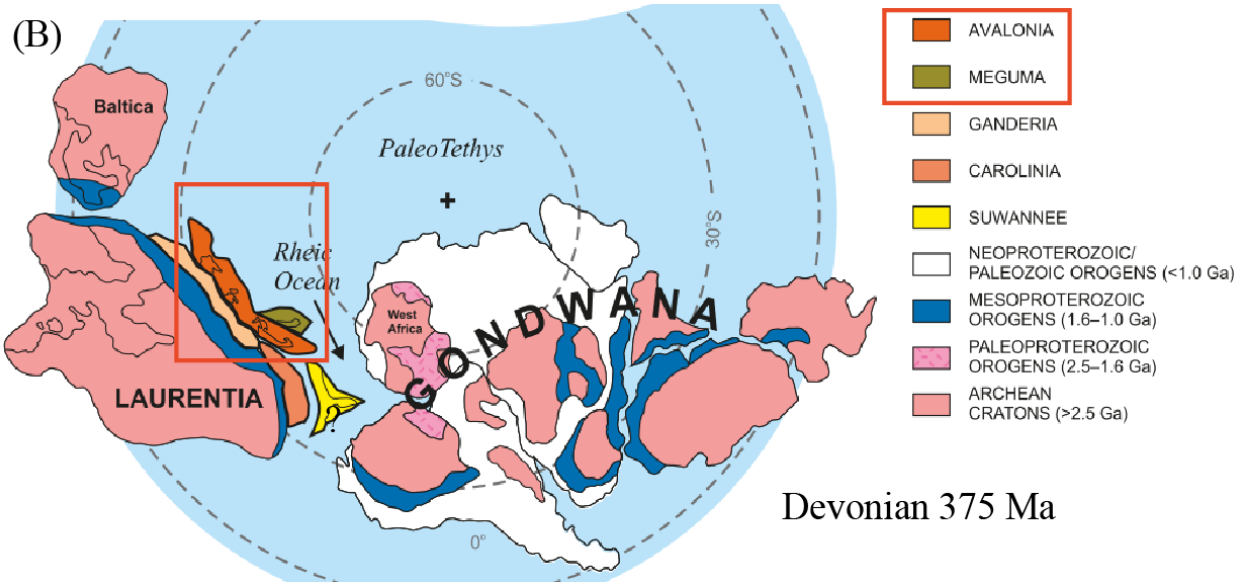

Figure 2.3: (A) The possible terrane locations and collisions at five time intervals in Cambrian-Ordovician time, showing the subduction zone, travel path of the Avalonia, and the closure of the Iapetus Ocean. But the exact location of the Meguma remains undiscussed (Modified from Waldron et al., 2014). (B) Devonian proposed paleogeographic reconstruction, showing the location of the Meguma (green color) and the Avalonia (orange color) at the age of 375 Ma (Modified from Pollock et al., 2012).

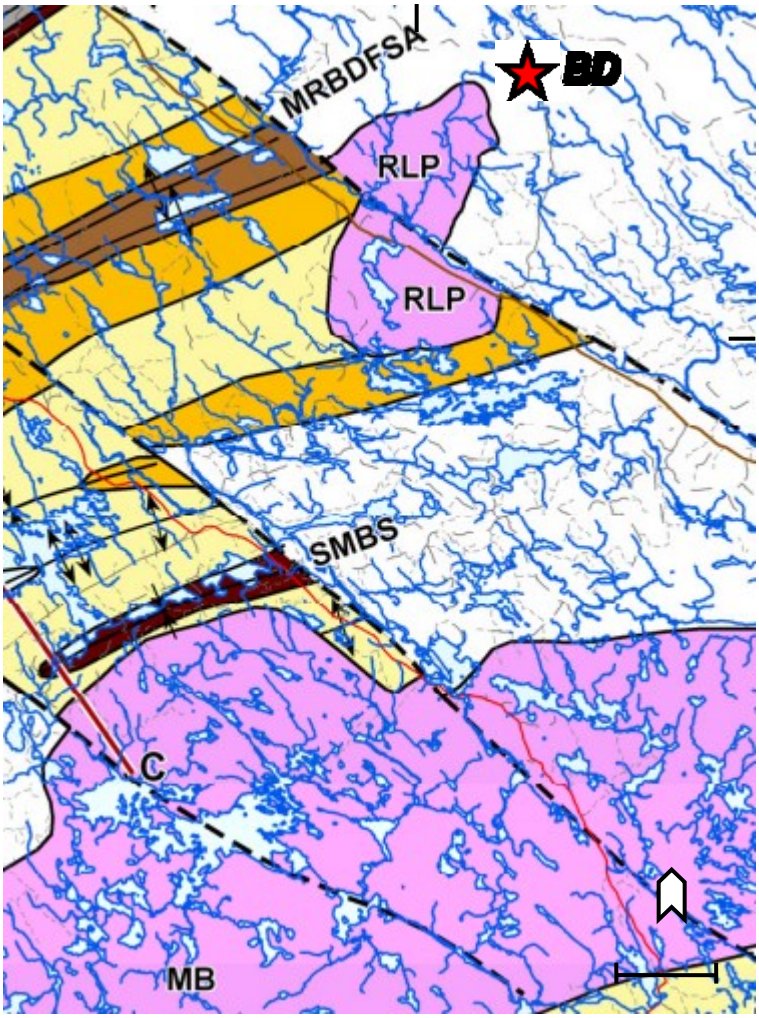

Figure 2.4: Part of the geological map of a transection of the Meguma Terrane on the Eastern Shore of Nova Scotia (modified from Horne and Pelley, 2006). RLP=River Lake pluton; MB= Musquodoboit Batholith; BD = Beaver Dam gold deposit; MRBDFMSA=Moose River-Beaver Dam-Fifteen Mile Stream Anticline; SMBS=St. Marys Bay Syncline.

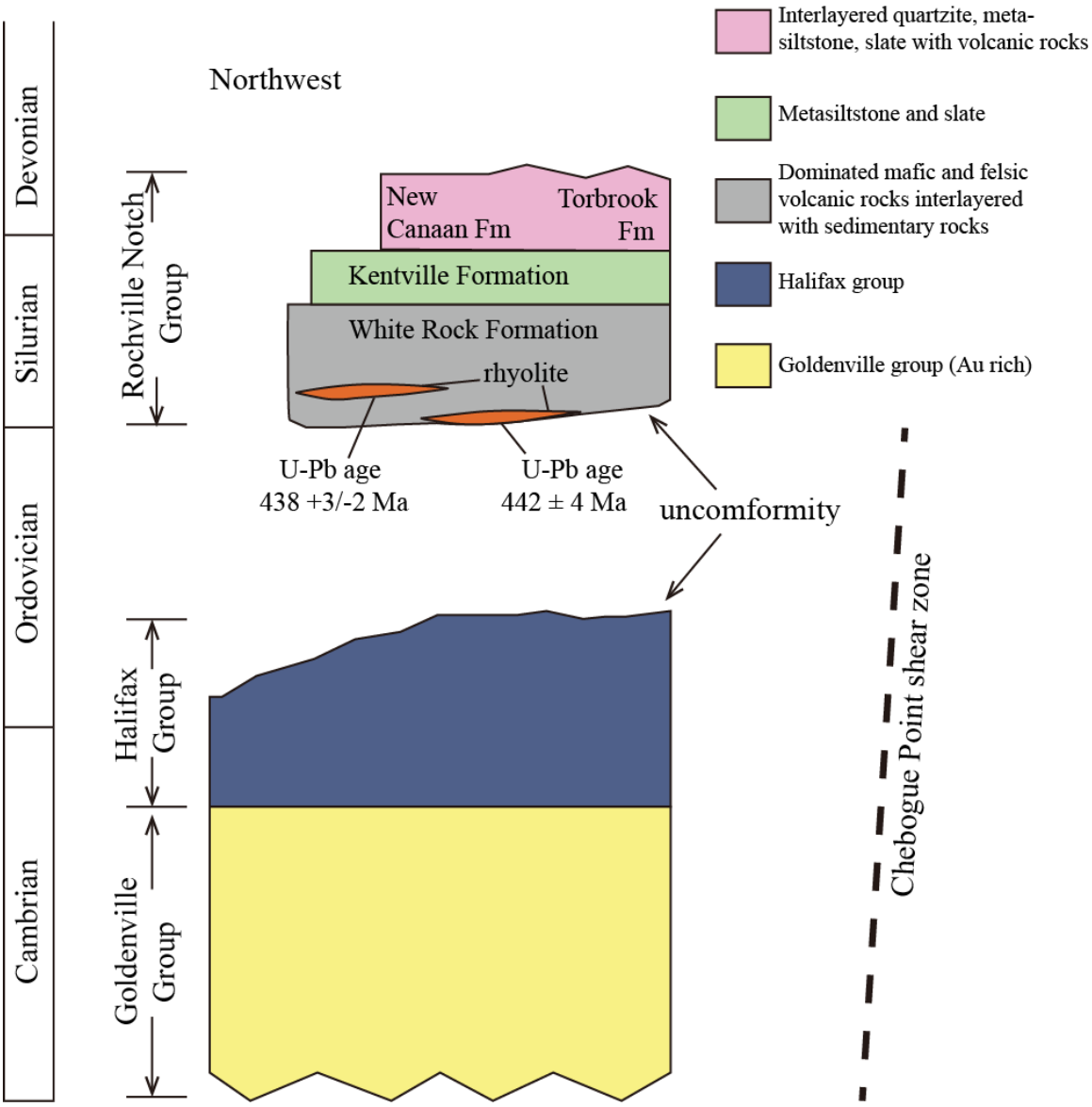

Figure 2.5: Stratigraphy in the Meguma terrane northwest of the Chebogue Point shear zone, showing the Silurian Rochville Notch Group (consisting of sedimentary and volcanic rocks) uncomformity deposited on Goldenville and Halifax Group. And the U-Pb age constrain of the White Rock Formation (modified from White et al., 2010, 2012).

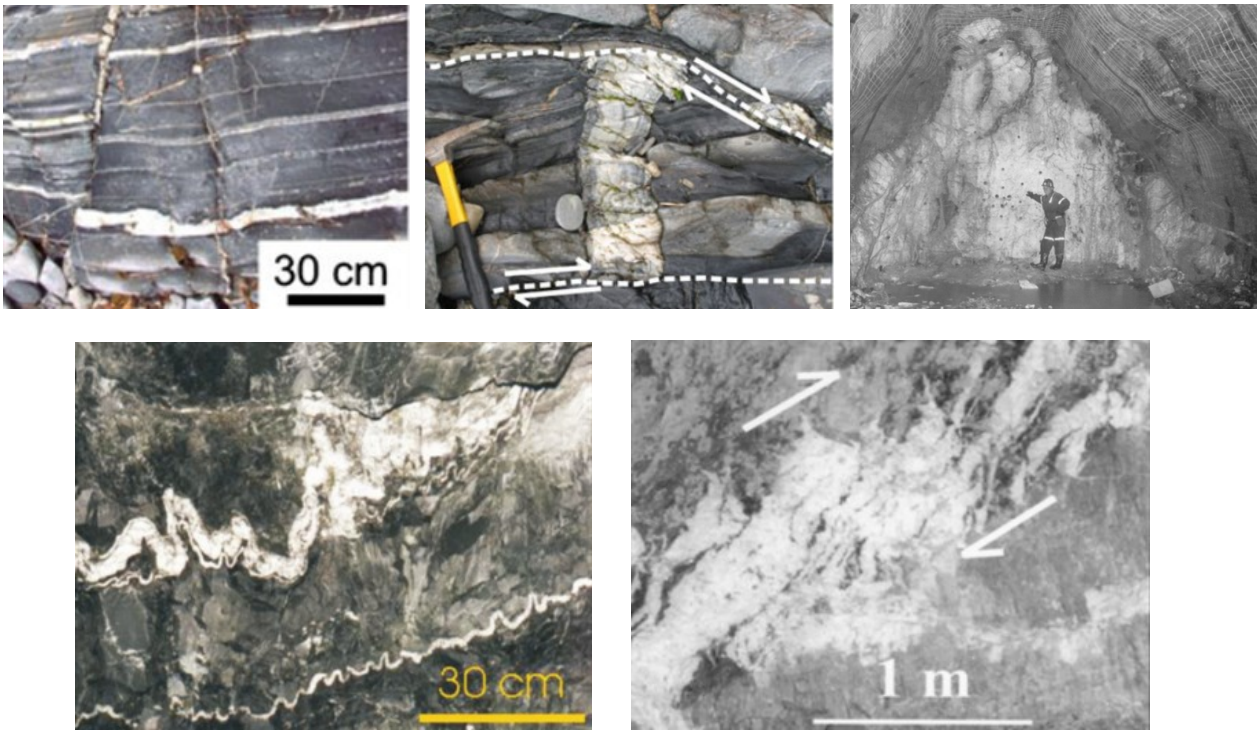

Figure 2.6: Different quartz vein types from gold deposits in the Maguma terrane: (A) Bedding-concordant (horizontal) and discordant (subvertical) veins cutting layered metasiltstone host rock, the Ovens (Kontak et al., 2011). (B) Discordant vein in metasiltstone, the Ovens (Kontak et al., 2011). (C) General cross-section of saddle-reef veins, Dufferin (Horne and Jodrey, 2001). (D) A buckled vein in the Tangier gold deposit (Kontak and Horne, 2010). (E) Strongly sheared en echelon veins in the Dufferin gold deposit (Horne and Jodrey, 2001).

Figure 2.7: Hand specimen images of arsenopyrite samples from quartz vein: (A) Small arsenopyrite crystals in quartz vein, LC-12-01, Moose River. (B) Arsenopyrite in vein, LC-12-02, Moose River. (C, D) Coarse arsenopyrite in quartz vein, LC-12-15, Beaver Dam. (E) Large arsenopyrite crystal in thin calcite vein, LC-12-16, Beaver Dam. (F) Arsenopyrite in quartz vein, LC-12-17, Beaver Dam.

Figure 2.8: Hand specimen images of host rocks, granite (outcrop) and visible gold: (A) Dark shale host-rock, LC-12-10, Beaver Dam. (B) Black shale host-rock, LC-12-14, Beaver Dam. (C) Granite LC-12-06 at outcrops, River Lake pluton. (D) Visible gold in the drill core BD-09-141, Beaver Dam.

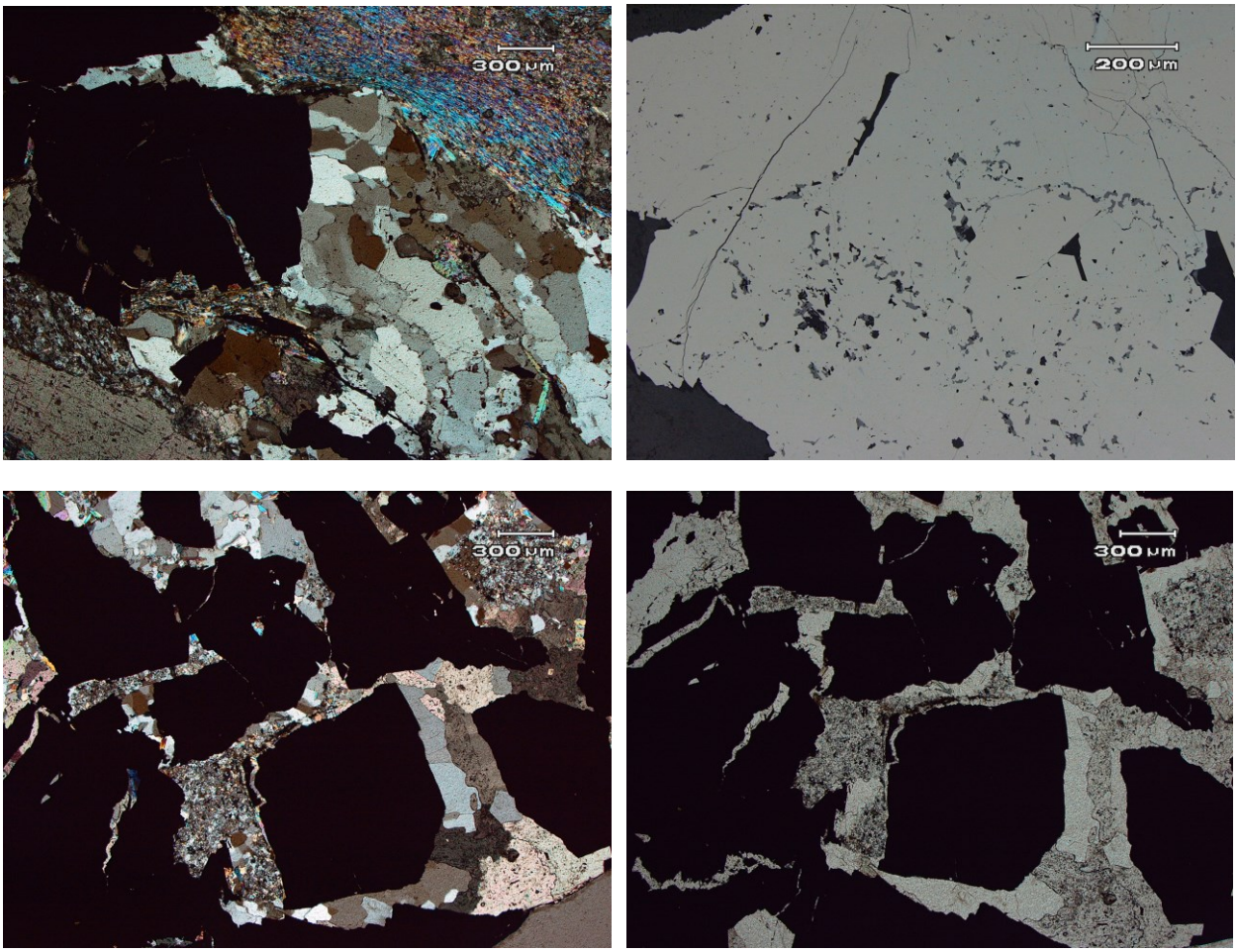

Figure 2.9: Thin section images of vein and arsenopyrite of sample LC-12-01: (A) Arsenopyrite from quartz vein, cross polarized transmitted light. (B) Inclusions in arsenopyrite crystal, plane polarized reflected light. (C) Arsenopyrite (opaque) crystals in quartz vein, cross polarized transmitted light. (D) Arsenopyrite (opaque) in quartz vein, plane polarized transmitted light.

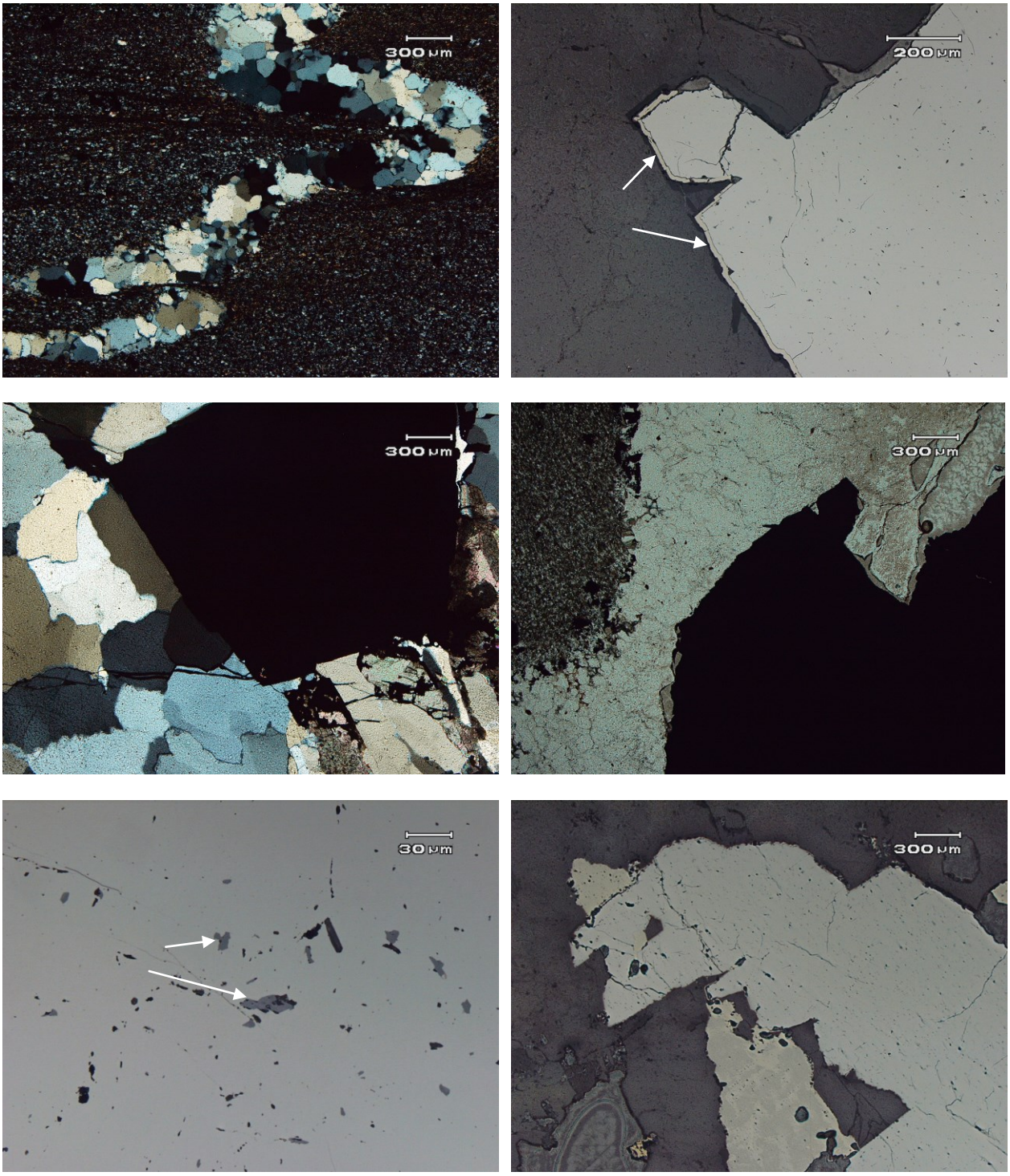

Figure 2.10: Thin section images of vein and arsenopyrite of sample LC-12-02: (A) Arsenopyrite bearing quartz vein, cross polarized transmitted light. (B) Pyrite rim out of arsenopyrite crystal, plane polarized reflected light. (C) Arsenopyrite crystal in quartz vein, cross polarized transmitted light. (D) Arsenopyrite in quartz vein in host rock, plane polarized transmitted light.

(E) Sphalerite inclusions in arsenopyrite crystal, plane polarized reflected light. (F) Arsenopyrite grows associated with pyrite, plane polarized reflected light.

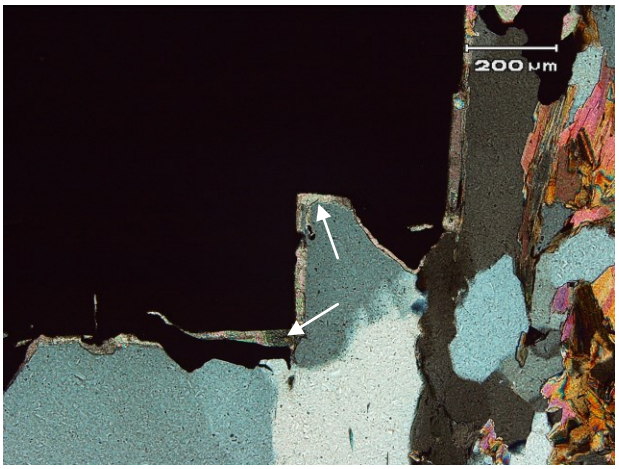

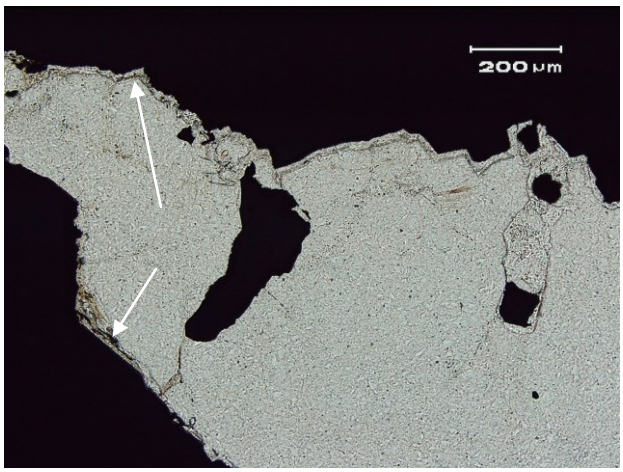

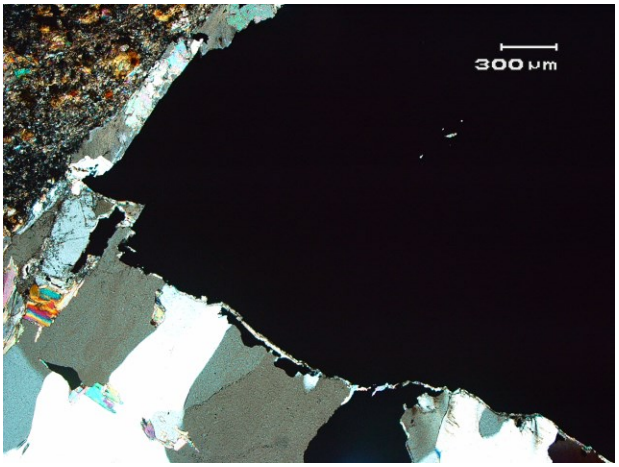

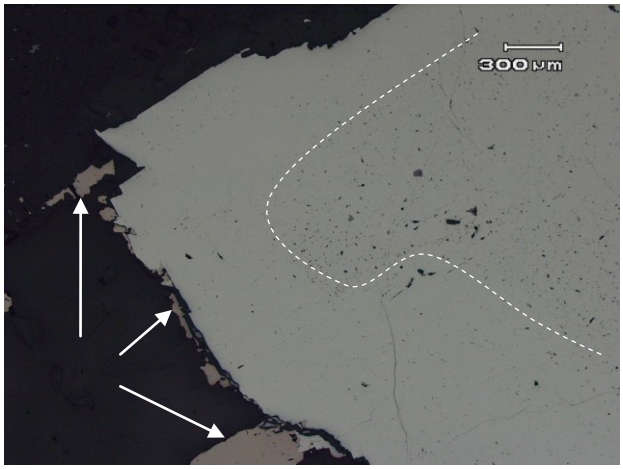

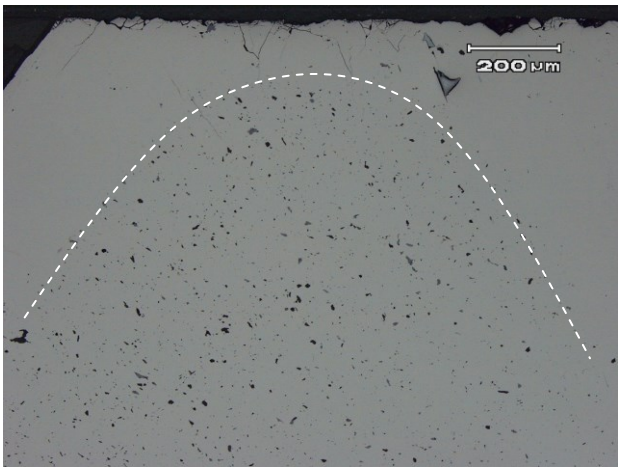

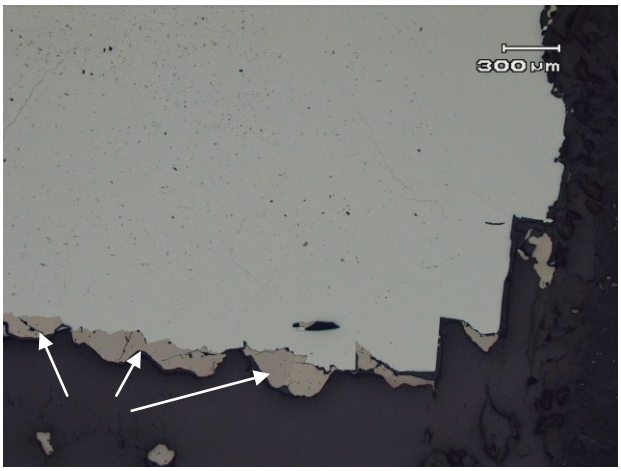

Figure 2.11: Thin section images of vein and arsenopyrite of sample LC-12-15: (A) Arsenopyrite crystal with calcite rim in quartz vein, cross polarized transmitted light. (B) Arsenopyrite crystal with calcite rim in quartz vein, plane polarized transmitted light. (C) Arsenopyrite bearing quartz vein in host rock, cross polarized transmitted light. (D) Pyrrhotite rim out of arsenopyrite crystal, inclusion rich core and clean rim of arsenopyrite crystal, plane polarized reflected light. (E) Arsenopyrite crystal, inclusion rich core and clean rim, plane polarized reflected light. (F) Coarse arsenopyrite with pyrrhotite rim, plane polarized reflected light.

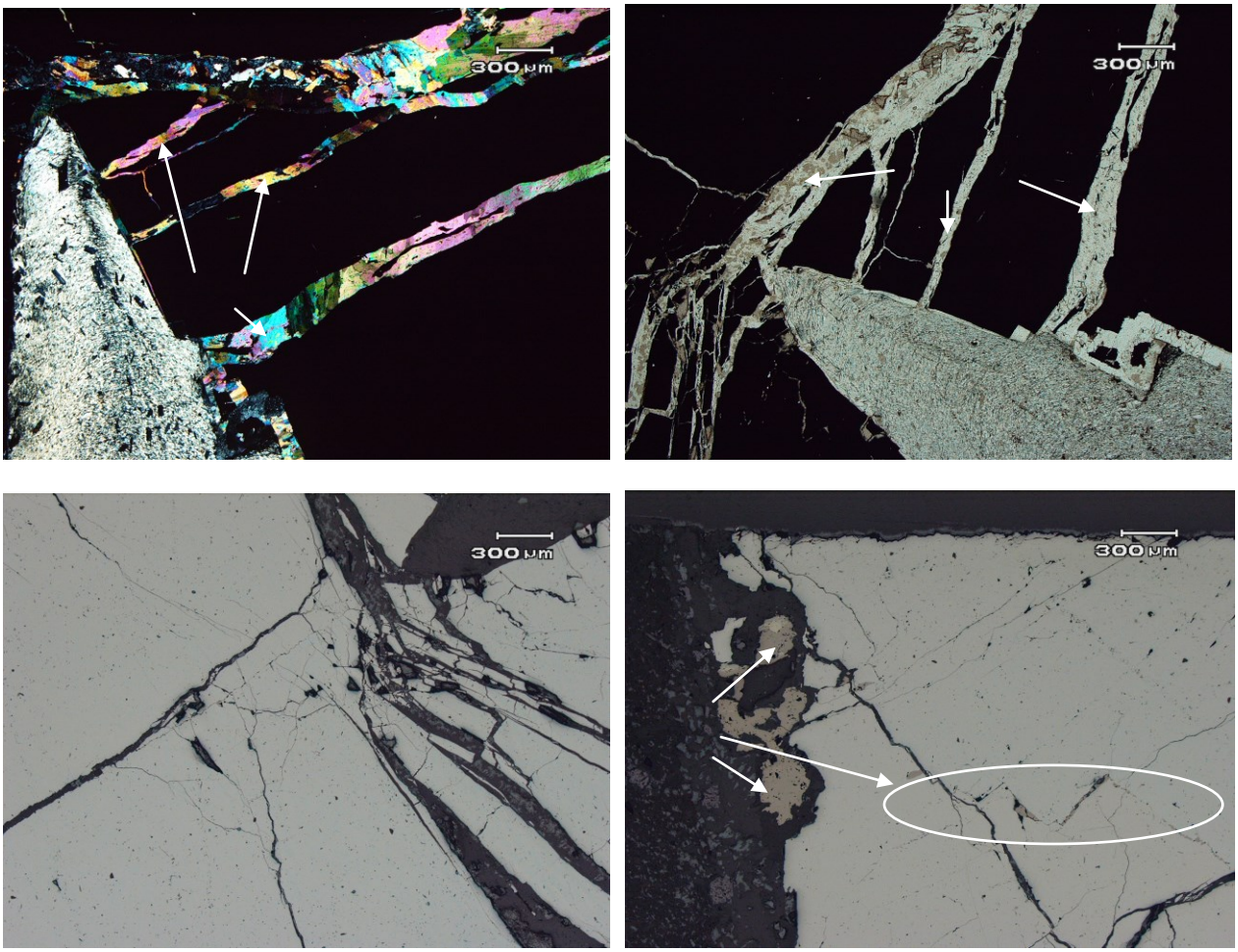

Figure 2.12: Thin section images of vein and arsenopyrite of sample LC-12-16: (A) Arsenopyrite crystal in thin calcite vein, cross polarized transmitted light. (B) Arsenopyrite crystal in thin calcite vein, plane polarized transmitted light. (C) Coarse arsenopyrite crystal, plane polarized reflected light. (D) Pyrrhotite with arsenopyrite crystal, plane polarized reflected light.

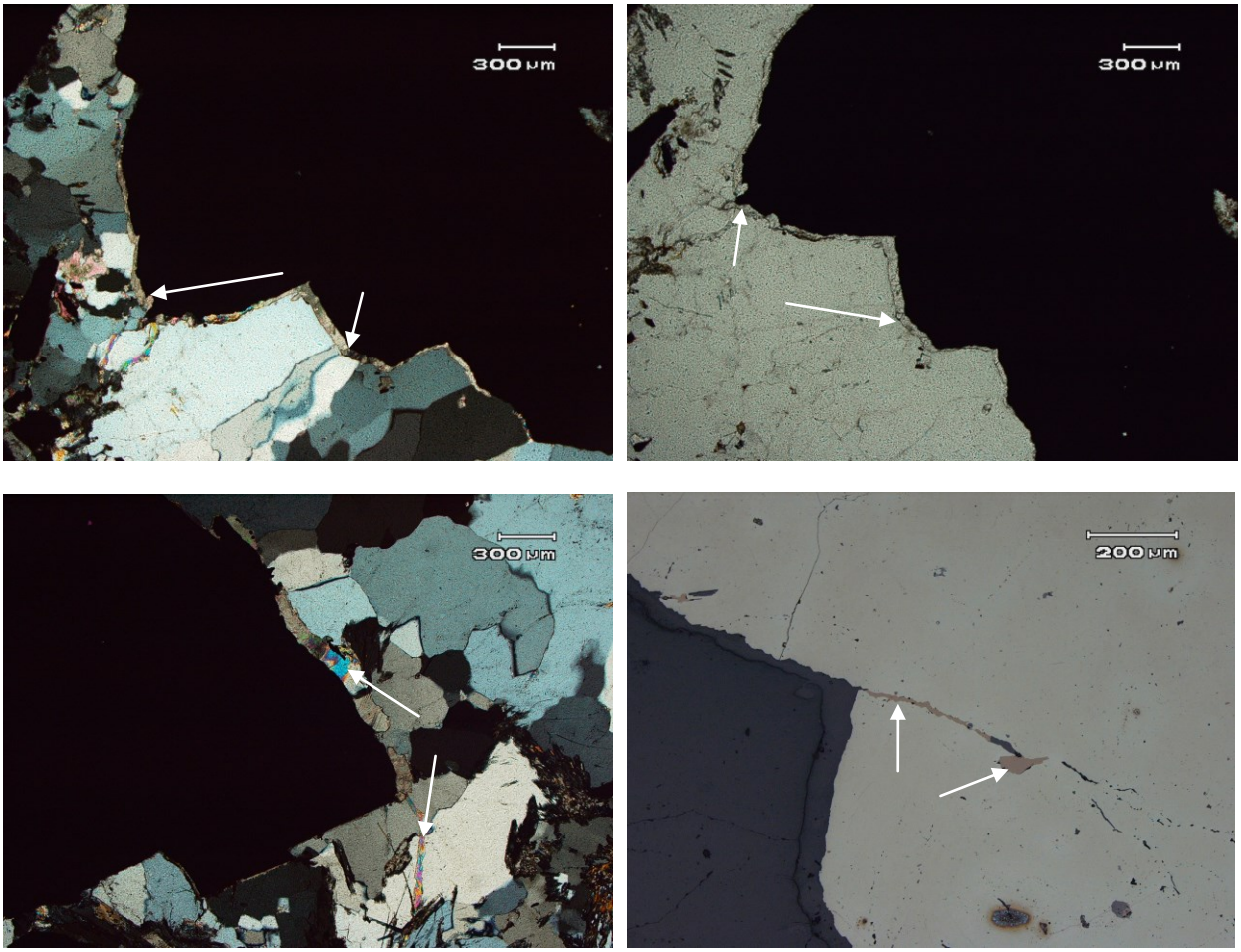

Figure 2.13: Thin section images of vein and arsenopyrite of sample LC-12-17: (A) Arsenopyrite crystal in thin calcite rim in quartz vein, cross polarized transmitted light. (B) Arsenopyrite with calcite rim in quartz vein, plane polarized transmitted light. (C) Coarse arsenopyrite crystal with calcite in quartz vein, cross polarized transmitted light. (D) Thin pyrrhotite vein inside arsenopyrite crystal, plane polarized reflected light.

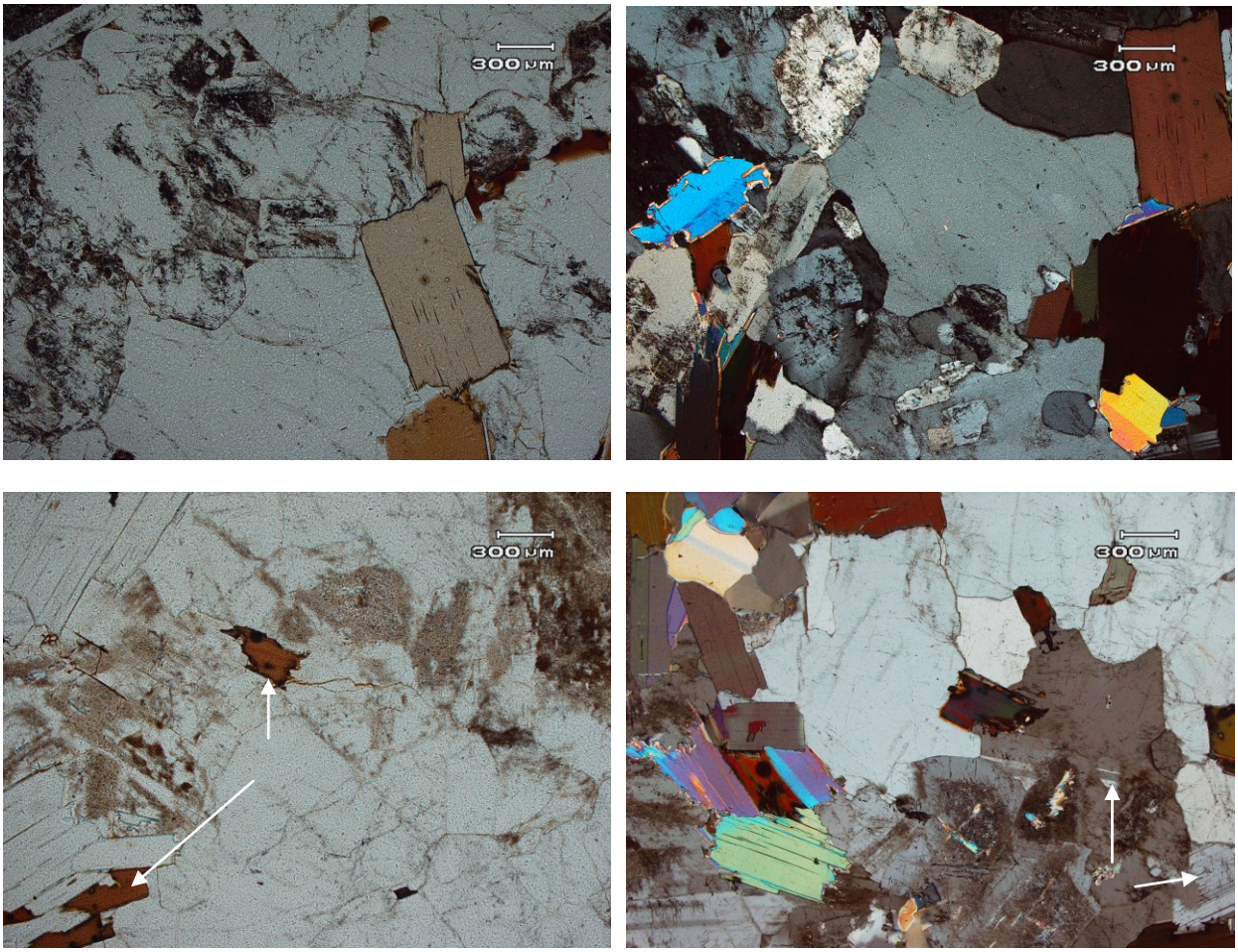

Figure 2.14: Thin section images of granite sample LC-12-05/06: (A) LC-12-05, plane polarized transmitted light. (B) LC-12-05, cross polarized transmitted light. (C) LC-12-06, plane polarized transmitted light. (D) LC-12-06, cross polarized transmitted light.

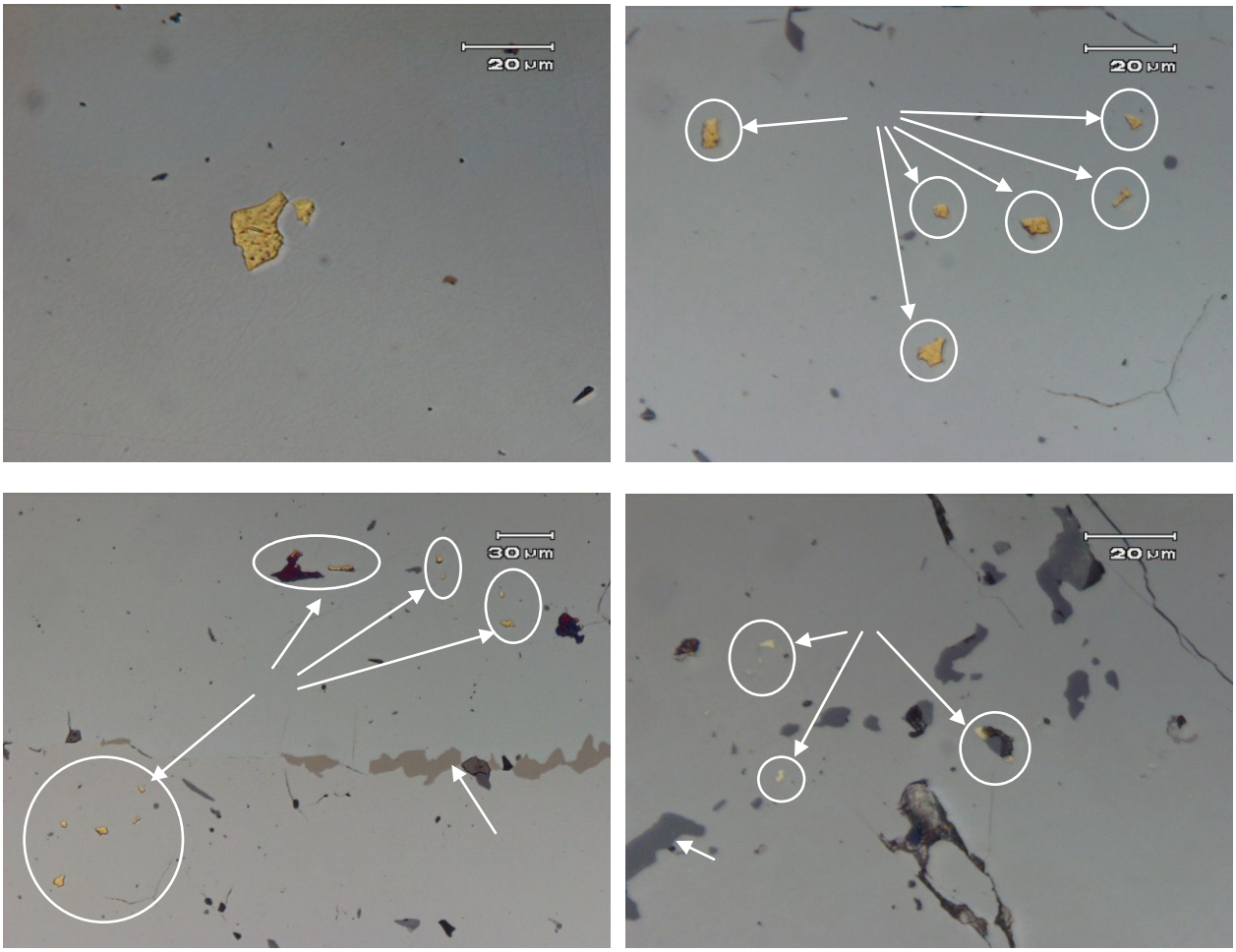

Figure 2.15: Thin section images of gold within arsenopyrite crystals: (A) Gold grain from LC-12-15, Beaver Dam. (B) Gold grains from LC-12-16, Beaver Dam. (C) Gold growing in arsenopyrite, associated with pyrrhotite, LC-12-16, Beaver Dam. (D) Gold grains in arsenopyrite with sphalerite (dark grey), LC-12-01, Moose River.

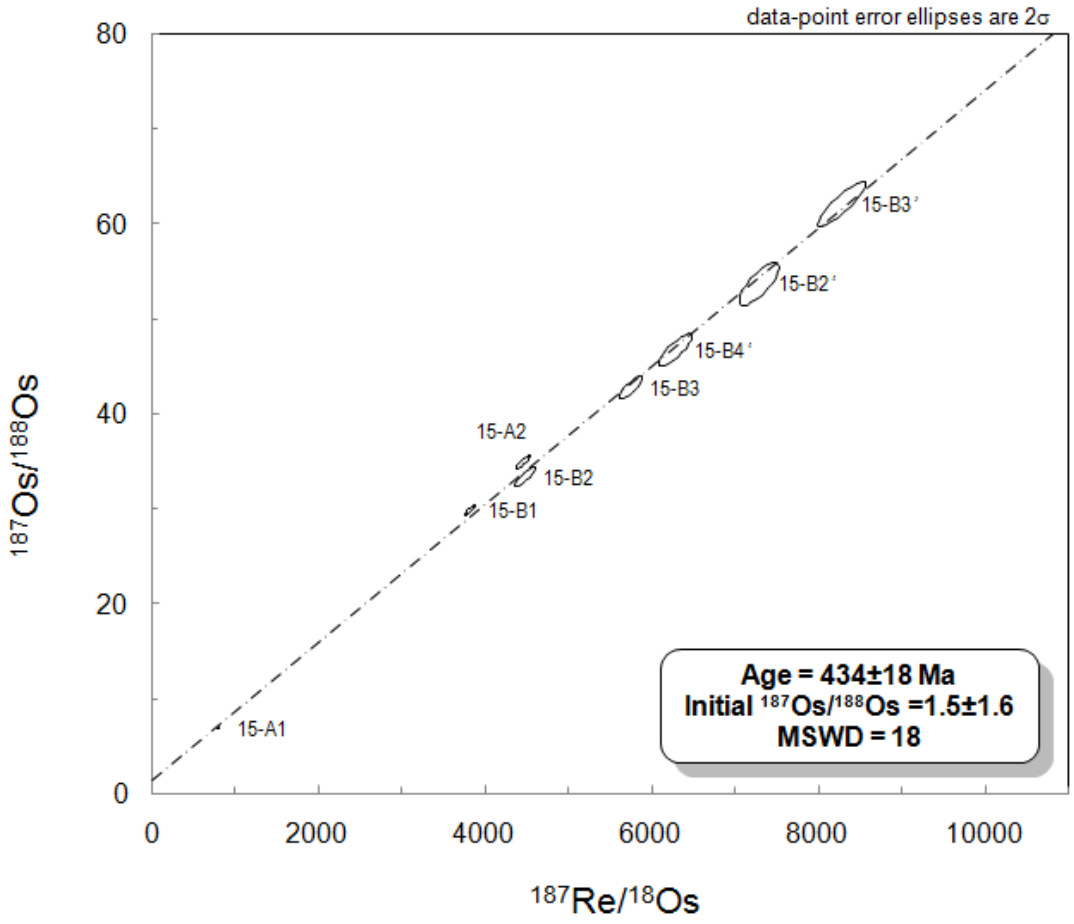

Figure 4.1: Re-Os isochron diagram of sample LC-12-15 from the Beaver Dam deposit.

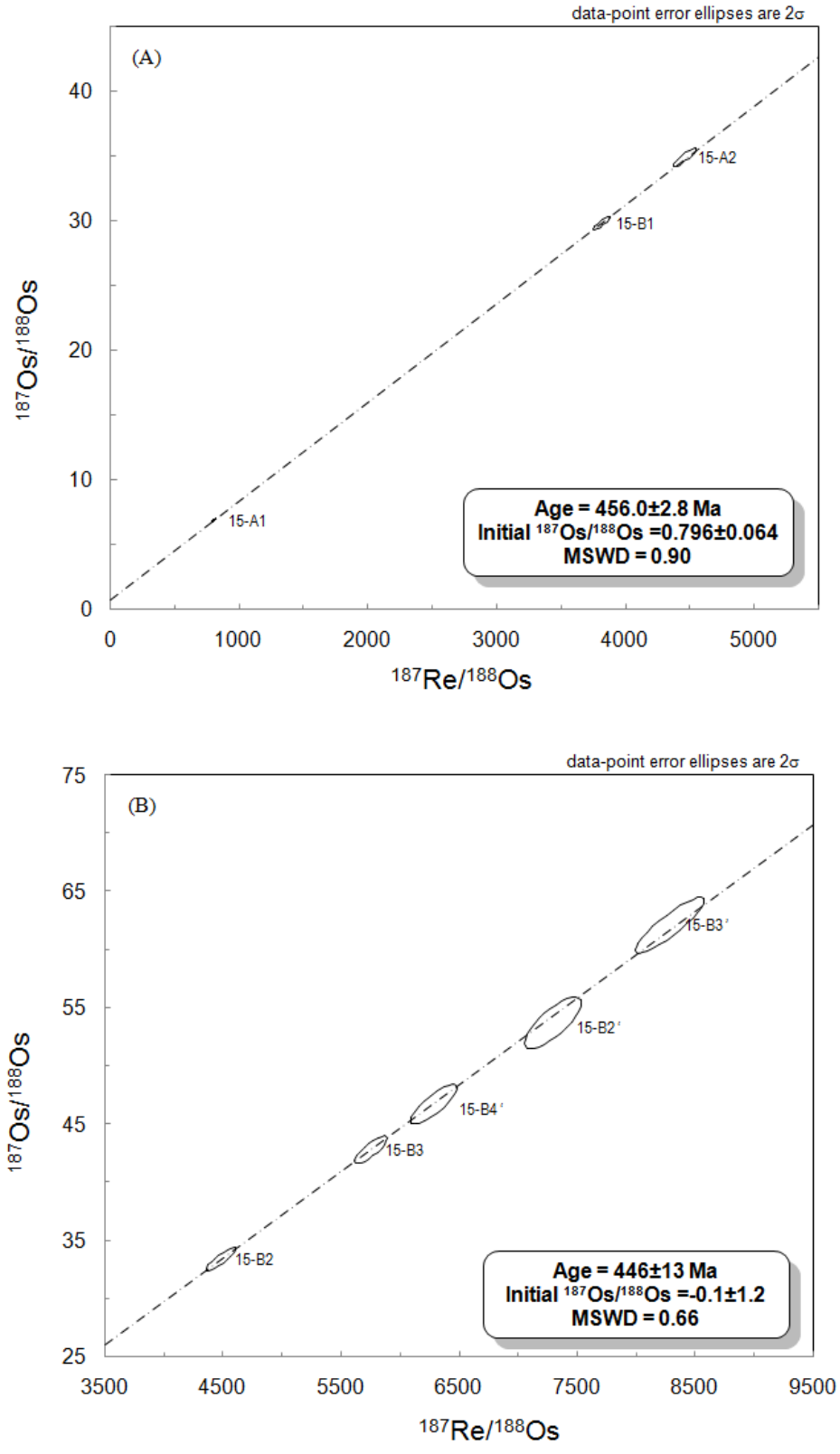

Figure 4.2: Re-Os isochron diagram of sample LC-12-15, separately plotting data into two groups.

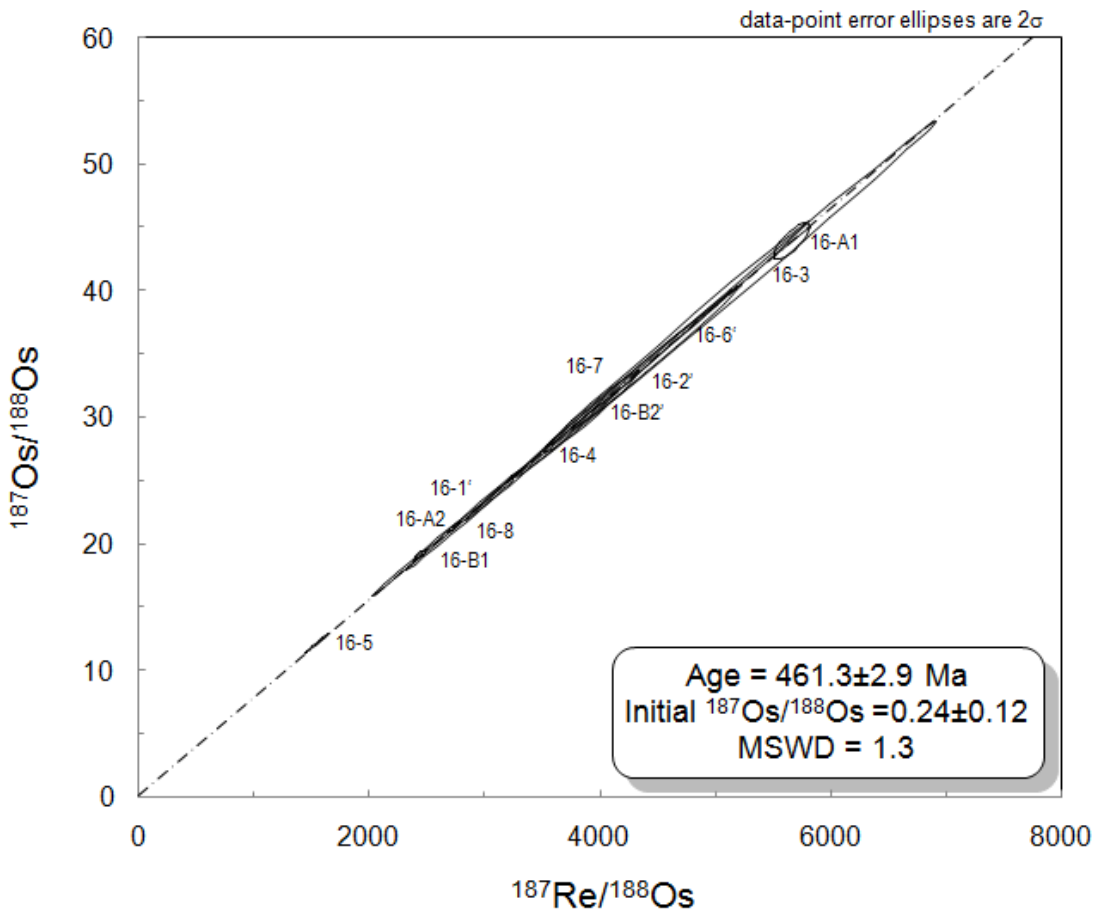

Figure 4.3: Re-Os isochron diagram of sample LC-12-16 from the Beaver Dam deposit.

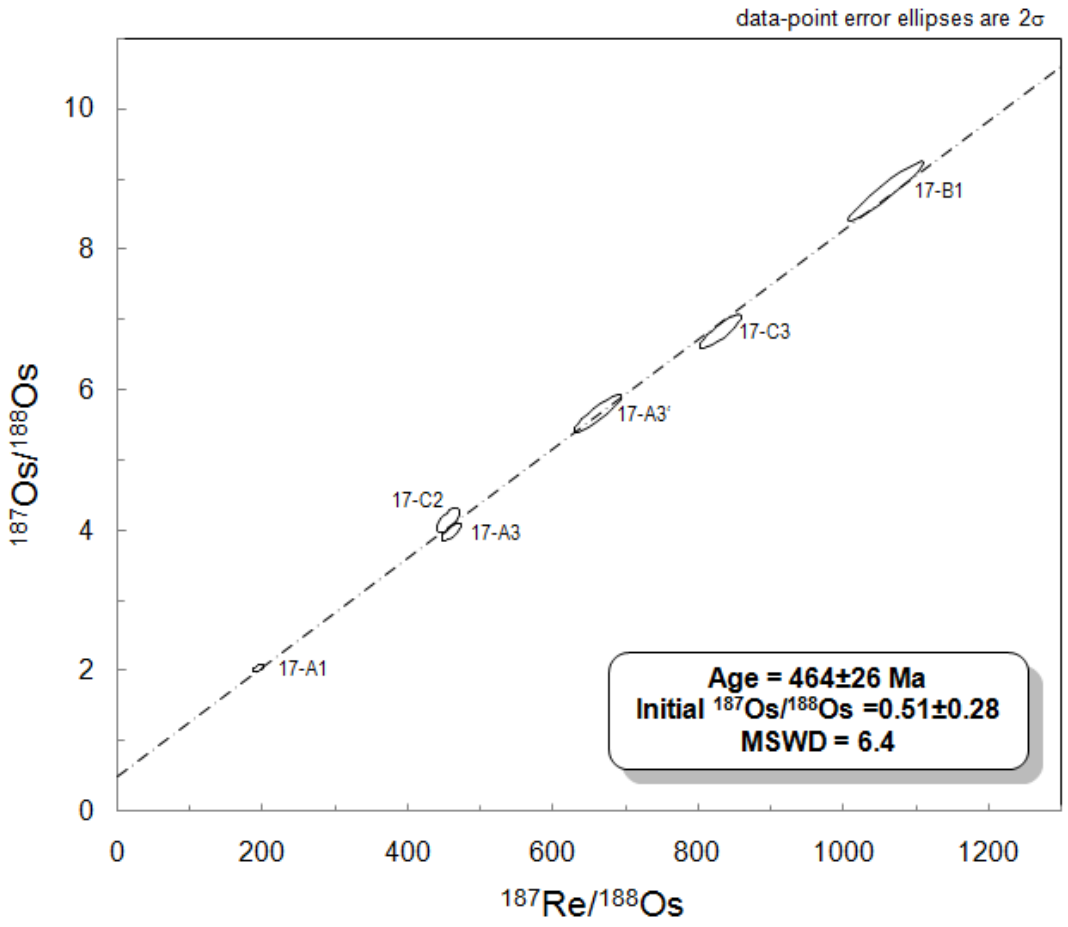

Figure 4.4: Re-Os isochron diagram of sample LC-12-17 from the Beaver Dam deposit.

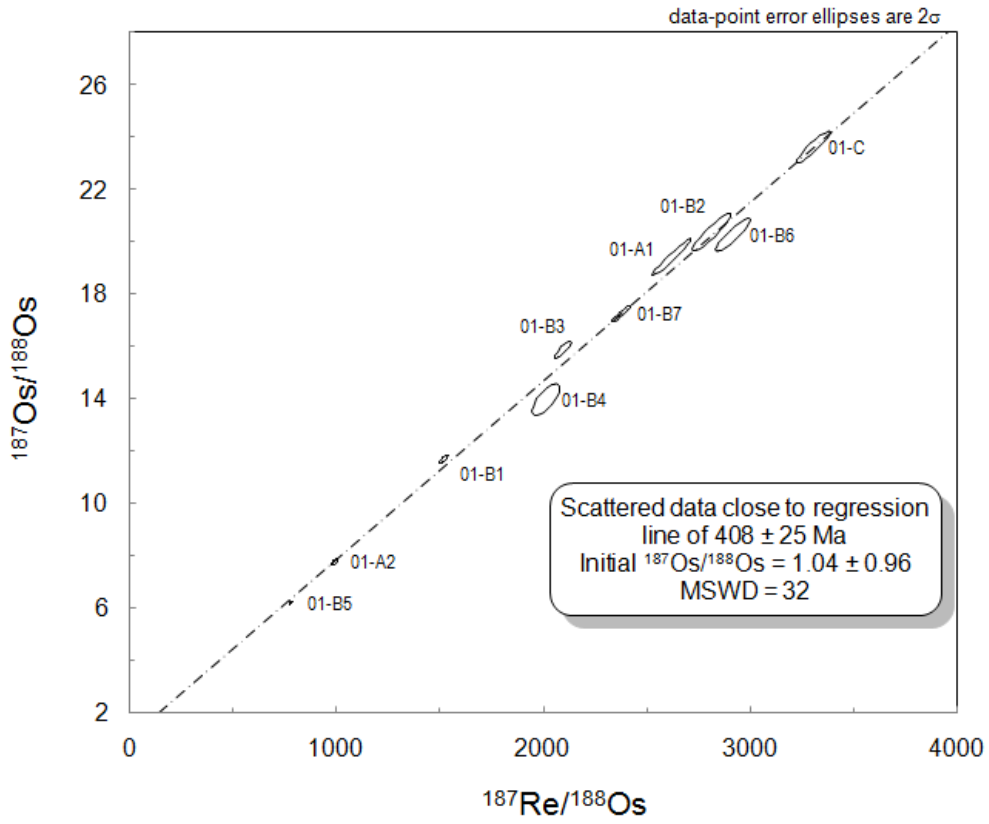

Figure 4.5: Re-Os isochron diagram of sample LC-12-01 from the Moose River deposit, 10 points are scattered around the regression line of age of 408 ± 25 Ma.

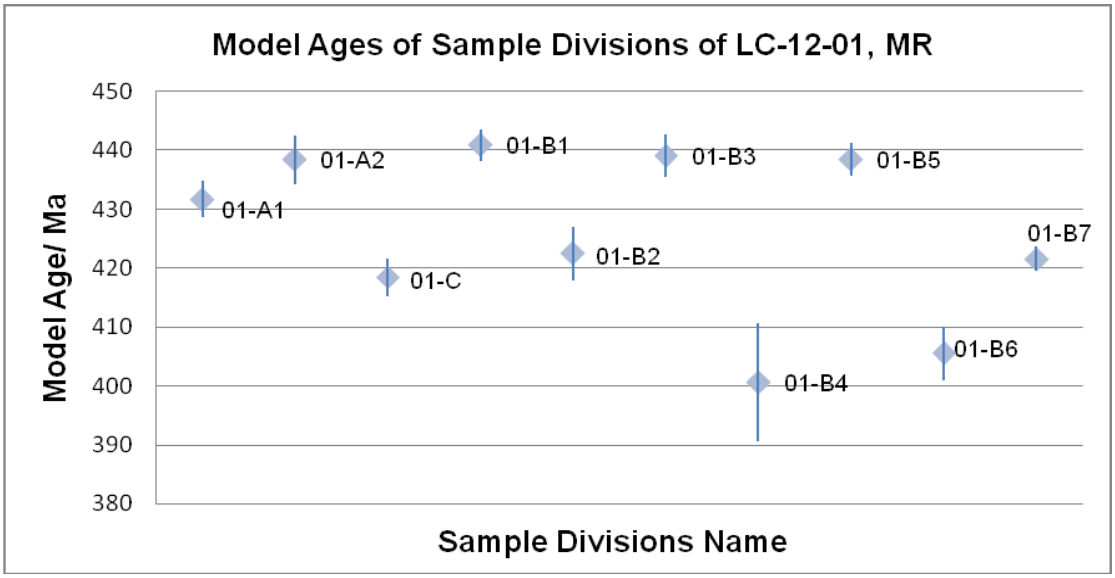

Figure 4.6: Re-Os model age diagram of sample divisions of LC-12-01.

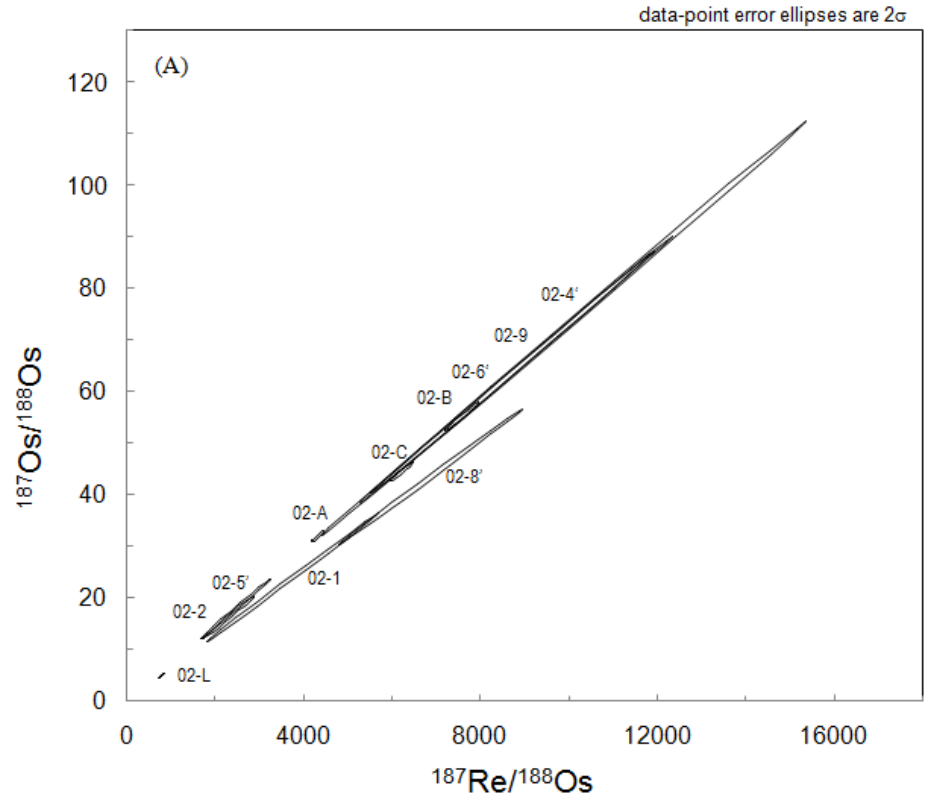
data-point error ellipses are 2σ
(A)
120
100
80
60
40
20
0
0
4000
8000
12000
16000
$^{187}Os/^{188}Os$
$^{187}Re/^{188}Os$
02-4'
02-9
02-6'
02-B
02-C
02-8'
02-A
02-5'
02-1
02-2
02-L

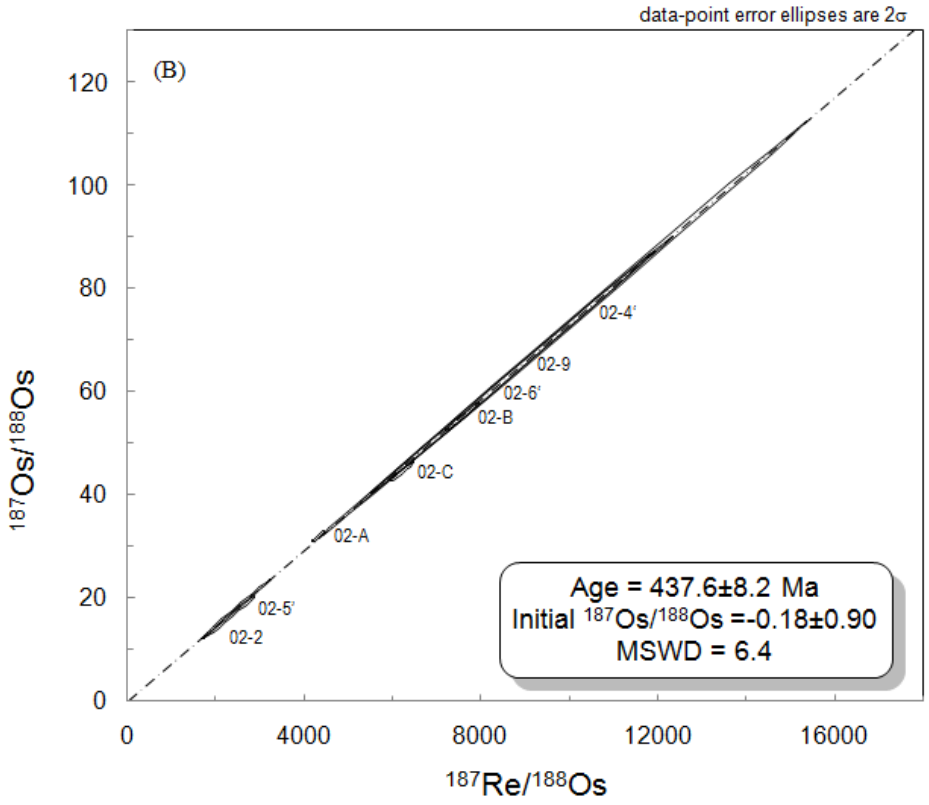
data-point error ellipses are 2σ
(B)
120
100
80
60
40
20
0
0
4000
8000
12000
16000
$^{187}Os/^{188}Os$
$^{187}Re/^{188}Os$
02-4'
02-9
02-6'
02-B
02-C
02-A
02-5'
02-2
Age = 437.6±8.2 Ma
Initial $^{187}Os/^{188}Os$ =-0.18±0.90
MSWD = 6.4

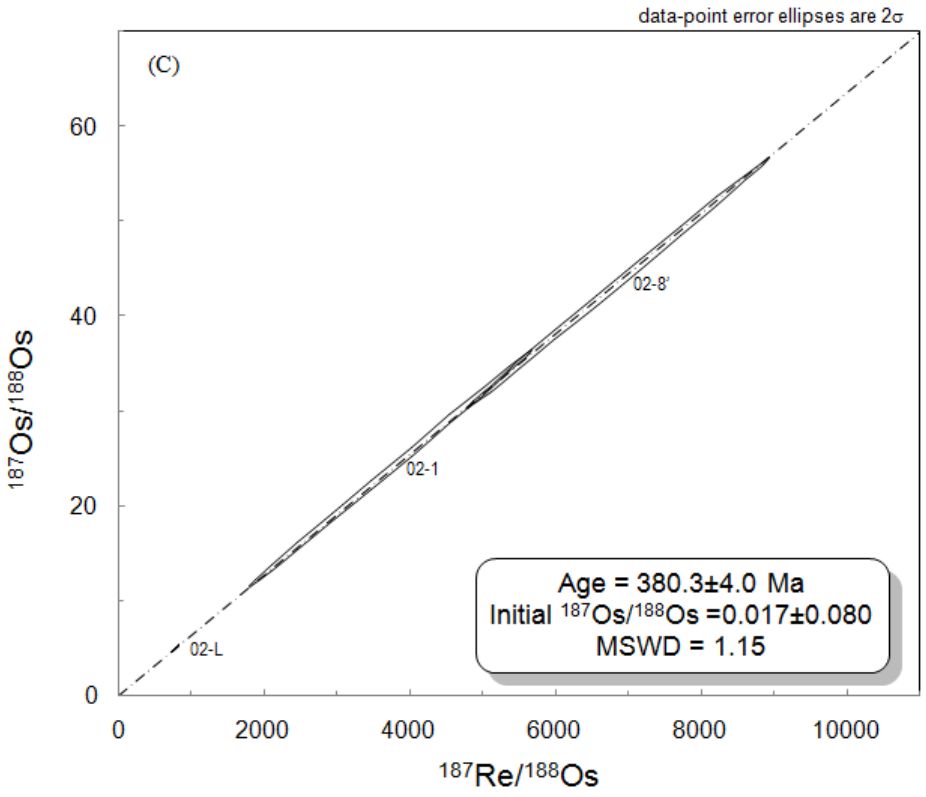

Figure 4.7: Re-Os isochron diagram of sample LC-12-02 from the Moose River deposit. (A) All 11 divisions plotting on regression lines with different slopes. (B) Eight divisions provide older age. (C) Three divisions yield younger age.

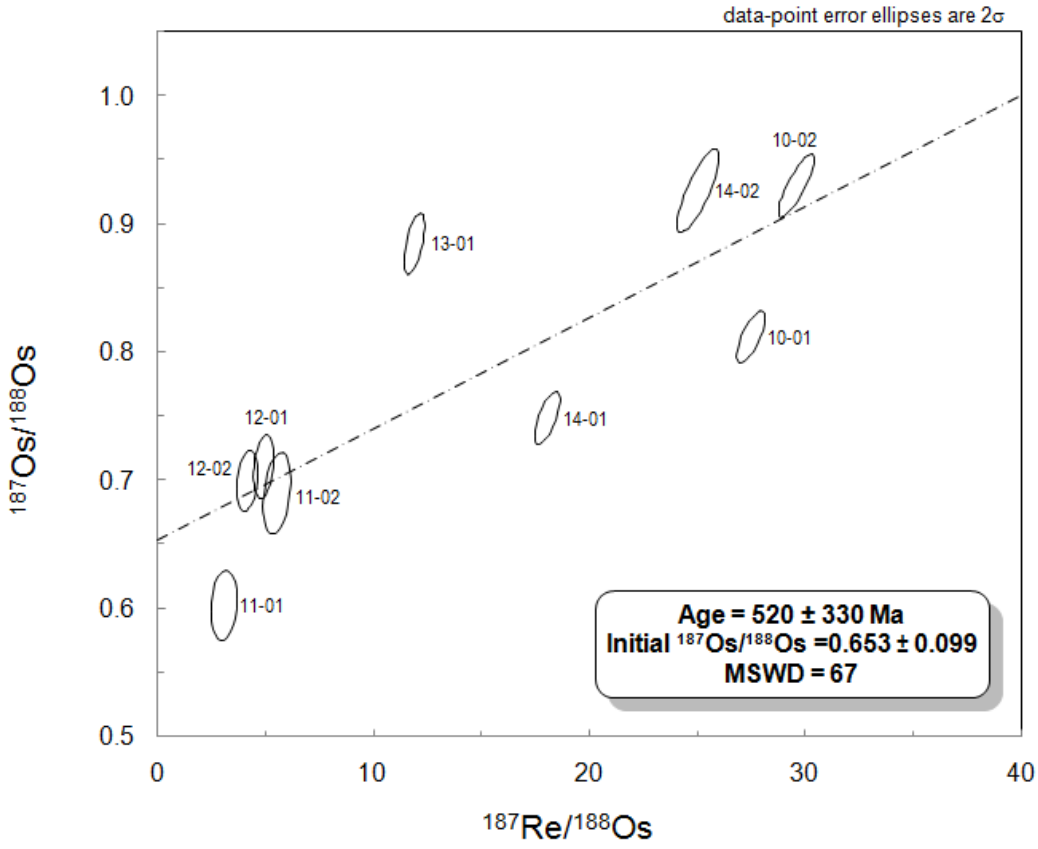

Figure 4.8: Re-Os isochron diagram of host rock black shale sample from the Beaver Dam deposit.

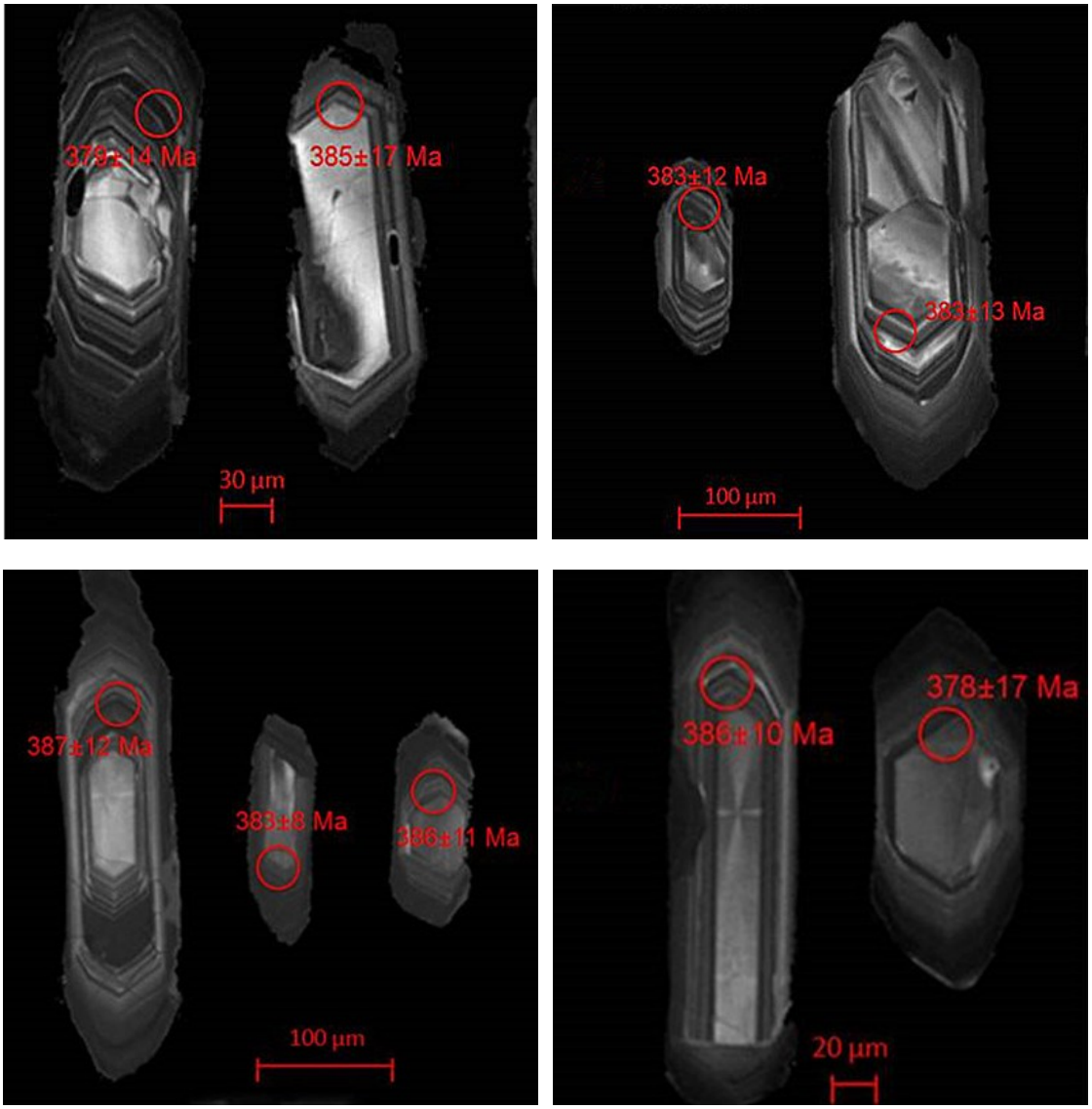

Figure 4.9: CL images of zircons from granite samples of the River Lake intrusion: LC-12-05 (top), LC-12-06 (bottom).

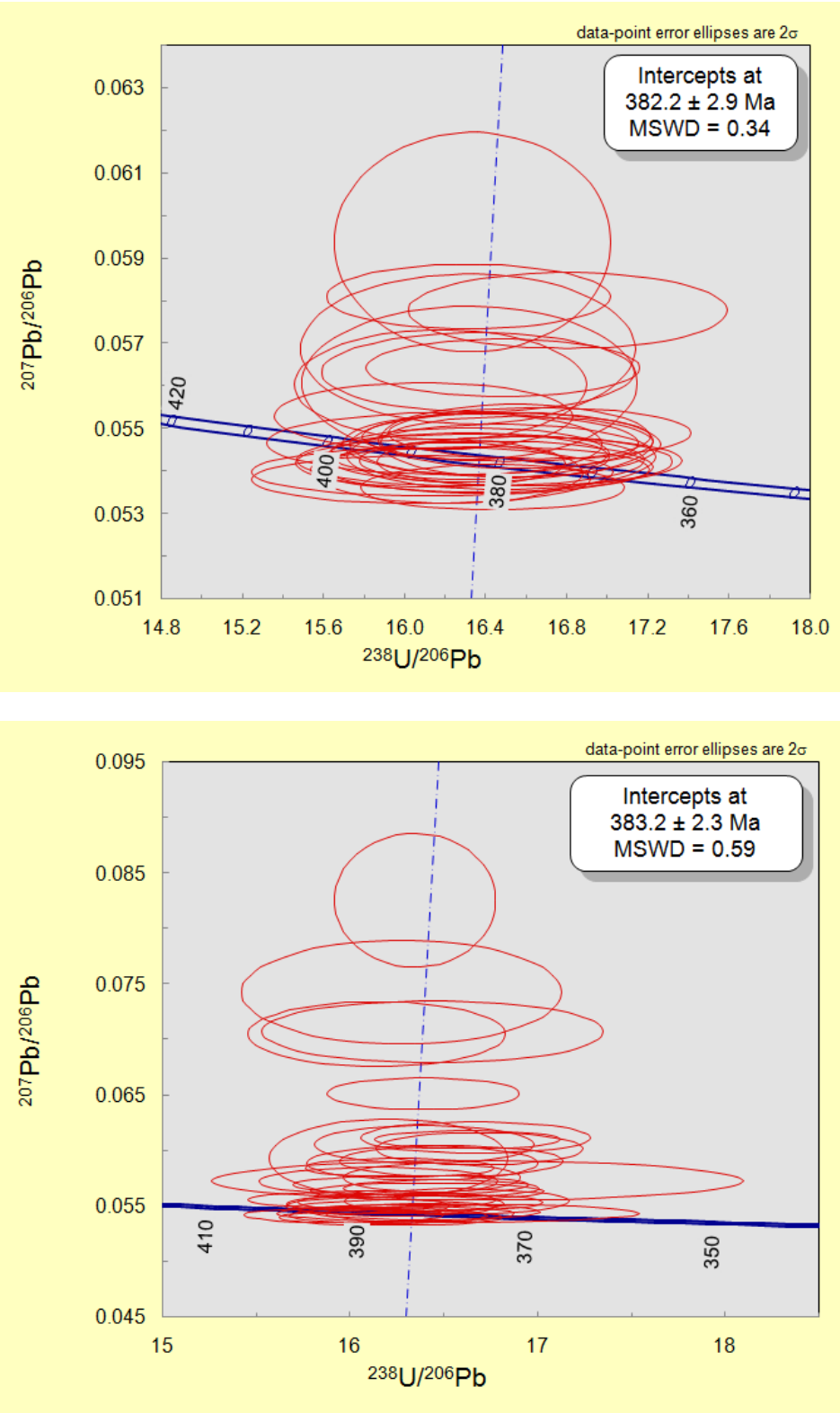

Figure 4.10: U-Pb LA-ICPMS Tera-Wasserburg diagram: (A) Determined from 29 zircons from granite LC-12-05. (B) Determined from 31 zircons from granite LC-12-06. Error ellipses are at 2σ levels.

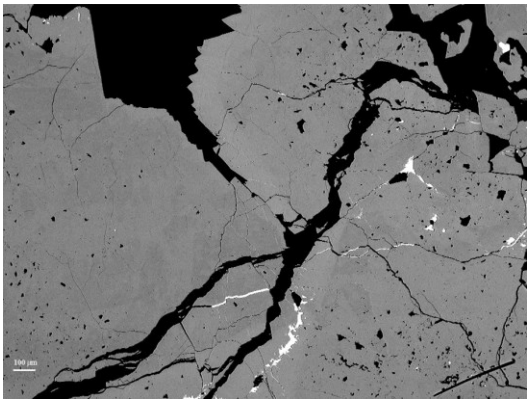
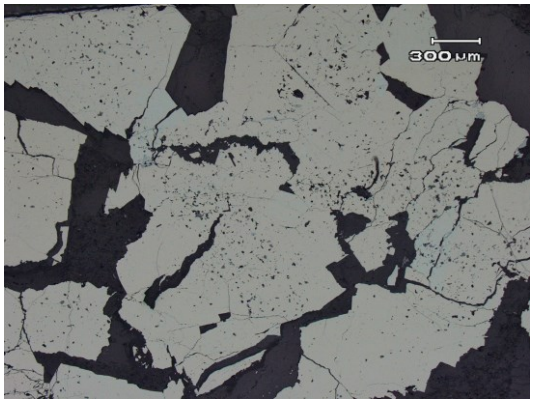
300 µm
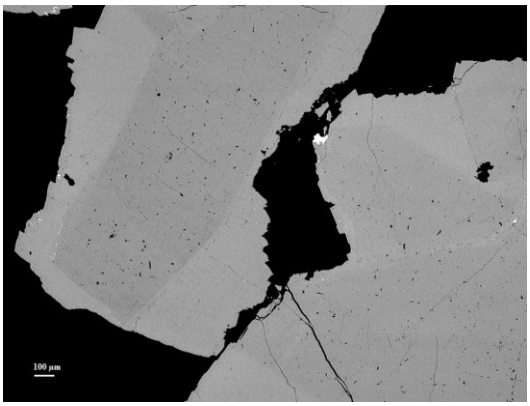
100 µm
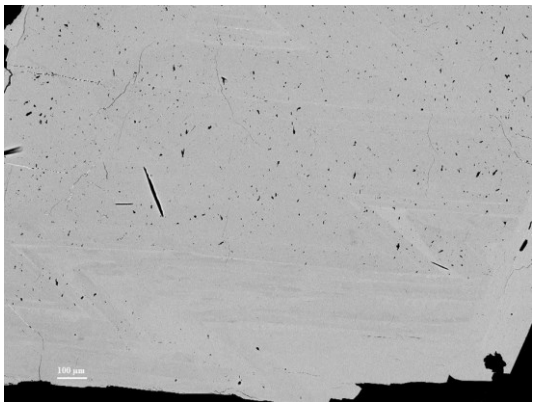
100 µm
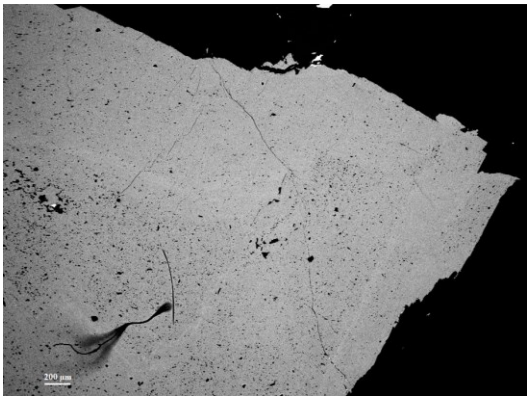
200 µm
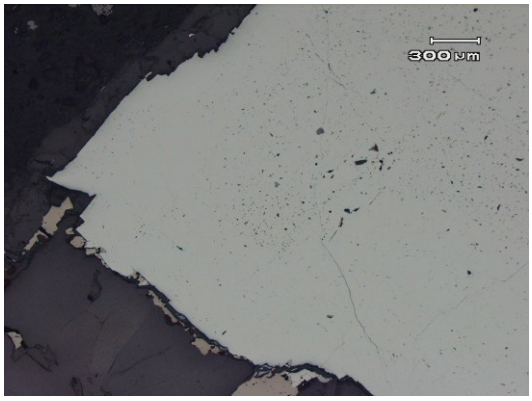
300 µm
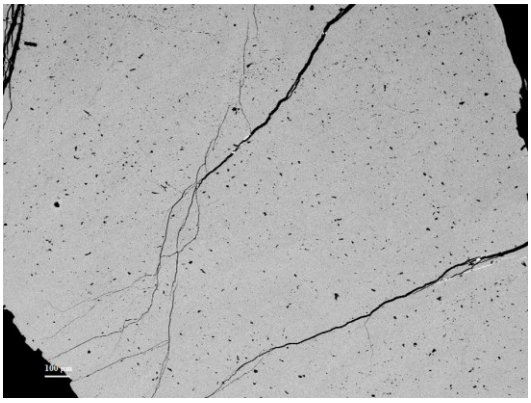
100 µm
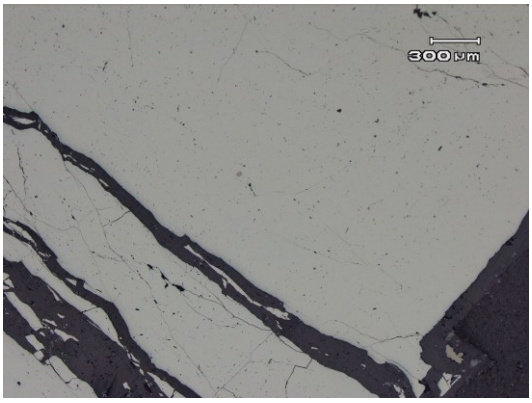
300 µm

Figure 4.11: Arsenopyrite thin section images and SEM images. (A, B) Arsenopyrite from sample LC-12-01, MR, inclusion rich core and inclusion free overgrouth rim, A is SEM image, B is thin section image. (C) Zoning appears in LC-12-01 SEM image. (D) Zigzag zoning in SEM image of LC-12-02, MR. (E, F) Arsenopyrite from sample LC-12-15, BD, inclusion rich core and inclusion free overgrouth rim, E is SEM image, F is thin section image. (G, H) Homogenous arsenopyrite from LC-12-16, BD, G is SEM image, H is thin section image.

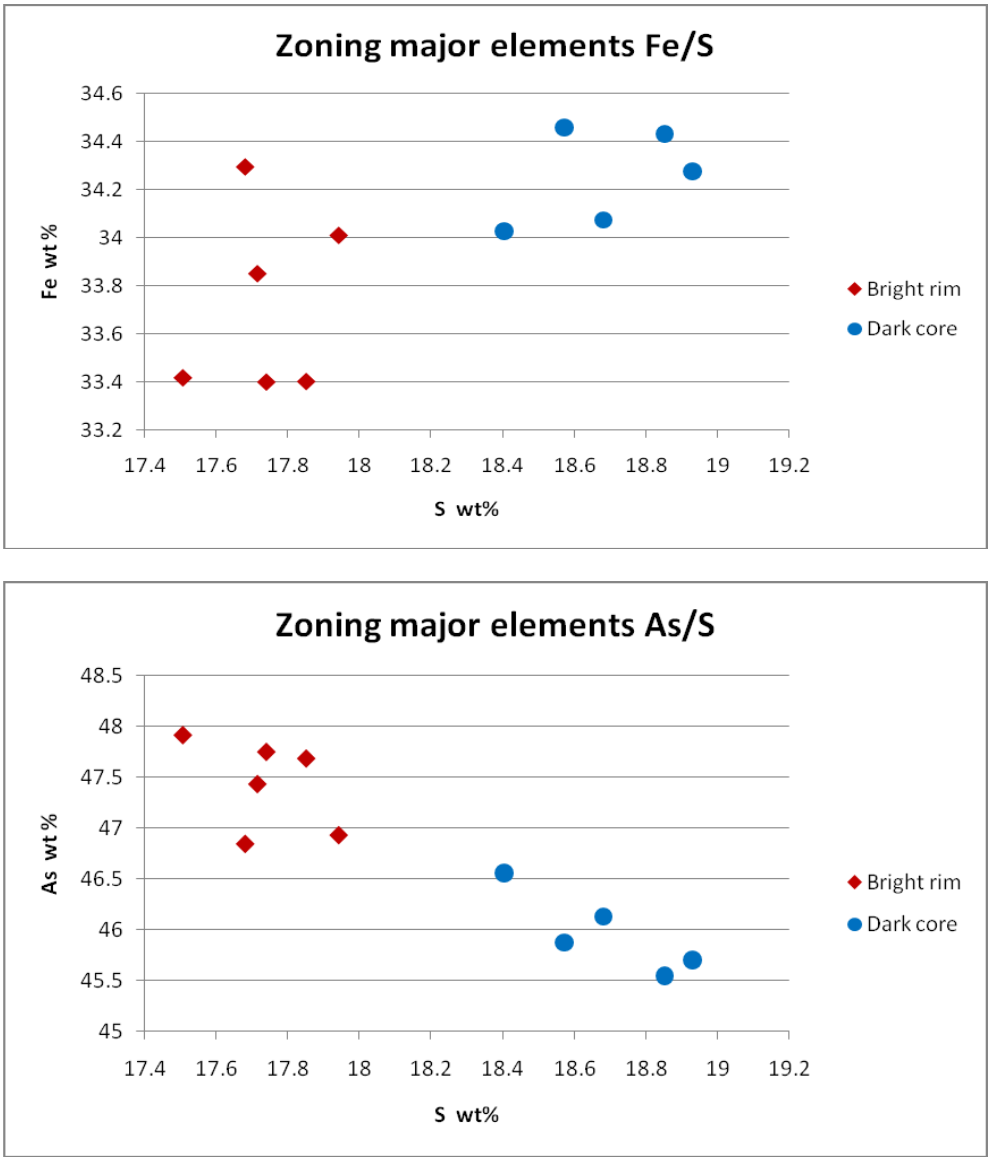

Figure 4.12: Major element analytical results of LC-12-01, LC-12-02 from the Moose River deposit by SEM, the core is rich of Fe and S but lack of As, the rim is in an opposite way.

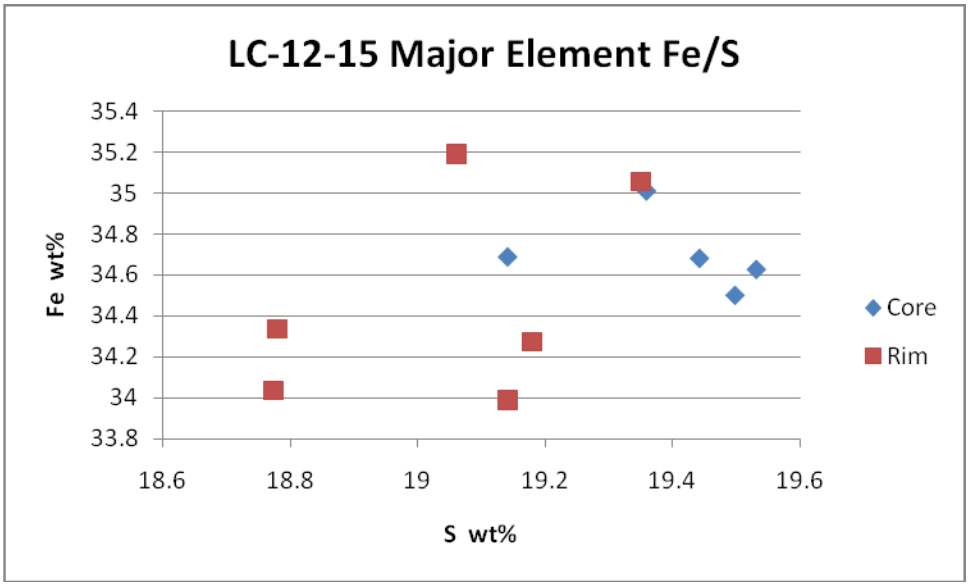

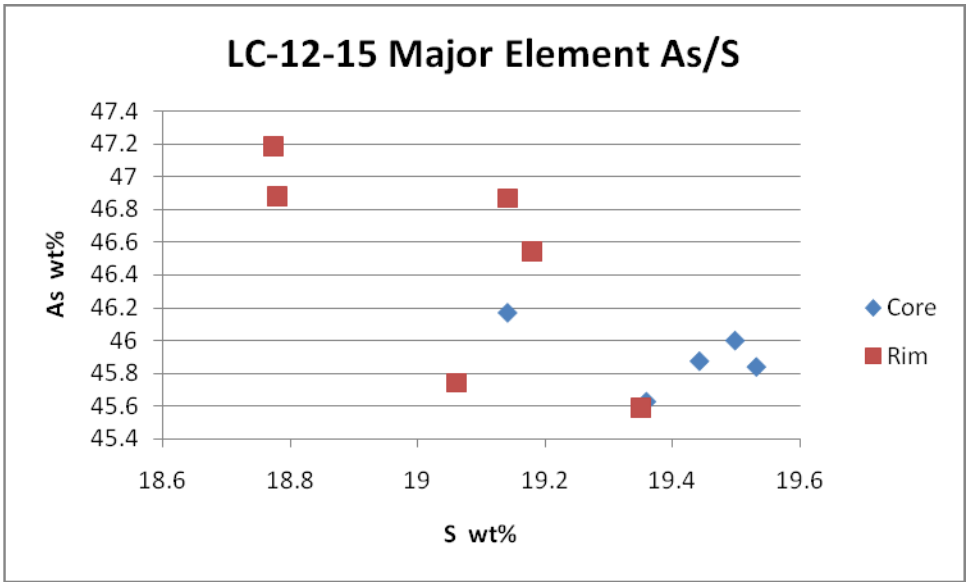

Figure 4.13: Major element analytical results of LC-12-15 from the Beaver Dam deposit by SEM , inclusions rich core is high in S while the clear rim is relatively low in S, As and Fe distribution does not show a clear difference.

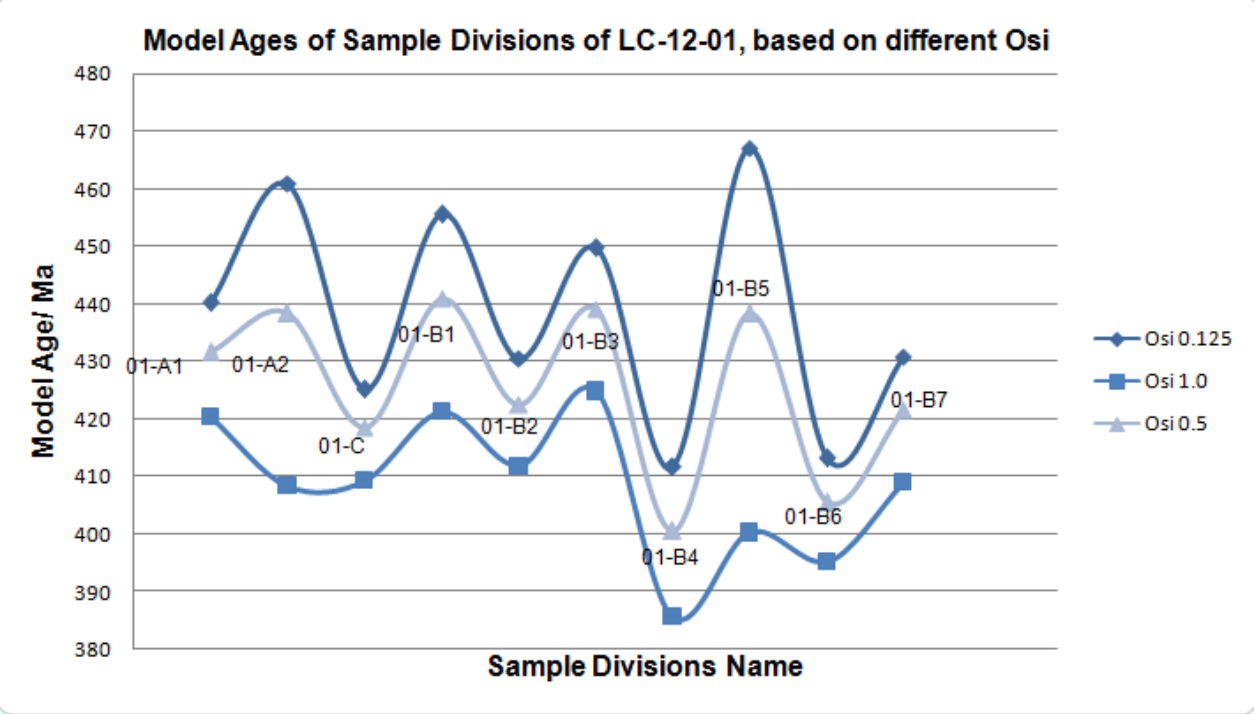

Figure 5.1: Re-Os model age diagram of sample divisions of LC-12-01. Different model ages when calculate using different $^{187}Os/^{188}Os$ initials, regardless the error. The upper line shows the model ages ranging from ca. 410-460 Ma when calculate using the Os_i of 0.125 (mantle $^{187}Os/^{188}Os$ value); the middle line shows the model ages varying from ca. 400-440 Ma when calculate using the Os_i of 0.5 (suggested values); the lower line shows the model ages from ca. 385-425 Ma when calculate using the Os_i of 1.0 (higher than all the previous defined Os_i value in the Meguma terrane, relatively impossible).

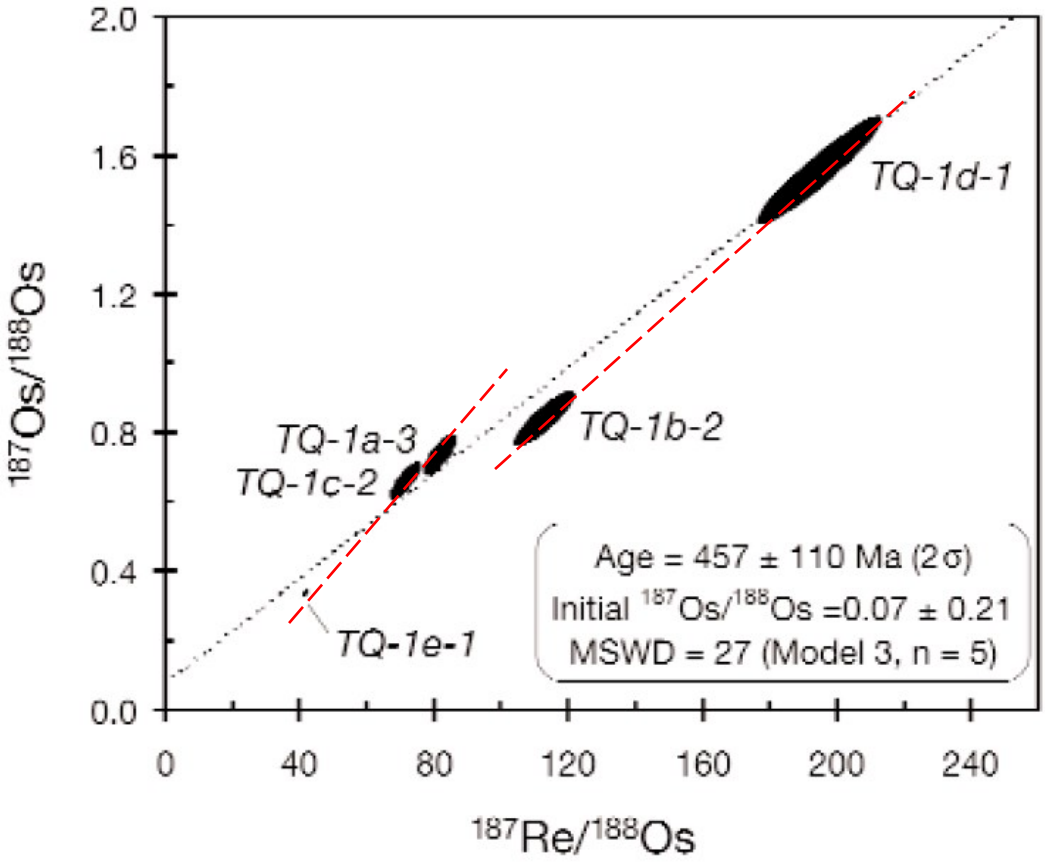

Figure 5.2: Re-Os isochron diagram of arsenopyrite analyses of samples from the disseminated Touquoy deposit, Moose River district (Morelli et al., 2005), red lines show the data regressed on different regression lines assuming that they are not homogenous.

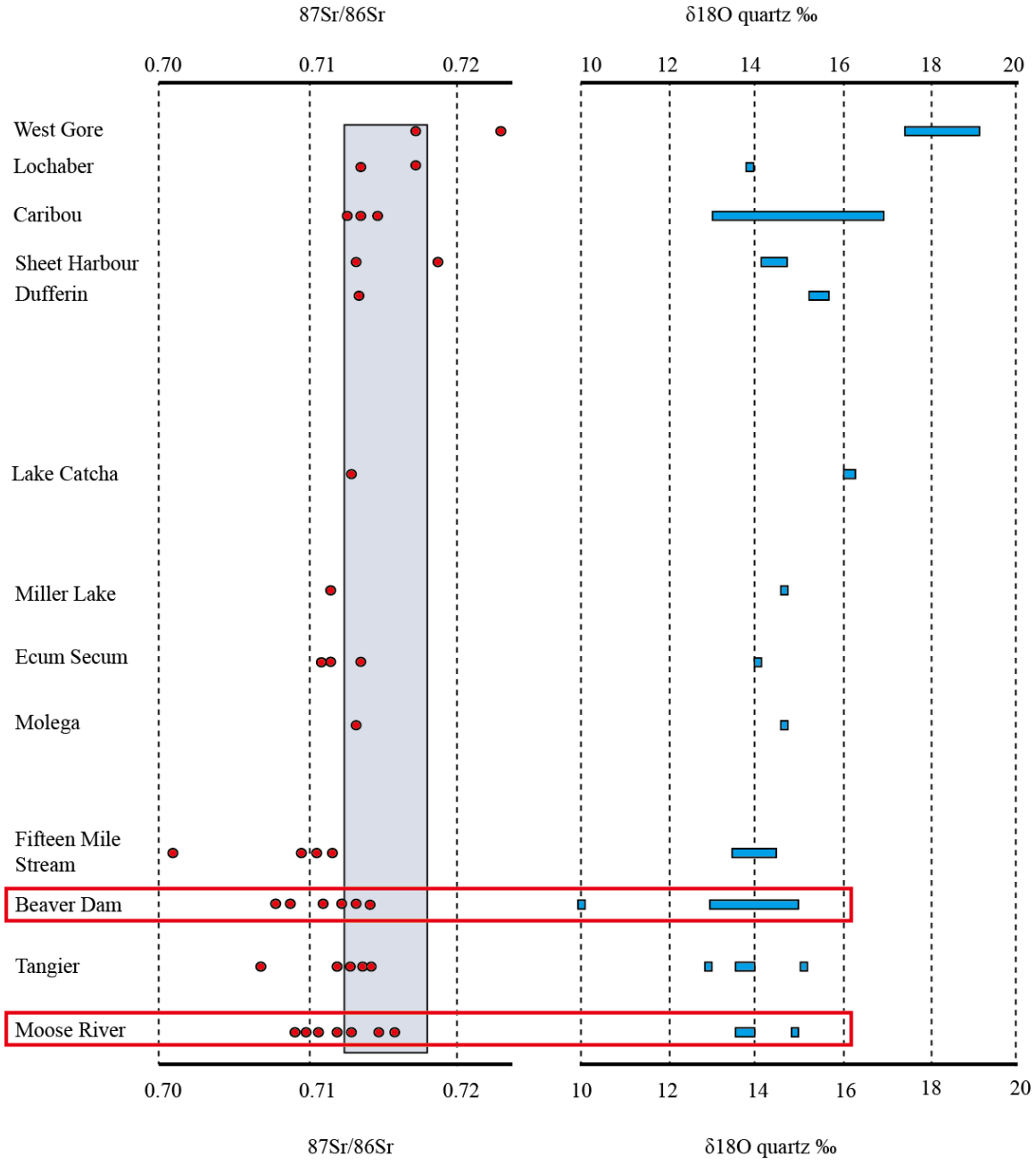

Figure 5.3: Left, Plot of $^{87}Sr/^{86}Sr$ for vein carbonate samples from gold districts arranged from base to top of the stratigraphy. The shaded box outlines the initial ratio for the Goldenville Group and Halifax Group (known as Meguma Supergroup) at 380 Ma; Right, summary of $\delta^{18}O$ ‰ for quartz from the Meguma gold deposits. Comparing Beaver Dam and Moose River deposit isotope data with other gold deposits, the ranges of both isotopes are wide (modified from Kontak and Kerrich, 1995; Kontak and Horne 2010).